arXiv:1402.5756v1 [cond-mat.mtrl-sci] 24 Feb 2014

Phonon-glass electron-crystal thermoelectric clathrates: Experiments and theory

Toshiro Takabatake* and Koichiro Suekuni

Graduate School of Advanced Sciences of Matter, Hiroshima University, Higashi-Hiroshima 739-8530, Japan

Tsuneyoshi Nakayama† ‡ and Eiji Kaneshita*†

†*Max Planck Institute for the Physics of Complex Systems, Dresden 01187, Germany and* ‡*Hokkaido University, Sapporo 060-0826, Japan*
**Sendai National College of Technology, Sendai 989-3128, Japan*

Type-I clathrate compounds have attracted a great deal of interest in connection with the search for efficient thermoelectric materials. These compounds constitute networked cages consisting of nano-scale tetrakaidecahedrons (14 hedrons) and dodecahedrons (12 hedrons), in which the group 1 or 2 elements in the periodic table are encaged as the so-called "rattling" guest atom. It is remarkable that, though these compounds have crystalline cubic-structure, they exhibit glass-like phonon thermal conductivity over the whole temperature range depending on the states of rattling guest atoms in the tetrakaidecahedron. In addition, these compounds show unusual glass-like specific heats and THz-frequency phonon dynamics, providing a remarkable broad peak almost identical to those observed in topologically disordered amorphous materials or structural glasses, the so-called Boson peak. An efficient thermoelectric effect is realized in compounds showing these glass-like characteristics. This decade, a number of experimental works dealing with type-I clathrate compounds have been published. These are diffraction experiments, thermal and spectroscopic experiments in addition to those based on heat and electronic transport. These form the raw materials for this article based on advances this decade. The subject of this article involves interesting phenomena from the viewpoint of not only physics but also from the view point of the practical problem of elaborating efficient thermoelectric materials. This review presents a survey of a wide range of experimental investigations of type-I clathrate compounds, together with a review of theoretical interpretations of the peculiar thermal and dynamic properties observed in these materials.

Contents

I. INTRODUCTION 2
A. History and motivation 2
B. The concept of "phonon-glass and electron-crystal" exploring efficient thermoelectric materials 3

II. BACKGROUND ON THERMOELECTRICITY 3
A. The Wiedemann-Franz law and the Lorenz number 3
B. Heat and electric transport as irreversible processes 4
1. Peltier and Seebeck coefficients 4
2. Figure of merit 5
3. The Mott formula for the Seebeck coefficient 6

III. CRYSTAL STRUCTURES OF TYPE-I CLATHRATE COMPOUNDS 6
A. Various types of clathrate compounds 6
1. Classification of clathrate compounds 6
2. Intermetallic clathrate compounds 7
3. Crystal chemistry of type-I clathrate 8
B. On-center and off-center positions of guest atoms in type-I clathrate compounds 9
1. X-ray and neutron diffractions and EXAFS 9

IV. SPECIFIC HEATS OF TYPE-I CLATHRATE COMPOUNDS 13
A. Observed characteristics of specific heats 13
1. Low temperature specific heats below 1 K 13
2. Excess specific heats over Debye phonons at temperatures of several Kelvin 13
3. Characteristic temperatures of excess specific heats 14

V. TRANSPORTS PROPERTIES OF TYPE-I CLATHRATE COMPOUNDS 16
A. Electrical resistivity and Seebeck coefficient 16
B. Phonon thermal conductivity 18

VI. SPECTROSCOPIES IN THz FREQUENCY REGION 20
A. Optical spectroscopies 20
1. Raman spectra and those assignments 20
2. Temperature, carrier-type, and pressure dependences of Raman spectra 22
3. Infrared spectroscopy in the terahertz (THz) frequency range 23
B. Inelastic neutron scattering 25
1. Dynamic structure factor and the flat dispersion relation of phonons 25
2. Inelastic neutron scattering experiments for on-center systems 26
3. Inelastic neutron scattering experiments on off-center systems 28

VII. PHONON DISPERSION RELATIONS 29
A. Theoretical aspects of THz frequency dynamics of type-I clathrate compounds 29
1. Molecular dynamics calculations 29
2. Anharmonic potential expressed in terms of the relative coordinate 31

*Electronic address: takaba@hiroshima-u.ac.jp
†Electronic address: tnaka@eng.hokudai.ac.jp

3. Spontaneous symmetry breaking of off-center systems 31
B. Equations of motion 32
1. Effect of charge fluctuation 32
2. Fourier-transformed representation of equations of motion 32
C. Phonon dispersion relations for off-center and on-center systems in the THz frequency region 33
1. On-center System 33
2. Off-center system 33
3. Comparison of calculated dispersion relations to INS experiments 35
4. The origin of Boson-peak like excess density of states 35

VIII. GLASS-LIKE SPECIFIC HEATS BELOW 1 [K] 36
A. Low temperature specific heats and two-level tunneling states 36
1. Two-level tunneling model 36
2. Specific heats below 1 [K] 37
3. Failure of the noninteracting picture for tunneling elements 37
B. Interacting-dipoles in type-I clathrate compounds 39
1. Multi-valley potentials in configuration space 39
2. Explicit form of specific heats below 1 K 40
3. Tunneling states in alkali-halide crystals containing CN^- ions 40

IX. UNDERLYING MECHANISMS OF GLASS-LIKE THERMAL CONDUCTIVITIES 40
A. Thermal conductivities below 1 K 41
B. Plateau region of thermal conductivities at around 5 K 42
1. Umklapp process for on-center systems 42
2. Plateau temperature region of off-center systems 42
C. T-linear rise above the plateau temperature region 43
1. Thermal transport due to the hopping of local modes associated with guest atoms 43
2. Overall interpretation of glass-like thermal conductivities 44

X. SUMMARY AND CONCLUSIONS 45

XI. ACKNOWLEDGMENTS 46

References 46

I. INTRODUCTION

A. History and motivation

Research on thermoelectricity has a long history. It started in the 1820's with the discovery of the Seebeck effect, i.e., converting temperature difference to electric current in metals (Seebeck, 1822, 1826). J. T. Seebeck discovered in 1821 that an electric current flows in a closed circuit made of two dissimilar metals when the two junctions are maintained at different temperatures. The reverse effect was found 10 years later by Peltier (1834).

A. F. Ioffe (1932) made a breakthrough in the 1930's, noting that semiconductor thermoelements are more practical than metals employed at that time. In fact, modern thermoelectric devices contain many thermocouples consisting of n-type (electron carriers) and p-type (hole carriers) semiconductors wired electrically in series and thermally in parallel as shown in Fig. 1. A. F. Ioffe is the first to use the quantity Z termed "material's figure of merit" describing the efficiency of the thermal-to-electrical conversion (A. F. Ioffe, 1958a; Vedernikov and Iordanishvili, 1998). How to increase the conversion efficiency can be found from the definition,

$$Z = \frac{S^2\sigma}{\kappa_{\rm tot}} \ \ [{\rm WK}^{-2}{\rm m}^{-1}], \tag{1}$$

where $S(T)\,[{\rm V/K}]$ is the Seebeck coefficient, $\sigma(T)\,[1/(\Omega{\rm m})]$ the electrical conductivity, and $\kappa_{\rm tot} = \kappa_{\rm el} + \kappa_{\rm ph}$ is the total thermal conductivity given by the sum of the electrical thermal conductivity $\kappa_{\rm el}$ and the phonon thermal conductivity $\kappa_{\rm ph}$. The physical meaning of Eq. (1) will be explained in II.B.2.

The design concept proposed by A. F. Ioffe is to reduce the phonon thermal conductivity $\kappa_{\rm ph}(T)$ by forming semiconducting mixed crystals with *narrow* band gaps composed of heavy elements. This approach has led to finding thermoelectric compounds based on Bi-Te alloys and Pb-Te alloys (Goldsmid and Douglas, 1954; A. V. Ioffe and A. F. Ioffe, 1954, 1956; Kanatzidis, 2010; LaLonde *et al.*, 2011; Sootsman *et al.*, 2009), which are in practical use at present, though the elements on the lower right of the periodic table are toxic to humans. Increasing interest in recent years in the recovery of waste heat has focused attention on earth and human friendly thermoelectric materials with improved efficiency.

Since Z of Eq. (1) contains the electrical conductivity σ in the numerator and the total thermal conductivity $\kappa_{\rm tot}$ in the denominator, high performance for thermoelectricity can be achieved for materials with the lowest possible thermal conductivity, the highest possible electrical conductivity and the highest possible Seebeck coefficient. According to those ideas, efficient thermoelectric effects should be achieved by materials possessing both glass-like phonon thermal conductivity and crystalline electrical conductivity. In this framework, Slack (1995) has proposed the important concept of "phonon-glass electron-crystal" for designing efficient thermoelectric materials. This is really a controversial concept from the aspect of materials science. If such materials can be synthesized, it truly becomes one of the most significant innovations in alternative energy technologies. Ioffe (1958b) noted in an article entitled "*The revival of thermoelectricity*" that "Evidently we stand on the threshold of a new era in power engineering, heating and refrigeration. This prospect flows from the now-rapid advance of thermoelectricity." We have reached a new stage of thermoelectricity since the concept of phonon-glass electron-crystal introduced (Slack, 1995).

General phenomena in thermoelectricity have been reviewed in a number of articles (Chen *et al.*, 2003; Dresselhaus and Thomas, 2001; Dresselhaus *et. al*, 2007; Goldsmid, 2010; Gonçalves and Godart, 2013; Koumoto *et al.*, 2006; LaLonde *et al.*, 2011; Mahan *et al.*, 1997; Mahan, 1998; Nolas *et al.*, 2001a,b; Rowe, 1995, 2003; Sales, 1998, 2002; Slack, 1995;

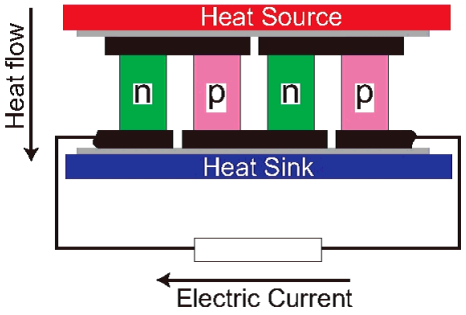

FIG. 1 (Color online) Thermoelectric devices contain many couples of n-type and p-type thermoelectric elements wired electrically in series and thermally in parallel.

Snyder and Toberer, 2008; Tritt, 2001).

B. The concept of "phonon-glass and electron-crystal" exploring efficient thermoelectric materials

The concept "phonon-glass electron-crystal" coined by Slack (1995) is actually a summary of ideas discussed by Ioffe in the 1950's (A. F. Ioffe, 1958a; Vedernikov and Iordanishvili, 1998). In general, glasses and amorphous materials, having no periodic arrangement of atoms, show the lowest thermal conductivities.

The concept has stimulated numerous attempts to search for efficient thermoelectric materials, and the first achievement was for skutterudite compounds (Nolas *et al.*, 1995, 1996; Sales *et al.*, 1996). The filled skutterudites are described with a chemical formula $\mathcal{R}_y\mathrm{T}_4\mathrm{X}_{12}$ ($0 \leq y \leq 1$), where $\mathcal{R}$ is a positive element of the lanthanides or actinides, or a group 1 or 2 element. The element T is a transition metal, and X is a pnictogen belonging to the group 15 elements (P, As, Sb). The crystal structure of skutterudite involves voids (or cages composed of $\mathrm{T}_8\mathrm{X}_{12}$) which are filled by $\mathcal{R}$ guests (Takabatake *et al.*, 2006). Because the radius of the $\mathcal{R}$ filler is significantly smaller than that of the voids, the fillers are trapped in largely anharmonic potentials and can vibrate with large amplitudes (Chakoumakos *et al.*, 1999).

Morelli *et al.* (1997) have reported the significant reduction in phonon thermal conductivity $\kappa_{\rm ph}$ of $\mathrm{Ce}_y\mathrm{Co}_4\mathrm{Sb}_{12}$ relative to unfilled skutterudite CoSb_3. It is remarkable that a small amount of Ce filler has a strong influence on the $\kappa_{\rm ph}$. The similar outcome was observed in La-filled skutterudite $\mathrm{La}_y\mathrm{Co}_4\mathrm{Sb}_{12}$ (Nolas *et al.*, 1998c). Furthermore, it has been revealed that all voids need not be occupied in order to achieve the maximum reduction in $\kappa_{\rm ph}$ (Tang *et al.*, 2001). For instance, the value of $\kappa_{\rm ph}$ of $\mathrm{Ce}_y\mathrm{Fe}_{4-x}\mathrm{Co}_x\mathrm{Sb}_{12}$ with y=0.7 has a minimum value lower than 2 $[\mathrm{Wm}^{-1}\mathrm{K}^{-1}]$ above room temperature (Uher, 2001).

The data strongly support that low phonon thermal conductivities $\kappa_{\rm ph}$ are obtained when guest atoms fill voids at random. At the same time, since electrical conduction is mainly due to the pnictogen orbitals in the group 15 elements, the carrier mobility remains large enough to maintain its crystalline character. Thus, in general, materials like skutterudites with voids, cavities, cages, and empty sublattices are thought to be favorable candidates for realizing the "phonon-glass electron-crystal" concept.

Following these works, Nolas *et al.* (1998a,b) demonstrated that type-I clathrate compounds have potential for use as high-efficiency thermoelectric materials. In fact, clathrate compounds belong to the category mentioned above. Highly efficient thermoelectric properties have been exhibited by these compounds encapsulating "rattlers". The terms "rattler" or "rattling" were introduced by Sales *et al.* (1997) for the atoms $\mathcal{R}$=La, Ce, Th in the filled skutterudite structure $\mathcal{R}_{1-y}\mathrm{Fe}_{4-x}\mathrm{Co}_x\mathrm{Sb}_{12}$ and Xe clathrate hydrates by Tse *et al.* (1997) which are weakly bound in an oversized atomic cage. Sales *et al.* (1997) have stated that rare earth elements, undergoing incoherent rattling motion in cages, lower the phonon thermal conductivity at room temperature down to a value comparable to that of vitreous silica. Tse *et al.* (1997) have noted that the coupling between guest modes and acoustic phonons arising from networked cages lead to the glass-like behavior in the thermal conductivity of clathrate hydrates.

The type-I clathrate compounds constitute networked cages consisting of nano-scale tetrakaidecahedrons with 14 flat faces (14 hedrons) and dodecahedrons with 12 flat faces (12 hedrons), in which the group 1 or 2 element in the periodic table can fill in the cages as the so-called "rattling" guest atom. We employ the term "guest" in this article, though some use "filler" instead. For $\mathcal{R}_8\mathrm{Ga}_{16}\mathrm{Ge}_{30}$ with the guest atom $\mathcal{R}$=Ba, Sr and Eu, Sales *et al.* (2001) have found, by means of neutron diffraction measurement, that the nuclear density of guest atoms Sr and Eu are distributed in off-center positions apart from a center of 14 hedrons, while Ba takes on-center position in 14 hedrons. Glass-like low phonon thermal conductivity has been realized in compounds with off-center guest atoms Sr and Eu, but not in those with on-center guest atom Ba. It is crucial, though scaffold networks take crystalline cubic-structure, that there emerge glass-like phonon thermal conductivities *depending on* the states of guest atoms in tetrakaidecahedrons.

II. BACKGROUND ON THERMOELECTRICITY

A. The Wiedemann-Franz law and the Lorenz number

Wiedemann and Franz (1853) found, when investigating the thermal conductivity $\kappa\,[\mathrm{W(mK)}^{-1}]$ and the electrical conductivity $\sigma\,[(\Omega\mathrm{m})^{-1}]$ of several metals, that the two quantities are linearly proportional to each other at

room temperature in the form

$$\kappa = \text{const.} \times \sigma. \tag{2}$$

This relation indicates that electric and thermal conductions are definitely correlated. 20 years later, L. V. Lorenz (1872) found, from the data of the temperature dependence of Eq. (2), the ratio is also proportional to the absolute temperature T as

$$\kappa = LT\sigma, \tag{3}$$

where L is a proportionality constant termed the Lorenz number. This relation is generally called the Wiedemann-Franz law or the Wiedemann-Franz-Lorenz law.

The first theoretical derivation of the Lorenz number was made by Sommerfeld (1927, 1928) using the Fermi-Dirac distribution function of degenerate metals, which provides

$$L_0 = \frac{\pi^2}{3}\left(\frac{k_\mathrm{B}}{e}\right)^2 = 2.44 \times 10^{-8}\,[\mathrm{W\Omega K^{-2}}], \tag{4}$$

where k_B is the Boltzmann constant, and e the electron charge. The L_0 defined via universal constants is called the Sommerfeld value of the Lorenz number. This relation can be simply derived from the free electron model. The expression of the conductivity σ is

$$\sigma = \frac{ne^2\tau_\mathrm{el}}{m_\mathrm{e}^*}, \tag{5}$$

where τ_el is the average collision time of the electrons, n the number of electrons per volume at the Fermi energy, and m_e^* is the effective mass of an electron. The electronic contribution to the thermal conductivity κ_el is expressed in the same way by the relation

$$\kappa_\mathrm{el} = \frac{1}{3}C_\mathrm{el}v_\mathrm{F}\ell_\mathrm{el} = \frac{\pi^2 n k_\mathrm{B}^2 T\tau_\mathrm{el}}{3m_\mathrm{e}^*}, \tag{6}$$

where C_el is the specific heat of the electrons, v_F the Fermi velocity, and ℓ_el the mean free path of the electrons.

The ratio of Eqs. (5) and (6) provides

$$\frac{\kappa_\mathrm{el}}{\sigma} = \frac{\pi^2}{3}\left(\frac{k_\mathrm{B}}{e}\right)^2 T = L_0 T, \tag{7}$$

where the collision time τ_el is canceled out. The mean free path ℓ_el is reduced by collision with impurities and phonons in impure metals or in disordered alloys or semiconductors. Note that Eq. (7) has been obtained from the average collision-time approximation for free electrons in addition to the assumption that only electrons carry heat.

The Wiedemann-Franz law is valid for the cases that the elastic scattering of electrons dominates. The Wiedemann-Franz law holds, to a good approximation, at low temperatures where the elastic scattering by impurities or defects is relevant and at high temperatures where the change in energy of each electron scattered by electron-electron or electron-phonon interactions is negligible compared with the energy scale $k_\mathrm{B}T$. At intermediate temperatures 10-200 [K], electronic energy-loss becomes of the order of $k_\mathrm{B}T$ and Eq. (7) is no longer valid. See, for example, Ashcroft and Mermin (1976) on the detailed arguments beyond the relaxation-time approximation for electron transport relevant to the Wiedemann-Franz law.

It had been already pointed out by Lorenz (1881a,b) that L is not a universal factor, but depends on the kind of metal. The actual values of the Lorenz number L are given, for example, in Kaye and Laby (1966) and Kumar *et al.* (1993) for elemental metals, semi-metals, metallic alloys and compounds, and degenerate semiconductors. These provide L=2.3−2.6×10^{-8} [WΩK^{-2}] close to the Sommerfeld value L_0 for almost all elemental metals and smaller values L=1.7−2.5×10^{-8} [WΩK^{-2}] in degenerate semiconductors. In contrast, the Lorenz numbers of transition metals deviate considerably from the Sommerfeld value (Chari and Chari, 1989, 1990a).

The experimental values of the thermal conductivity κ in Eq. (3) is the total thermal conductivity κ_tot including the phonon contribution to heat transport. The phonon component of the thermal conductivity κ_ph can be estimated by subtracting the electric component κ_el from the measured total thermal conductivity κ_tot. Suppression of the electronic contribution to the thermal conductivity, and hence the separation of the phonon and electronic parts of conductivity can be achieved by applying a transverse magnetic field.

In the presence of a magnetic field, the Lorenz number varies with it. In this connection, we should mention the Nernst-Ettingshausen effect (Ettingshausen and Nernst, 1886). This is a thermomagnetic phenomenon where an electric current is generated perpendicular to an applied magnetic field and a temperature gradient. This was discovered by Etttingshausen and his student Nernst in 1886 when heating one side of the sample during the investigation of the Hall effect in bismuth. The reverse effect is called the Ettingshausen effect in which a temperature gradient appears when applying a current and a magnetic field. There is a close correspondence between the expressions on cooling power and the coefficient of performance obtained by using Ettingshausen and Peltier effects (O'Brien and Wallace, 1958). The Ettingshausen refrigerator requires only one material, so the issue of matching n-type and p-type transport does not arise. Detailed discussions about the Ettingshausen effect are given, for example, in Nolas *et al.* (2001a).

B. Heat and electric transport as irreversible processes

1. Peltier and Seebeck coefficients

The Onsager reciprocal relations express the equality of certain ratios between generalized fluxes and forces

based on the principle of detailed balance when a notion of local equilibrium is applicable. The thermoelectric effects discussed here deal with the relations between two kinds of flux (the heat flux density $\boldsymbol{Q}$ and the particle flux density $\boldsymbol{J}$), which are associated with two kinds of generalized forces (the gradient of the inverse of temperature $\nabla(1/T)$ and the gradient of electrochemical potential $\nabla\mu$). Callen (1948, 1952) have developed a general argument of the application of Onsager's theory to thermoelectric phenomena. The relations given by Callen (1948) are expressed in the form of linear combinations among the generalized fluxes and forces,

$$-\boldsymbol{J} = L_{11}\tfrac{1}{T}\nabla\mu + L_{12}\nabla\left(\tfrac{1}{T}\right), \tag{8}$$

$$\boldsymbol{Q} = L_{21}\tfrac{1}{T}\nabla\mu + L_{22}\nabla\left(\tfrac{1}{T}\right), \tag{9}$$

where μ is the electrochemical potential composed of both a chemical potential μ_C and an electrical one μ_E with $\mu = \mu_C + \mu_E$. For the charge e of a particle, $\mu_E = e\phi$, where ϕ is the electrostatic potential. The chemical potential μ_C is a function of the temperature T and the particle density n, and the $\nabla\mu_C$ plays a minor role in electrical conductors. The Onsager reciprocal relation (Onsager, 1931) states that

$$L_{12} = L_{21}. \tag{10}$$

Provided that an applied magnetic field $\boldsymbol{H}$ exists, this relation becomes $L_{ij}(\boldsymbol{H}) = L_{ji}(-\boldsymbol{H})$.

The kinetic coefficients L_{ij} are closely related to the electrical $\sigma\,[(\Omega\mathrm{m})^{-1}]$ and thermal conductivity $\kappa\,[\mathrm{W(Km)}^{-1}]$ as seen by expressing Eqs. (8) and (9) in terms of σ ad κ. Here σ is defined as the electrical current density $\boldsymbol{j} = e\boldsymbol{J}$ per unit electric field $\boldsymbol{E} = -\nabla\mu_E/e$ in an isothermal system, which provides

$$\sigma = \frac{\boldsymbol{j}}{\boldsymbol{E}} = -\frac{\boldsymbol{j}}{\nabla\mu_E/e}, \quad \text{for} \quad \nabla T = 0. \tag{11}$$

Substituting Eq. (11) into Eq. (8), we have the relation

$$\sigma = \frac{e^2 L_{11}}{T}. \tag{12}$$

The thermal conductivity κ is the heat current $\boldsymbol{Q}$ per unit temperature gradient given by

$$\kappa = -\frac{\boldsymbol{Q}}{\nabla T}, \quad \text{for} \quad \boldsymbol{j} = 0. \tag{13}$$

The above can be related to the kinetic coefficient L_{ij} using Eqs. (8) and (9), which is written down as

$$\kappa = \frac{L_{11}L_{22} - L_{12}^2}{T^2 L_{11}}. \tag{14}$$

The Seebeck effect implies the temperature gradient ∇T yields the electric field $\boldsymbol{E}'$ in a system. This is expressed as $\boldsymbol{E}' = -S\nabla T$, where $S[\mathrm{V/K}]$ is called the Seebeck coefficient or the thermoelectric power of a medium. The use of S enables us to rewrite Eqs. (8) and (9) in terms of the electric field $\boldsymbol{E}\,[\mathrm{V/m}]$ and the temperature gradient $\nabla T\,[\mathrm{K/m}]$ as

$$\boldsymbol{j} = \sigma\left(\boldsymbol{E} - S\nabla T\right), \tag{15}$$

$$\boldsymbol{Q} = \sigma S T\boldsymbol{E} - \kappa\nabla T, \tag{16}$$

where $S = -eL_{12}/(\sigma T^2)$.

Equations (15) and (16) recover the Onsager reciprocal relation $L_{12} = L_{21} = -T^2\sigma S/e$. From Eqs. (15) and (16) with $\nabla T = 0$, the Peltier coefficient Π is defined by

$$\boldsymbol{Q} = TS\boldsymbol{j} \quad \longrightarrow \quad S = \frac{\Pi}{T}. \tag{17}$$

Thus, the Peltier and the Seebeck effects are essentially the same in thermoelectrics. The Peltier coefficient has a simple physical meaning of the energy carried by charged particles per unit charge.

The Seebeck coefficient S becomes negative for electron carriers such as the case of n-type semiconductors, and positive for hole carriers in p-type semiconductors.

2. Figure of merit

The direct expression of the heat current $\boldsymbol{Q}$ driven by an electrical current $\boldsymbol{j}$ and the temperature gradient ∇T is obtained from Eqs. (15) and (16). This yields

$$\boldsymbol{Q} = ST\boldsymbol{j} - \kappa_{\mathrm{tot}}\nabla T, \quad \text{with } \kappa_{\mathrm{tot}} \equiv \kappa\left(1 - Z'T\right), \tag{18}$$

where $Z' \equiv \sigma S^2/\kappa$. Since κ_{tot} is a positive quantity, Z' is bounded by the inequality $Z'T < 1$ as seen from Eq. (18).

Instead of Z', let us introduce the quantity called the material's figure of merit defined by (Mahan, 1998)

$$Z = \frac{\sigma S^2}{\kappa_{\mathrm{tot}}} = \frac{Z'}{1 - Z'T}, \tag{19}$$

where Z has the dimension of inverse temperature, so the efficiency of thermoelectric conversion is alternatively defined by the dimension-less parameter ZT termed "dimensionless figure of merit", which is given by

$$ZT = \frac{S^2\sigma T}{\kappa_{\mathrm{eh}} + \kappa_{\mathrm{ph}}}. \tag{20}$$

Here $\kappa_{\mathrm{tot}} = \kappa_{\mathrm{ph}} + \kappa_{\mathrm{eh}}$ is the total thermal conductivity composed of the phonon part κ_{ph} and the electronic part κ_{eh}. We use the notation of κ_{eh} expressing hole or electron carriers in semiconductors. When electron-hole pairs are present at temperatures comparable to the gap energy, a bipolar term contributing to the electric thermal conductivity should be taken into account. See, for example, Yang (2004).

The Carnot limit (also known as the Carnot efficiency) specifies limits on the maximum efficiency that any heat engine can obtain. The Carnot limit solely depends on the temperature difference between the hot (T_{H}) and cold (T_{C}) temperature reservoirs. It is clear that the hotter

the heat source, the higher the possible efficiency. The maximum efficiency $\eta_{\rm Carnot}$ is given by the dimensionless ratio between the temperature difference $\Delta T = T_{\rm H} - T_{\rm C}$ and $T_{\rm H}$. The formula for the actual efficiency η of a thermoelectric generator is expressed by using $\eta_{\rm Carnot}$ as (Goldsmid, 2010)

$$\eta = \eta_{\rm Carnot} \frac{\sqrt{1+ZT}-1}{\sqrt{1+ZT}+T_{\rm C}/T_{\rm H}}. \tag{21}$$

Thus the performance of thermoelectric materials is characterized by ZT determined by three parameters: the Seebeck coefficient $S\,[{\rm V/K}]$, the electrical conductivity $\sigma\,[(\Omega{\rm m})^{-1}]$, and the thermal conductivity $\kappa\,[{\rm W(Km)}^{-1}]$. Since it is required for efficient η to take values above around 10% at the temperature difference of 300 [K], thermoelectric materials satisfying the relation $ZT >1$ are thought to be especially efficient in practical applications.

3. The Mott formula for the Seebeck coefficient

In three dimensional systems, the x-component of the electric current density j_x and the electric heat flux density Q_x under the electric field F_x can be expressed in terms of the electron mobility $\mu(E)$ of the charge $-e<0$ as

$$j_x = eF_x \int \mu(E) f\,(1-f)\,N(E) dE, \tag{22}$$

$$Q_x = -F_x \int \mu(E)\,(E-\zeta)\,f\,(1-f)\,N(E) dE, \tag{23}$$

where $N(E)$ is the electron density of states, ζ the chemical potential, and $f(E)$ the Fermi-Dirac distribution function. Equation (22) provides the conductivity expressed by an integral over the single electron states (Fritzsche, 1971)

$$\sigma = e \int \mu(E) f\,(1-f)\,N(E) dE \equiv \int \sigma(E) dE, \tag{24}$$

where $\sigma(E)dE$ is the conductivity in the energy interval between E and $E+dE$.

The product of the Peltier coefficient Π and the conductivity σ is obtained by differentiating Eq. (23) with respect to the electric field F_x. The Seebeck coefficient is obtained from Eqs. (16) and (23) in comparison,

$$S(T) = -\frac{k_{\rm B}}{e} \int \left(\frac{E-\zeta}{k_{\rm B}T}\right) \frac{\sigma(E)}{\sigma} dE. \tag{25}$$

This yields $S<0$ for electrons, and $S>0$ for holes taking account of the signs of $-e$.

We can set $f(1-f) = -k_{\rm B}T\partial f/dE$ when only states near the Fermi energy $E_{\rm F}$ contribute to the conductivity. By expanding $\sigma(E)$ defined in Eq. (24) around $E=E_{\rm F}$ up to the order $(k_{\rm B}T/E_{\rm F})^2$, we have the convenient expression of the Seebeck coefficient from Eq. (25) of the form

$$S(T) \cong -\frac{\pi^2 k_{\rm B}^2 T}{3e} \left[\frac{\partial {\rm ln}\sigma(E)}{\partial E}\right]_{E=E_{\rm F}}. \tag{26}$$

This is the Mott formula (Mott and Jones, 1936), showing that the Seebeck coefficient S is proportional to the logarithmic derivative of $\sigma(E)$ or $\mu(E)N(E)$ with respect to the energy at $E=E_{\rm F}$.

The Mott formula can be applied not only to monovalent metals, but also to other metals or degenerate semiconductors. It is valid even for alloys at temperatures above the Debye temperature $\theta_{\rm D}$, and at low temperatures as long as the residual resistivity is large compared with the resistivity due to phonon scattering, in addition to doped semiconductors exhibiting the metal-insulator Anderson transition (Cutler and Mott, 1969). Since the Mott relation is correct only to second order in $k_{\rm B}T/\zeta$, it is not applicable to transition metals with narrow bands and at high temperatures (Chari and Chari, 1989, 1990a). Kirchner *et al.* (2013) have theoretically discussed the effect of nonlinear thermoelectric response for systems with narrow band structures.

Equation (25) shows that the Seebeck coefficient $|S|$ is proportional to the resistivity $\rho = 1/\sigma$ and the energy difference $E-\zeta$ from the chemical potential. This indicates that heavily-doped degenerate semiconductors are suitable for increasing $|S|$. Equation (26) in the degenerate limit yields, for example, from the definitions $\mu(E) \propto E^{\alpha}$, with α characterizing the scattering mechanisms, and the energy dependence of the electron density of states $N(E) \propto E^{3/2}$,

$$S \cong -\frac{\pi^2 k_{\rm B}^2 T}{3eE_{\rm F}} (\alpha + 1.5), \tag{27}$$

where α=−0.5 for scattering by acoustic phonons and α=1.5 for ionized impurity scattering. The actual evaluation of the above equation gives $S \cong -2.44\times10^{-2} T\,(\alpha+1.5)\,/E_{\rm F}[{\rm eV}]$ in units of [μV/K]. This is a measure of the Fermi energy $E_{\rm F}$.

The discussion given above has been focused on degenerate electrons. In semiconductors, the Fermi level lies in the gap and there exist positively charged holes. These positive carriers contribute to the transport in addition to negatively charged electrons. One needs to assign different time-scales to electrons and holes depending on the band index (Nolas *et al.*, 2001b; Yang, 2004).

III. CRYSTAL STRUCTURES OF TYPE-I CLATHRATE COMPOUNDS

A. Various types of clathrate compounds

1. Classification of clathrate compounds

Clathrates or clathrate compounds consist of regular lattices of cages in which guest atoms or molecules are

encapsulated. Cages with restricted geometry form the basic framework of a lattice with translational invariance. Clathrates are also called host-guest complexes. Typical examples of host-guest complexes are inclusion compounds and intercalation compounds. Gas hydrate is a special type of clathrate compound consisting of water molecules and gas molecules. The history of gas hydrates can be traced back to the work of 200 years ago by Davy (1811a,b), who discovered chlorine hydrate in the combination of water host molecule (H_2O) and guest chlorine molecule (Cl_2) when pressurizing water with chlorine gas below 9 °C. Davy and his assistant Michael Faraday continued the research on chlorine hydrate at the Royal Institution of London from 1813. Faraday (1823) determined the composition of chlorine clathrate hydrate of nearly 1 part of Cl_2 and 10 parts of H_2O molecules.

The water molecule H_2O forms a variety of cages different in size and in geometrical structure. Typical examples of hydrate-forming substances include CH, CO, and HS molecules. The terms "gas hydrate" and "clathrate hydrates" have been used for these solids (Davidson, 1973). Oxygen atoms forming a cage are tetrahedrally connected by hydrogen bonds, which make cages with open space for guest atoms/molecules. In the early stages of this research, the vast majority of clathrate hydrates had been classified into two types, which are type-I and type-II belonging to the cubic space groups $Pm\bar{3}n$ and $Fd\bar{3}m$, respectively (Claussen, 1951a,b,c; Müller and von Stackelberg, 1952; Pauling and Marsh, 1952; von Stackelberg and Müller, 1951a,b). Jeffrey (1984) has classified clathrate hydrates into seven types by introducing five further types of clathrate hydrates in addition to type-I and -II structures. Crystal structures of type-III, -VIII, and -IX in addition to type-I and -II are shown in Fig. 2.

The unit cell of the type-I structure consists of 46 water molecules which form two types of small and large cages. The small cages in the unit cell are two against six large ones. The small cage has the shape of a pentagonal dodecahedron (5^{12}), and the large one that of a tetrakaidecahedron ($5^{12}6^2$), as given in Fig. 2. Typical guests in type-I clathrate hydrates are CO_2 in carbon dioxide hydrate and CH_4 in methane hydrate. Methane hydrates have attracted much interest as a possible new energy source, in which large amounts of methane gas are contained both in permafrost formations and under the ocean seabed (Englezos, 1993; Hester and Brewer, 2009). Hydrogen storage in clathrates is expected to have potentially important energy applications (Struzhkin *et al.*, 2007).

The unit cell of type-II clathrate hydrates consists of 136 water molecules, forming also small and large cages. The small cages in the unit cell are sixteen against eight large ones. The small cage is again a pentagonal dodecahedron (5^{12}), but the large one is a hexakaidecahedron ($5^{12}6^4$). Type-II hydrates contain larger molecules like CCl_4 and SF_6 than in type-I hydrates.

The compositions of the type-I and II hydrates are expressed as $2D{\cdot}6T{\cdot}46H_2O$ and $16D{\cdot}8H{\cdot}136H_2O$, respectively, where D, T, and H represent, respectively, the guest atoms/molecules in a cage of pentagonal dodecahedron, tetrakaidecahedron, and hexakaidecahedron composed of water molecules.

2. Intermetallic clathrate compounds

Intermetallic clathrates are inorganic inclusion compounds structurally related to the hydrates (Rogl, 2006). The clathrates composed of the group 14 elements were discovered as prospective thermoelectric materials which realize the "phonon-glass electron-crystal" concept (Blake *et al.*, 1999; Iversen *et al.*, 2000; Nolas *et al.*, 1998b; Slack, 1995). The group 14 clathrates have been intensively investigated because of their high potential for converting temperature differences to electric energy (Christensen *et al.*, 2006c; Kleinke, 2010; Kuznetsov *et al.*, 2000; Saramat *et al.*, 2006; Sootsman *et al.*, 2009).

Frameworks of the group 14 clathrate compounds are constructed from face-sharing polyhedron. Five structures given in Fig. 2 are known as type-I ($2D{\cdot}6T{\cdot}46F$), type-II ($16D{\cdot}8H{\cdot}136F$), type-III ($10D{\cdot}16T{\cdot}4P{\cdot}172F$), type-VIII ($8D'{\cdot}46F$), and type-IX ($8D{\cdot}12O{\cdot}4C{\cdot}100F$) (Karttunen *et al.*, 2011; Mudryk *et al.*, 2002; Rogl, 2006). Here P, D′, O, and C express guests in pentakaidecahedron, distorted dodecahedron, open cage, and distorted cube, respectively, and F means a framework (cage) atom. D, T, and H are defined in the previous paragraph. The type-VIII and IX have no representatives among hydrate structures.

A silicon clathrate, for example, is formed by the covalently bonded Si atoms. Thereby, Si atoms and sp^3 hybridized orbital electrons play roles of O atoms and H atoms in clathrate hydrates due to their tetrahedral coordination and hydrogen bonding by "ice rules" (Bernal and Fowler, 1933; Pauling, 1948). Kasper *et al.* (1965) discovered the first silicon clathrates, type-I Na_8Si_{46} and type-II Na_xSi_{136}, where cationic Na guests are enclosed in the silicon framework. The synthesis of Ge- and Sn-based type-I clathrates with alkali metal atoms as guests was reported by Gallmeier *et al.* (1969).

Ternary type-I clathrates $\mathcal{R}_8M_{16}Z_{30}$, where $\mathcal{R}$ belongs to the group 2, M the group 13, and Z the group 14 elements, respectively, were first synthesized by Eisenmann *et al.* (1986). The $\mathcal{R}$ guest atom is encapsulated by the cage formed by M and Z elements. The combination of M and Z elements makes it possible to tune the size of cages. When the cage has a large open-space, the encapsulated guest atoms are weakly bounded to the cage. Such a loosely bound guest is referred to as a "rattler" (Sales *et al.*, 1997). The present article is concerned with type-I $\mathcal{R}_8M_{16}Z_{30}$ clathrate with potential application to efficient thermoelectric materials.

Structural and thermoelectric properties for var-

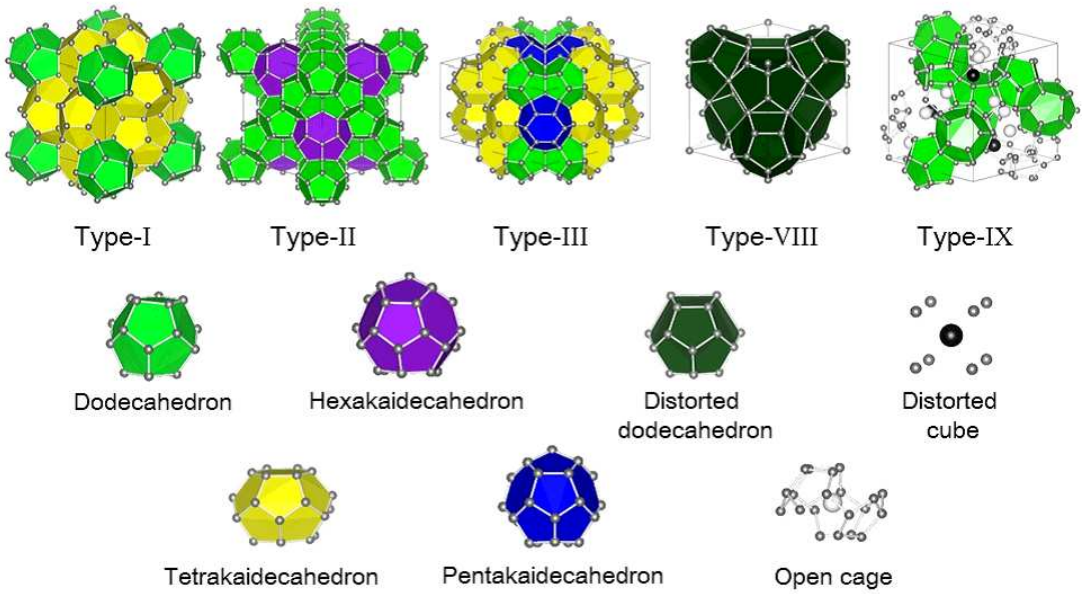

FIG. 2 (Color online) Crystal structure of type-I, type-Ⅱ, type-Ⅲ, type-Ⅷ, and type-Ⅸ intermetallic clathrates.

ious types of intermetallic clathrates, including type-Ⅱ and type-Ⅲ clathrates, have been treated in the following works: type-I $\mathcal{R}'_8M_8Z_{38}$ with alkali metal guest $\mathcal{R}'_8$ (Bobev and Sevov, 2000; Hayashi *et al.*, 2010; Myles *et al.*, 2001; Nolas *et al.*, 2000; Tanaka *et al.*, 2010); type-I with transition metal element as cage atom (Akai *et al.*, 2005; Anno *et al.*, 2003; Christensen *et al.*, 2009, 2010; Johnsen *et al.*, 2007; Melnychenko-Koblyuk *et al.*, 2009a; Nasir *et al.*, 2010; Nguyen *et al.*, 2010; Xu *et al.*, 2012; Zhang *et al.*, 2011); type-I mainly constructed from the group 15 elements (As and Sb) (He *et al.*, 2012; Liu *et al.*, 2009); type-Ⅱ (Beekman and Nolas, 2008; Beekman *et al.*, 2010; Kasper *et al.*, 1965), type-Ⅲ (Bobev and Sevov, 2001; Zaikina *et al.*, 2008, 2010), and type-Ⅸ clathrates (Carrillo-Cabrera *et al.*, 2000; Fukuoka *et al.*, 2000; Kim *et al.*, 2000, 2007a,b; Kröner *et al.*, 1988; Paschen *et al.*, 2002; Rachi *et al.*, 2005); "inverse clathrates" with halogen/tellurium guests (Falmbigl and Rogl, 2012r; Kishimoto *et al.*, 2006, 2007; Menke and von Schnering, 1973; Zaikina *et al.*, 2010).

3. Crystal chemistry of type-I clathrate

Among various types of intermetallic clathrate compounds, the type-I structure of $\mathcal{R}_8M_{16}Z_{30}$ and $\mathcal{R}'_8M_8Z_{38}$ stoichiometry has been mostly adopted, where $\mathcal{R}$ is a guest atom of the group 2 (Ba, Sr) or a divalent rare-earth element (Eu), and $\mathcal{R}'$ a group 1 element (Na, K, Rb, and Cs). The cage constituents M and Z are the elements of the group 13 (Al, Ga, and In) and the group 14 (Si, Ge, and Sn), respectively (Bobev and Sevov, 2000; Eisenmann *et al.*, 1986) It should be noted that only $Ba_8Ga_{16}Sn_{30}$ and $Eu_8Ga_{16}Ge_{30}$ are known to form the type-Ⅷ structure with the same composition as the type-I (Carrillo-Cabrera *et al.*, 2002; Eisenmann *et al.*, 1986; Leoni *et al.*, 2003; Paschen *et al.*, 2001; von Schnering *et al.*, 1998). Large single crystals of type-I and type-Ⅷ $Ba_8Ga_{16}Sn_{30}$, which are shown in Fig. 3, were grown by a flux method using excess amounts of Ga and Sn (Suekuni *et al.*, 2008a). The type-Ⅷ structure can be formed in alloyed compounds $Sr_8Al_xGa_{16-x}Si_{30}$ ($8 \leq x \leq 13$) and $Sr_8Al_xGa_yGe_{46-x-y}$ ($6 \leq x \leq 7$ and $10 \leq y \leq 11$) (Kishimoto *et al.*, 2008; Sasaki *et al.*, 2009;

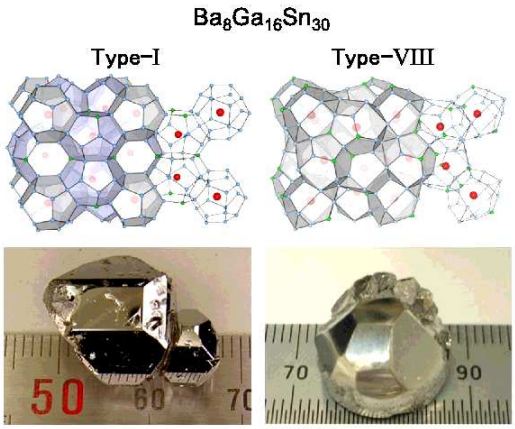

FIG. 3 (Color online) Crystal structures and single crystals of type-I and type-Ⅷ $Ba_8Ga_{16}Sn_{30}$. The units of rulers are given in millimeter. After the work of Suekuni *et al.* (2008a)

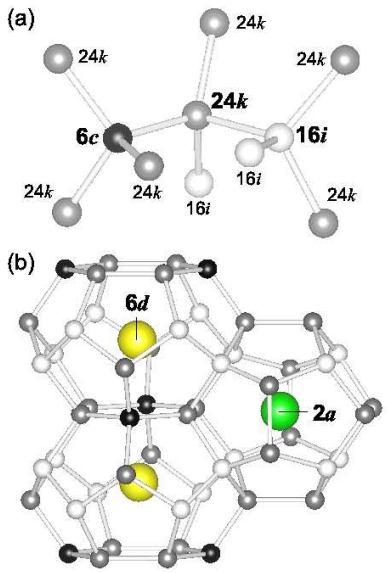

FIG. 4 (Color online) (a) Tetrahedral bonds of framework atoms, and (b) guests in dodecahedral and tetrakaidecahedral cages for type-I clathrates.

Shimizu *et al.*, 2009b). This structure is cubic (space group No.217; $I\bar{4}3m$) and the unit cell consists of eight distorted dodecahedra, as shown in Fig. 2. Aspects of the chemistry and synthesis of intermetallic clathrates have been reported in review articles (Kovnir and Shevelkov, 2004; Shevelkov and Kovnir, 2011).

Most of the type-I and the type-VIII clathrates follow the so-called Zintl concept (Paschen *et al.*, 2003; Rodriguez *et al.*, 2010; Shevelkov and Kovnir, 2011; Toberer *et al.*, 2010). In a Zintl compound, each constituent attains a closed valence shell by combining a formal charge transfer with covalent bonds. In intermetallic clathrate compounds, the cage atom Z is partially substituted by the acceptor atoms M for charge compensation between the guest and the cage. Consequently, the cage atoms are tetrahedrally bonded by a sp^3 hybridized orbital as shown in Fig. 4.

In the type-I structure the guests occupy two sites as shown in Fig. 4(b): the 2*a* site in the dodecahedron and the 6*d* site in the tetrakaidecahedron. The cage atoms M and Z in type-I $\mathcal{R}_8M_{16}Z_{30}$ and $\mathcal{R}'_8M_8Z_{38}$ occupy three crystallographic sites 6*c*, 16*i*, and 24*k* sites. The 6*c* site is bound to four 24*k* sites; the 16*i* site, to three 24*k* sites and one 16*i* site; the 24*k* sites, to one 6*c* site, two 16*i* sites, and one 24*k* site. Note that there are no equivalent positions around the 6*c* site. The M and Z atoms do not order in the host framework, but are distributed by a certain rule (see below). First-principles calculations by Blake *et al.* (1999, 2001) and Gatti *et al.* (2003) have suggested that the M atoms in $\mathcal{R}_8M_{16}Z_{30}$ preferentially occupy the 6*c* site which does not have adjoining equivalent sites. This is because the bonds between M atoms are energetically unfavorable. In fact, as described in the next subsection, the preferential occupation of the M atom at 6*c* sites was experimentally proved from analysis of x-ray and neutron diffraction experiments (Bentien *et al.*, 2005; Christensen *et al.*, 2006a, 2007, 2010; Eisenmann *et al.*, 1986; Zhang *et al.*, 2002). For type-I $Ba_8Ga_{16}Sn_{30}$, extended x-ray absorption fine-structure (EXAFS) analyses have shown that the Ga-Ga bond is unfavorable; only 15% of the Ga nearest neighbors are Ga (Kozina *et al.*, 2009).

First-principles calculations have pointed out that type-I clathrates with $\mathcal{R}_8M_{16}Z_{30}$ stoichiometry have a semiconducting electronic structure (Akai *et al.*, 2009; Blake *et al.*, 1999, 2001; Kono *et al.*, 2010; Madsen *et al.*, 2003; Nenghabi and Myles, 2008; Uemura *et al.*, 2008). Despite the balanced electron count $[\mathcal{R}^{2+}]_8[M^{1-}]_{16}[Z^0]_{30}$, these compounds often behave like a metal or a doped semiconductor in their electrical conduction. This is attributed to a minor off-stoichiometry: $[\mathcal{R}^{2+}]_8[M^{1-}]_{16+x}[Z^0]_{30-x}$ and/or vacancy formation on the cage sites. It is crucial for efficient thermoelectric materials that the carrier type and the carrier density can be tuned by adjusting x in $\mathcal{R}_8M_{16+x}Z_{30-x}$. For instance, in type-I $Ba_8Ga_{16+x}Ge_{30-x}$, a positive value of x yields p-type conduction and negative x leads to n-type (Anno *et al.*, 2002, 2003; Avila *et al.*, 2006a,b; Tang *et al.*, 2010b). A tunable carrier type in one compound has the advantage of the possibility of constructing a thermoelectric module using p- and n-type legs.

B. On-center and off-center positions of guest atoms in type-I clathrate compounds

1. X-ray and neutron diffractions and EXAFS

This subsection describes the atomic configuration in type-I clathrate compounds determined by means of x-ray diffraction (Bentien *et al.*, 2005; Christensen *et al.*, 2006a, 2010; Nolas *et al.*, 2000), neutron diffraction (Chakoumakos *et al.*, 2000, 2001; Christensen *et al.*, 2006a, 2010; Sales *et al.*, 2001), and extended x-ray absorption fine-structure (EXAFS) (Baumbach *et al.*, 2005; Jiang *et al.*, 2008; Kozina *et al.*, 2009; Mansour *et al.*, 2012).

In type-I clathrates, the guest sites in the dodecahedron and tetrakaidecahedron are denoted by guest (1) and (2) sites, respectively. Chakoumakos *et al.* (2000) have investigated the vibrational characteristics of Sr(2) guest-atom encaged in type-I $Sr_8Ga_{16}Ge_{30}$ in terms of neutron diffraction at room temperature, claiming that the isotropic atomic displacement parameter (ADP) for Sr(2) is enormous. Taking into account the anisotropic displacement, the vibrations of Sr(2) show a large ADP in the plane parallel to the six-member ring cage. These results suggest that the site of Sr(2) could be equally described by a fractionally occupied four-fold split-site. In fact, the differential Fourier map around the cage center 6*d* site shows a residual nuclear density with lobes in the directions of the split positions 24*k*. Following the

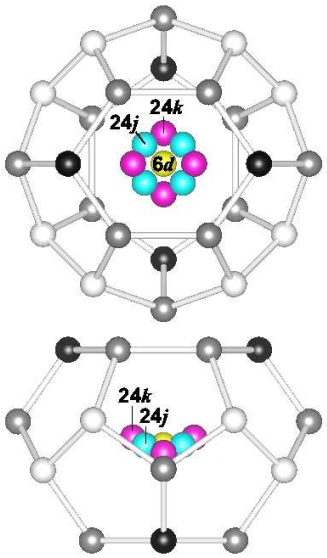

FIG. 5 (Color online) Split $24j$ and $24k$ sites for guest (2) atoms around $6d$ sites in tetrakaidecahedral cages for type-I clathrate.

above work, Sales *et al.* (2001) and Chakoumakos *et al.* (2001) have performed a neutron diffraction study on single crystals of type-I $\mathcal{R}_8Ga_{16}Ge_{30}$ ($\mathcal{R}$=Ba, Sr, Eu). Difference Fourier maps suggest that the nuclear density of Ba(2) is centered at the cage center, while those of Sr(2) and Eu(2) move off to one of four off-center sites $24k$, 0.3 Å and 0.4 Å away from the cage center, respectively. Refinements result in similar residual factors for two models with a four split site on $24k$ and $24j$, as shown in Fig. 5. Therefore, the disorder of the guest position is more complex than the case of just four sites. In fact, Fujiwara *et al.* (2012) have reported that the Sr(2) are widely distributed to $24k$ and $24j$ sites.

By combining x-ray and neutron diffraction methods, Christensen *et al.* (2006a, 2010) have revealed that the Ba(2) guests in *n*- and *p*-type $Ba_8Ga_{16}Ge_{30}$ also occupy slightly off-center sites $24k$ or $24j$. A more definite off-center $24k$ site for Ba(2) situated 0.43 Å away from the center was found in type-I $Ba_8Ga_{16}Sn_{30}$ (β-BGS), where the cage size is larger by 8 % than that of $Ba_8Ga_{16}Ge_{30}$. The off-center displacement of 0.43 Å is comparable to that of Eu(2) (Avila *et al.*, 2008; Suekuni *et al.*, 2008a).

EXAFS has also been employed to investigate the rattling sites of the guests in $\mathcal{R}_8Ga_{16}Ge_{30}$ ($\mathcal{R}$=Ba, Sr, Eu) (Baumbach *et al.*, 2005; Jiang *et al.*, 2008; Mansour *et al.*, 2012). The analysis has confirmed that Eu(1) is located at the center $2a$ sites, but Eu(2) is located an off-center site 0.445 Å away from the center of the cage. For $\mathcal{R}$=Sr, ∼75% of Sr(2) atoms take off-center sites 0.40 Å away from the center and the rest reside at the center. The results of EXAFS were in reasonable agreement with those of x-ray and neutron diffraction. Furthermore, the analysis for $\mathcal{R}$=Ba indicates a somewhat off-center site for Ba(2).

To summarize, it has been revealed that the degree of off-center displacement of the guest(2) atoms primarily depends on the relative size of the cage to that of the guest atom. Actually, neutron diffraction experiments have shown that the guest(2) atoms occupy four off-center positions away from the center of the cages when the size of the cage is large enough, or equivalently, the ionic radius of the guest atom is small enough (Sales *et al.*, 2001).

Table I gives the sets of the data obtained from various types of experimental methods on characteristic properties of type-I and type-VIII $\mathcal{R}_8M_{16}Z_{30}$. This is useful for the purpose of overviewing the characteristics of actual clathrate compounds.

Table 1: Key properties of type-I and type-VIII clathrates $\mathcal{R}_8M_{16}Z_{30}$. The samples are in the forms of poly-crystallines, powders, or single crystals. Listed are carrier types *n* or *p*, $\kappa_{ph}(T)$, on- or off-center state of the guest atom $\mathcal{R}(2)$, and two characteristic temperatures θ of $\mathcal{R}(2)$. Features of $\kappa_{ph}(T)$ are denoted by C: crystalline or G: glass-like. The exponents of the temperature dependence of $\kappa_{ph}(T)$ below 1 [K] are given for single crystals. The states of guest atom $\mathcal{R}(2)$, on- or off-center, have been judged by various experiments; x-ray diffraction (XRD), neutron diffraction (ND), resonant x-ray diffraction (RXD), extended x-ray absorption fine structure spectroscopy (EXAFS), resonant ultrasound spectroscopy (RUS), Mössbauer spectroscopy (Mössbauer), microwave absorption spectroscopy (MW), specific heat (SH), electrical resistivity (ER), Raman scattering (Raman), THz spectroscopy (THz), inelastic neutron diffraction (INS), and nuclear inelastic scattering (NIS). Two characteristic temperatures θ on $\mathcal{R}(2)$ correspond to vibrational modes in out-of-the plane/on-the-plane perpendicular to the four-fold axis of the tetrakaidecahedron. Single or non-separated values denote the cases not distinguished or assumed off-center $24k$ or $24j$ sites. The values in parentheses may include the components of $\mathcal{R}(1)$ in the dodecahedron in addition to $\mathcal{R}(2)$. For type-VIII clathrates, the characteristic temperature θ is for the guest atom in a distorted dodecahedron.

Compounds Type of $\mathcal{R}_8M_{16}Z_{30}$	Sample form	Carrier types	$\kappa_{ph}(T)$	Experiments (Temperature)	Rattling states of $\mathcal{R}(2)$	θ [K] for $\mathcal{R}(2)$	References
I-$Ba_8Al_{16}Si_{30}$	Poly	n	C				Mudryk *et al.* (2002)
	Single			XRD	on-center	92,100/68,74	Christensen *et al.* (2010)
($Ba_8Al_{14}Si_{31}$)	Single	n	C	ND(298 [K])	on		Condron *et al.* (2006)
I-$Sr_8Al_{10}Si_{36}$	Single			XRD(90 [K])	on		Roudebush *et al.* (2012)
I-$Sr_8Al_{11}Si_{35}$	Single	n	C	SH		125/67	unpublished our data
I-$Ba_8Ga_{16}Si_{30}$	Single			ND	on	98/69	Bentien *et al.* (2002)

[a] $E_g(1)/E_g(A),T_{2g}(1)$ rattling modes in the tetrakaidecahadron

table continued on next page

continued from previous page

Compounds Type of $\mathcal{R}_8M_{16}Z_{30}$	Sample form	Carrier types	$\kappa_{ph}(T)$	Experiments (Temperature)	Rattling states of $\mathcal{R}(2)$	θ [K] for $\mathcal{R}(2)$	References
	Powder	n	C	ND	off-center	85	Qiu *et al.* (2004)
	Single			ND	off		Bentien *et al.* (2005)
	Powder			XRD	on	101/77	Bentien *et al.* (2005)
	Single			XRD	on	92-95/66-69	Christensen *et al.* (2010)
($Ba_8Ga_{12}Si_{33}$)	Powder			XRD(R.T.)	on		Mudryk *et al.* (2002)
($Ba_8Ga_{15-16}Si_{31-30}$)	Powder			XRD(R.T.)	on	88-96/53-57	Anno *et al.* (2012)
	Single			Raman(4 [K])	off	-/59	Takasu *et al.* (2008)
I-$Sr_8Ga_{16}Si_{30}$	Single	n	C	SH		120/59	Suekuni *et al.* (2007)
	Single	n	C	Raman(50 [K])	off	-/56	Takasu *et al.* (2008)
I-$Ba_8Al_{16}Ge_{30}$	Single			XRD	on	81-85/61-69	Christensen *et al.* (2007)
	Single			XRD	off	81-84	Christensen *et al.* (2007)
	Single			ND(20 [K])	off		Christensen *et al.* (2007)
	Poly	n	C				Christensen *et al.* (2007)
I-$Ba_8Ga_{16}Ge_{30}$				XRD(R.T.?)	on	(51)	Eisenmann *et al.* (1986)
							Sales *et al.* (1999)
	Single		C	ND(15 [K])	?		Keppens *et al.* (2000)
	Single			ND	on		Chakoumakos *et al.* (2001)
	Single	n		ND	on	64	Sales *et al.* (2001)
		n		XRD(293 [K])	off	72	Paschen *et al.* (2001)
	Powder			XRD	on	101/73	Bentien *et al.* (2005)
	Single	p		ND	on	90/62	Christensen *et al.* (2006a)
	Single	p		XRD	on	87/60	Christensen *et al.* (2006a)
	Single	n		ND	on	89/59	Christensen *et al.* (2006a)
	Single	n		XRD	on	84/60	Christensen *et al.* (2006a)
	Single	p		ND	off	88	Christensen *et al.* (2006a)
	Single	p		XRD	off	82	Christensen *et al.* (2006a)
	Single	n		ND	off	88	Christensen *et al.* (2006a)
	Single	n		XRD	off	81	Christensen *et al.* (2006a)
	Single	p		XRD(20 [K])	off:65%,on:33%		Fujiwara *et al.* (2012)
	Single	n		XRD(20 [K])	on		Fujiwara *et al.* (2012)
	Powder	n,p		EXAFS	off	86	Jiang *et al.* (2008)
	Poly	n	C				Uher *et al.* (1999)
	Single	n	C	SH		(60)	Sales *et al.* (2001)
		n		SH		(80)	Paschen *et al.* (2001)
	Single		G: $T^{\sim 1.8}$				Paschen *et al.* (2003)
	Single	p	G: $T^{1.5}$	SH		38	Bentien *et al.* (2004)
				SH		80	Bentien *et al.* (2005)
	Single	p	G: T^2	SH		42	Umeo *et al.* (2005)
	Single	p	G: T^2	SH		87/49	Avila *et al.* (2006a,b)
	Single	n	C: T^2	SH		87/49	Avila *et al.* (2006a,b)
	Single	n		SH		74	Xu *et al.* (2011)
	Single	n, p		Raman(2 [K])	off	92/47,45-47[a]	Takasu *et al.* (2006, 2010)
	Single	p		THz(6.6 [K])		86/55	Mori *et al.* (2009)
	Poly			INS(295 [K])		55	Hermann *et al.* (2005)
	Powder	p		INS		-/50	Christensen *et al.* (2006b)
	Powder	n		INS		65/52	Christensen *et al.* (2006b)
	Single	n		INS(R.T.)		-/52	Lee *et al.* (2007a)
	Single	n		INS		87/53	Christensen *et al.* (2008)
I-$Ba_8In_{16}Ge_{30}$	Powder			XRD	on	65/65	Bentien *et al.* (2005)
	Single	n	C				Bentien *et al.* (2006)
(with vacancy)	Poly	n	G				Bentien *et al.* (2006)
	Single	n	C	SH		99/38	Suekuni *et al.* (2008b)
I-$Sr_8Ga_{16}Ge_{30}$	Powder			XRD(R.T.)	on	85/39	Schujman *et al.* (2000)
	Pow.,Sin.			ND	off		Chakoumakos *et al.* (2000)
	Pow.,Sin.			ND	off or on	85	Chakoumakos *et al.* (2000)

[a] $E_g(1)/E_g(A)$,$T_{2g}(1)$ rattling modes in the tetrakaidecahadron

table continued on next page

continued from previous page

Compounds Type of $\mathcal{R}_8M_{16}Z_{30}$	Sample form	Carrier types	$\kappa_{ph}(T)$	Experiments (Temperature)	Rattling states of $\mathcal{R}(2)$	θ [K] for $\mathcal{R}(2)$	References
	Single			XRD(R.T.)	on	74	Nolas *et al.* (2000)
	Single		G	ND(15 [K])	off		Keppens *et al.* (2000)
	Powder			XRD		90/29	Iversen *et al.* (2000)
	Single	n	G	ND	off		Sales *et al.* (2001)
	Single	n	G	ND	on	80	Sales *et al.* (2001)
	Powder			RXD(R.T.)	off		Zhang *et al.* (2002)
	Powder	n	G	ND	off	76	Qiu *et al.* (2004)
	Powder			XRD	on	104/163	Bentien *et al.* (2005)
	Single	n		XRD(20 [K])	off:98%,on:2%		Fujiwara *et al.* (2012)
	Poly	n	G: T^2				Nolas *et al.* (1998a)
							Cohn *et al.* (1999)
	Poly	n	G/C				Uher *et al.* (1999)
	Poly	n	G				Nolas *et al.* (1998b)
			G				Nolas *et al.* (2000)
	Powder	n		EXAFS	off	126-128	Baumbach *et al.* (2005)
	Powder	n		EXAFS	off:75%,on:25%	147-156	Baumbach *et al.* (2005)
				SH		(50)	Chakoumakos *et al.* (2000)
	Single	n	G	SH		(53)	Sales *et al.* (2001)
				SH		(79)	Paschen *et al.* (2001)
				SH		80	Bentien *et al.* (2005)
	Single	n	G	SH		34	Umeo *et al.* (2005)
	Single	n	G	SH		90/35	Suekuni *et al.* (2007)
	Single	n		SH		80	Xu *et al.* (2011)
	Single			RUS		45	Keppens *et al.* (2002)
	Poly			Raman(300 [K])		-/46	Nolas *et al.* (2000b)
	Single	n		Raman(2 [K])	off	95/42,42[a]	Takasu *et al.* (2006)
	Poly			INS(295 [K])		49	Hermann *et al.* (2005)
	Powder	n		INS		62/48	Christensen *et al.* (2006b)
	Single	n		INS		-/46	Lee *et al.* (2008)
I-$Eu_8Ga_{16}Ge_{30}$	Single			XRD(R.T.)	on	53	Nolas *et al.* (2000)
	Single			ND	off		Chakoumakos *et al.* (2001)
	Single	n	G	ND	off		Sales *et al.* (2001)
	Single	n		XRD(293 [K])	off	45	Paschen *et al.* (2001)
	Powder	n		EXAFS	off	93-96	Baumbach *et al.* (2005)
			G				Nolas *et al.* (2000)
	Single	n	G	SH		(30)	Sales *et al.* (2001)
	Poly	n	G				Paschen *et al.* (2001)
	Poly	n	G				Bentien *et al.* (2005b)
	Single			RUS		22	Zerec *et al.* (2004)
	Poly			Mössbauer, MW	off	-/31	Hermann *et al.* (2006)
	Poly			Raman(300 [K])		-/33	Nolas *et al.* (2000b)
	Single	n		Raman(2 [K])	off	69/26,26[a]	Takasu *et al.* (2006)
	Powder			NIS(25 [K])		87,57,35	Hermann *et al.* (2005)
VIII-$Eu_8Ga_{16}Ge_{30}$	Single	n		XRD(293 [K])		45	Paschen *et al.* (2001)
	Poly	n	C	SH		72	Paschen *et al.* (2001)
I-$Ba_8Ga_{16}Sn_{30}$	Single	p	G: $T^{\sim 2}$	XRD	off		Suekuni *et al.* (2008a)
	Single	n	G: $T^{\sim 2}$	XRD	off	78/60	Suekuni *et al.* (2008a)
	Single	n	G: $T^{\sim 2}$	SH	off	-/20	Avila *et al.* (2008)
	Single	p	G: $T^{\sim 2}$	SH	off	-/20	Suekuni *et al.* (2008a)
		p?		SH		55,14	Zheng *et al.* (2012)
		p?		ER		54	Zheng *et al.* (2012)
	Single	n		Raman(4 [K])	off	68/27,20[a]	Suekuni *et al.* (2010)
	Single	p		Raman(4 [K])	off	-/27,21[a]	Suekuni *et al.* (2010)
	Single	n		THz(7 [K])		64/34	Mori *et al.* (2011)
				NMR	off	-/20	Zheng *et al.* (2011)

[a] $E_g(1)/E_g(A)$,$T_{2g}(1)$ rattling modes in the tetrakaidecahadron

table continued on next page

continued from previous page

Compounds Type of $\mathcal{R}_8M_{16}Z_{30}$	Sample form	Carrier types	$\kappa_{\rm ph}(T)$	Experiments (Temperature)	Rattling states of $\mathcal{R}(2)$	θ [K] for $\mathcal{R}(2)$	References
VIII-$Ba_8Ga_{16}Sn_{30}$	Sin.,Pow.	n		XRD		64	Huo *et al.* (2005)
	Single	n	C	SH		50	Huo *et al.* (2005)
							Avila *et al.* (2006b)
	Single	p	G	SH		50	Avila *et al.* (2006b)

[a] $E_g(1)/E_g(A)$,$T_{2g}(1)$ rattling modes in the tetrakaidecahadron

IV. SPECIFIC HEATS OF TYPE-I CLATHRATE COMPOUNDS

It is common to use an appropriate energy scale in each experiment. These are Joule (J) or Kelvin (K) for thermal measurements, cm^{-1} or THz for optical spectroscopies, and eV for inelastic neutron or x-ray scatterings. The conversion relation is $1\,[\mathrm{THz}] = 47.99\,[\mathrm{K}] = 33.36\,[\mathrm{cm}^{-1}] = 4.136\,[\mathrm{meV}]$. This relation will be helpful for readers in connection with the following descriptions on the dynamical behaviors of type-I clathrate compounds.

A. Observed characteristics of specific heats

Heat capacity provides fundamental information on the thermal properties of materials. It represents the amount of energy needed to raise the temperature of a given material by one degree. The heat capacity per unit mass is called specific heat. Molar specific heat is referred to as specific heat $C_{\rm V}$ in the present article. Temperature dependences of specific heats reflect the phonon density of states, the electronic one at $E_{\rm F}$, the magnetic degree of freedom, superconducting properties, and so on.

Three characteristic temperature-regions are manifested in the observed specific heats of type-I clathrate compounds by subtracting the electronic contribution. These are temperature regions below 1 [K], around several [K], and above several 10 [K]. We will describe in details these characteristics in the following subsections.

1. Low temperature specific heats below 1 K

A series of specific heat experiments on type-I clathrate compounds have made clear that the characteristics critically depend on the states of guest atoms in cages (Avila *et al.*, 2006a,b; Bentien *et al.*, 2004, 2005; Cohn *et al.*, 1999; Nolas *et al.*, 1995, 1996, 1998a,b,b,c, 2000, 2001a; Sales *et al.*, 1996; Sales, 1998; Sales *et al.*, 2001; Suekuni *et al.*, 2007, 2008a,b, 2010; Xu *et al.*, 2010). The most intriguing findings in the regime below about 1 [K] are that the temperature dependences and the magnitude are almost identical to those of glasses for type-I clathrate compounds with *off-center* guest atoms.

The specific heats of type-I clathrates with off-center guest atoms are scaled in the following form

$$C_{\rm V}(T) \cong \alpha T^{1+\delta} + \beta T^3. \tag{28}$$

The first term proportional to $T^{1+\delta}$ is not exactly linear in T at temperatures below 1 [K] with the positive small factor δ, a dependence that is identical to that of structural glasses (Freeman and Anderson, 1986; Stephens, 1973; Zeller and Pohl, 1971). This term has no connection with conduction electron specific heat proportional to γT.

From careful measurements of specific heats of type-I $Ba_8Ga_{16}Sn_{30}$ (β-BGS), it has been estimated that $\alpha \cong 30\,\left[\mathrm{mJ\,mol^{-1}\,K^{-2}}\right]$ and $\beta \cong 50\,\left[\mathrm{mJ\,mol^{-1}\,K^{-4}}\right]$ with $\delta = 0.2$ (Suekuni *et al.*, 2008a,b). In silica glass (Zeller and Pohl, 1971), $\alpha \cong 0.072\,\left[\mathrm{mJ\,mol^{-1}\,K^{-2}}\right]$ and $\beta \cong 0.108\,\left[\mathrm{mJ\,mol^{-1}\,K^{-4}}\right]$ with the positive small factor $\delta \cong 0.2$. Most carefully measured silica glass (Lasjaunias *et al.*, 1975) gives $\delta = 0.22 - 0.30$ between T=25 [mK] and 0.9 [K].

The coefficient of the second term β should be separated into $\beta_{\rm D}$ and $\beta_{\rm B}$, where $\beta_{\rm D}$ is the coefficient from the Debye phonon specific heat and $\beta_{\rm B}$ is that of the excess specific heat originating from the tail of the hump observed at around $T \simeq$4 [K] in β-BGS.

2. Excess specific heats over Debye phonons at temperatures of several Kelvin

Atomic vibrations of type-I clathrates containing off-center guest atoms display glass-like low-lying modes. Actually, the excess densities of states in type-I clathrate compounds have been observed as a hump in specific heat experiments in the temperature range around several K, i.e., broad peaks observed in the temperature range at 10−100 times smaller than the Debye temperature $\theta_{\rm D} = \hbar\omega_{\rm D}/k_{\rm B}$. The characteristics are almost identical to those of structural glasses observed by a variety of measurements such as optical spectroscopies, inelastic neutron scattering, and specific heats in the THz frequency range (see, for example, a review by Nakayama (2002)). The Debye frequency $\omega_{\rm D}$ is related to the velocities of transverse $v_{\rm t}$ and longitudinal v_ℓ acoustic phonons by

$$\omega_D^3 = \frac{18\pi^2 N}{V}\left(\frac{2}{v_t^3} + \frac{1}{v_\ell^3}\right)^{-1}. \tag{29}$$

Here N is the number of atoms in the volume V. The experimental values of velocities of silica glass are $v_{\rm t} = 3.767\times10^5\,[\mathrm{cm\,s^{-1}}]$ and $v_\ell = 5.970\times10^5\,[\mathrm{cm\,s^{-1}}]$. These give a Debye frequency $\omega_{\rm D}/2\pi$ of 10.40 [THz] corresponding to the Debye temperature $\theta_{\rm D}$=500 [K] from the re-

lation $\theta_{\rm D} = \hbar\omega_{\rm D}/k_{\rm B}$. The specific heat of the Debye phonons is expressed by

$$C_{\rm ph}(T) \cong \frac{12\pi^4 N k_{\rm B}}{5V}\left(\frac{T}{\theta_{\rm D}}\right)^3. \qquad (30)$$

This formula for the phonon specific heat holds in the temperature regime $T \ll \theta_{\rm D}$. However, observed specific heats of structural glasses do not show the temperature dependence of Eq. (30) at low temperatures but manifest the excess humps in the temperature range around several [K].

Flubacher *et al.* (1959) and Anderson (1959) have observed the excess specific heat of silica glass at around 10 [K] over the Debye contribution of Eq. (30). This is clearly realized by plotting $C_{\rm V}(T)/T^3$ vs. T (Buchenau *et al.*, 1986; Pohl, 1981; Zeller and Pohl, 1971). These observations have been ascribed to the presence of excess vibrational states over the Debye density of states $D(\omega) \propto \omega^2$. The term "Boson peak" refers to this excess contribution to the conventional Debye density of states. The issue in structural glasses has been revitalized according to the advent of various experimental techniques. However, the nature of these vibrational states in glasses has been the subject of a very intensive and controversial debate for decades.

The humps in $C_{\rm V}/T^3$ of type-I $Ba_8Ga_{16}Sn_{30}$ (β-BGS) and type-I $Sr_8Ga_{16}Ge_{30}$ appear around $T \simeq 5$ [K] (Avila *et al.*, 2008; Suekuni *et al.*, 2007, 2008a,b; Umeo *et al.*, 2005; Xu *et al.*, 2011). See Fig. 7. This excess hump possess almost identical characteristics to the so-called Boson peak.

3. Characteristic temperatures of excess specific heats

The data on specific heats have been used to characterize vibrational properties of type-I clathrate compounds. Analysis based on the Einstein model has been carried out on type-I EGG, SGG, and BGG single crystals by Sales *et al.* (2001), where the cages and the guests were assumed to behave as a Debye lattice and Einstein oscillators, respectively. At temperatures above 80 [K], the specific heat data were the same among three samples to within the experimental error, and well described by the Debye specific heat with a $\theta_{\rm D}$ of about 300 [K]. At low temperatures, however, the Einstein oscillators predicted significantly different behaviors to the three samples. The Einstein temperatures $\theta_{\rm E}$ corresponding to the vibrations of Ba, Sr, and Eu guest atoms were estimated to be 60, 53, and 30 [K], respectively.

Paschen *et al.* (2001) have reported different analysis for these three compounds. The data of $C_{\rm V}$ vs. T were fitted by including lattice and electronic contributions given by $C_{\rm ph}$ and $C_{\rm e}$. The fitting parameters are $\theta_{\rm D}$, $\theta_{\rm E}$, and numbers of atoms $N_{\rm D}$ and $N_{\rm E}$ contributing to the Debye and Einstein specific heats, respectively, where their sum $N_{\rm D}+N_{\rm E}$ is taken as 54. For BGG, the obtained parameters were $\theta_{\rm D}$= 355 [K], $\theta_{\rm E}$=80 [K], $N_{\rm D}$=39, and $N_{\rm E}$=15. Similar results were obtained for SGG. The fits to the data for BGG and SGG yield $N_{\rm E}$=15 and 16, respectively, instead of the number of guests equal to 8. For β-EGG, $\theta_{\rm E}$ was not evaluated due to the large magnetic contribution of Eu^{2+} at temperatures up to 50 [K]. The value of $\theta_{\rm D}$ was estimated to be 302 [K] using $\theta_{\rm E}$ obtained from room-temperature isotropic ADP and $C_{\rm V}(T)$ data at temperatures above the Curie temperature of 36 [K].

Bentien *et al.* (2004) have analyzed $C_{\rm V}$ for BGG using two kinds of the Einstein oscillators. The obtained characteristic temperatures are $\theta_{\rm D}$=324(4) [K], $\theta_{\rm E1}$=78(2) [K], and $\theta_{\rm E2}$=38(1) [K] with $N_{\rm D}$=2.8(6), $N_{\rm E1}$=9.7(5), and $N_{\rm E2}$=1.5(5), respectively. A linear fit to the data of $C_{\rm V}/T$ vs. T^2 between 1.5 [K^2] and 4 [K^2] gave $\theta_{\rm D}$=311(10) [K], in agreement with the result from the fitting of the data $C_{\rm V}$ vs. T above 5 [K]. The Sommerfeld coefficient γ was estimated to be 14 [mJ/K^2mol].

In the above analysis on BGG, $N_{\rm D}$ and $N_{\rm E}$ are free fitting parameters. Bentien *et al.* (2005) then imposed the constraints $N_{\rm D}$=46 and $N_{\rm E1} + N_{\rm E2}$=8. By using $\theta_{\rm D}$=312 [K] obtained from the temperature dependence of the ADP of cage atoms, the parameters were evaluated to be γ=35 [mJ/K^2mol], $\theta_{\rm E1}$=80 [K] and $N_{\rm E1}$=6.5, and $\theta_{\rm E2}$=42 [K] and $N_{\rm E2}$1.5, respectively. For type-I SGG, the evaluated parameters were γ = 40 [mJ/K^2mol], $\theta_{\rm E1}$=80 [K], and $\theta_{\rm E2}$=33 [K]. They have argued that $N_{\rm E1}$ and $N_{\rm E2}$ almost correspond to the numbers of the large and small cages. However, the result disagreed with the fact that the guest in a small cage has a higher vibrational energy (Christensen *et al.*, 2010).

Avila *et al.* (2006b) have analyzed the specific heat data of BGG by plotting $C_{\rm V}/T^3$ vs. T. The contributions of the guest atoms from these systems appear as broad peaks over electronic and Debye *backgrounds* originating from the stiff cage. This treatment has reproduced the specific heat data for type-VIII $Ba_8Ga_{16}Sn_{30}$ (Huo *et al.*, 2005). It should be recalled that six Ba(2) atoms at the 6*d* site in the tetrakaidecahedra show strongly anisotropic vibration with larger amplitudes within the plane perpendicular to the four-fold axis. So, at least two characteristic temperatures are required to describe the vibrations of Ba(2) when applying the Einstein model: in plane $\theta_{\rm E2}^{\parallel}$ and out of plane $\theta_{\rm E2}^{\perp}$. Furthermore, the characteristic temperature of a Ba(1) atom at a 2*a* site in the dodecahedra was assumed to be the single parameter $\theta_{\rm E1}$ because of the isotropic shape of the cage. The dimensionality and the numbers of oscillators were predefined: $D \times N_{\rm E1}$=3×2, $D \times N_{\rm E2}^{\parallel}$=2×6, and $D \times N_{\rm E2}^{\perp}$=1×6. Additional constraints $\theta_{\rm E2}^{\parallel} < \theta_{\rm E2}^{\perp}$ and $\theta_{\rm E2}^{\parallel} < \theta_{\rm E1}$ were imposed. The values of γ and $\theta_{\rm D}$ determined from the plot of C/T vs. T^2 were fixed together with the number $N_{\rm E}$. Therefore, only three fitting parameters were left, which characterize the vibrational energies of the Ba guests. The best fits give the values $\theta_{\rm E1}$=87.2 [K], $\theta_{\rm E2}^{\perp}$=87.1 [K], and $\theta_{\rm E2}^{\parallel}$=49.4 [K].

Specific heat experiments on cage-size tuned $Sr_8Ga_{16}Si_{30-x}Ge_x$ have been performed

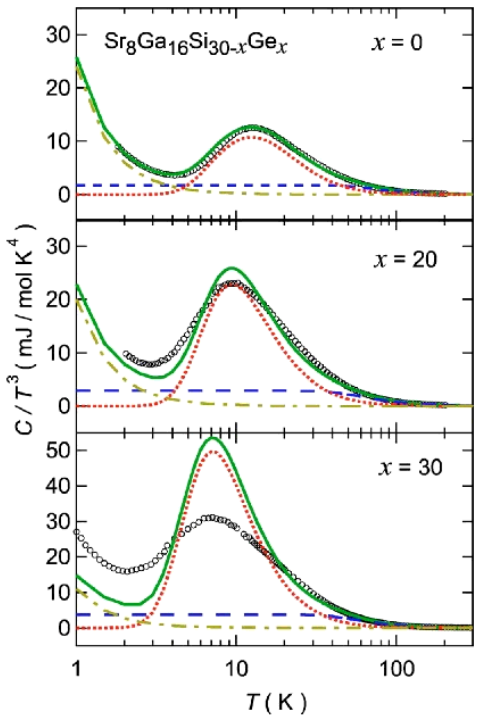

FIG. 6 (Color online) The specific heat data plotted as $C_{\rm V}(T)/T^3$ vs. T (open circles) for type-I $Sr_8Ga_{16}Si_{30-x}Ge_x$. The dotted, dashed, and dashed-dotted lines are from the Einstein model, the Debye model, and from electronic components, respectively. After the work of Suekuni *et al.* (2007).

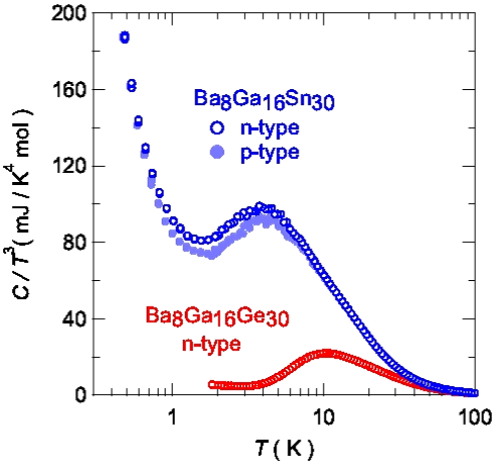

FIG. 7 (Color online) The specific heat data plotted as $C_{\rm V}/T^3$ vs. T on n-type type-I $Ba_8Ga_{16}Ge_{30}$ and n- and p-type type-I $Ba_8Ga_{16}Sn_{30}$ single crystals. Adopted from Avila *et al.* (2006b, 2008); Suekuni *et al.* (2008a).

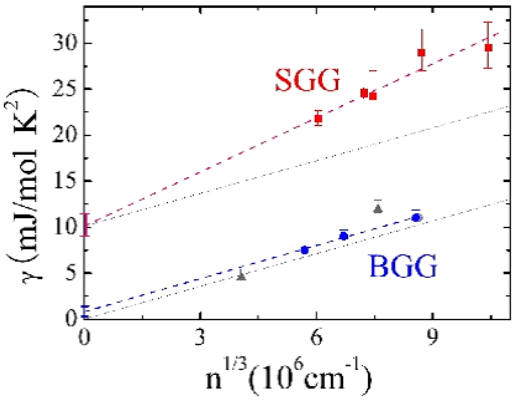

FIG. 8 (Color online) The temperature-linear factor γ of low-temperature specific heat for type-I $\mathcal{R}_8Ga_{16}Ge_{30}$ ($\mathcal{R}$=Sr and Ba) plotted as a function of the carrier concentration $n^{1/3}$. Adopted from Xu *et al.* (2010).

by Suekuni *et al.* (2007). With increasing x from 0 to 30, the cage size was expanded by 8%. The data in Fig. 6 plotted as $C_{\rm V}/T^3$ vs. T show that the peak temperatures of the Boson-peak like hump shift lower from 10.5 to 7 [K] with increasing hump heights. These observations do not depend on the carrier density, whose contribution becomes vanishingly small at temperatures above 4 [K]. In the analysis based on the Einstein model, the constraints $\theta_{\rm E2}^{\parallel}=\theta_{\rm EL}$ and $\theta_{\rm E2}^{\perp}=\theta_{\rm E1}=\theta_{\rm EH}$ were imposed, and the rest of the fitting parameters were taken as the lower and higher characteristic temperatures $\theta_{\rm EL}$ and $\theta_{\rm EH}$. For x=0, a good fit was obtained with $\theta_{\rm EL}$=59 [K] and $\theta_{\rm EH}$=120 [K], indicating the validity of the Einstein model for Sr guests in $Sr_8Ga_{16}Si_{30}$. However, for x=20, 30, the Einstein model apparently did not yield an adequate fitting to the observed data, as seen in Fig. 6. These discrepancies indicate the relevance of the anharmonic potential for the Sr(2) sites on increasing cage size for x=20, 30.

Avila *et al.* (2008) and Suekuni *et al.* (2008a) have reported specific heat measurements on type-I BGS, which has a larger cage and a larger off-center displacement of Ba(2) than that of BGG. The C/T^3 vs. T plot for β-BGS shows larger Boson-peak like hump around 4 [K] than that around 10 [K] (see Fig 7). The temperature of 4 [K] is the lowest among type-I clathrates, and corresponds to a vibrational energy equivalent to 20 [K] for Ba(2) in the plane perpendicular to the four-fold axis. The height of the hump for β-BGS was not reproduced by the Einstein model unlike BGG, that indicates a strong anharmonicity of Ba(2) vibrations. The low-temperature T-linear coefficient for n-type β-BGS was estimated to be 29 [mJ/K^{2}mol], which is about 5 times larger than 6 [mJ/K^{2}mol] for n-type BGG, regardless of a lower carrier density in β-BGS. It was argued that the larger coefficient in β-BGS is attributed to a tunneling contribution of Ba(2) among the off-center sites. The Boson-peak like hump at low temperature and the anomalously large temperature-linear coefficient in β-BGS are almost identical to that in vitreous silica.

Xu *et al.* (2010) have made an analysis of the data of low-temperature specific heats of type-I BGG and SGG. By using the relation $\gamma = \alpha + \gamma_e = \alpha + cm_e^* n^{1/3}$ (c

is a known constant) together with the measured values of γ and the carrier density n, they have obtained α and the carrier effective mass m_e^*. The relationships between γ and $n^{1/3}$ are shown in Fig. 8. The α value of $10.1\pm1.5\,[\mathrm{mJ/K^2mol}]$ for type-I SGG is larger than that of $0.8\pm0.4\,[\mathrm{mJ/K^2mol}]$ for BGG. It has been suggested that the finite α value in these clathrates presumably results from the random displacement of Ga and Ge in the host framework. The larger α value in type-I SGG indicates large disorder. The m_e^* was obtained from the slopes of the γ vs. $n^{1/3}$ plot to be $1.68m_0$ for type-I SGG and $1.01m_0$ for BGG, where m_0 is the free-electron mass. The enhancement of m_e^* was interpreted in terms of electron-phonon interactions. The value of m_e^* is described as $m_e^* = m_0(1 + \lambda_{\mathrm{e-ph}} + \lambda_{\mathrm{s}})$, where $\lambda_{\mathrm{e-ph}}$ is the electron-phonon term and λ_{s} is the spin fluctuation one. The last term is not important in SGG and BGG, and then values of the $\lambda_{\mathrm{e-ph}}$ were estimated to be 0.68 for SGG and 0.01 for BGG, respectively. For BGG, the low value of $\lambda_{\mathrm{e-ph}}$ indicates the weak interaction between electrons and vibrations of guest atoms. In contrast, $\lambda_{\mathrm{e-ph}}$ is enhanced for SGG. This enhancement is attributed to the anharmonic phonon of the Sr(2).

V. TRANSPORTS PROPERTIES OF TYPE-I CLATHRATE COMPOUNDS

A. Electrical resistivity and Seebeck coefficient

The type-I clathrates exhibit semiconducting or metallic behaviors in the electrical transport and thermoelectric properties depending on the magnitude of gap energy and doping level. Semiconducting behaviors are characterized by the exponential decrease of ρ and the $1/T$ dependence of $|S|$ with increasing temperature, which can be attributed to the thermal excitations of electrons over the intrinsic energy gap between the valence and conduction bands, or hopping excitations between impurity states and the band edge. Metallic behaviors are characterized by the increase of the ρ and $|S|$ with increasing temperature, which are caused by heavily-doped electrons or holes. The self-doping is due to the off-stoichiometry and/or vacancy in the cage structure. Binary and ternary type-I clathrates have gained much attention because of high thermoelectric performance.

Among type-I Si clathrates, $Na_2Ba_6Si_{46}$ and Ba_8Si_{46} are superconductors with the transition temperatures T_{sc} of 4 [K] and 8 [K], respectively (Yamanaka *et al.*, 1995, 2000). The superconductivity in such a compound based on the covalent sp^3 network has attracted great attention. It was followed by the discovery of the superconductivity in diamond (Ekimov *et al.*, 2004) and diamond-structured Si (Bustarret *et al.*, 2006). False superconductivity in BGG was observed for a polycrystalline sample of $Ba_{7.62}Ga_{17.30}Ge_{28.70}$ (Bryan *et al.*, 1999). Magnetic measurement for the finely grounded sample showed a diamagnetic signal below T_{sc}=7.5 [K]. The diamagnetic signal was approximately 40% of the shielding expected for a perfect diamagnet. The *ac* resistance measurement on the pelletized sample showed a resistive transition below 4.8 [K]. The higher T_{sc} in the diamagnetic signal was attributed to the surface oxidation and the non-stoichiometric surface states in the polycrystalline grains.

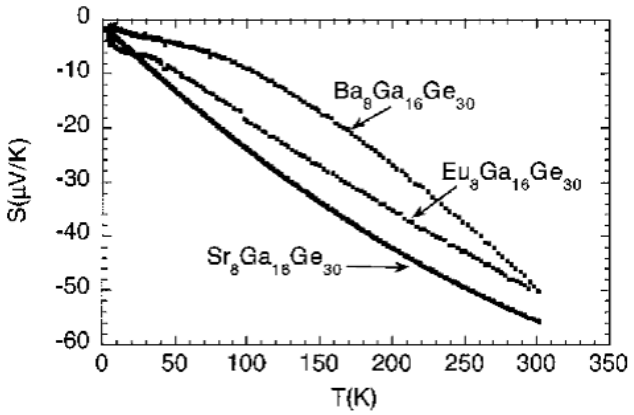

FIG. 9 Temperature dependences of the thermopower $S\,[\mu\mathrm{V/K}]$ for $\mathcal{R}_8Ga_{16}Ge_{30}$ ($\mathcal{R}$= Ba, Sr, Eu) single crystals. After Sales *et al.* (2001).

Sales *et al.* (2001) have carefully examined the superconducting properties by using single crystals. The crystal of BGG was grown by slowly cooling molten mixtures of the stoichiometric elements. The crystal with a carrier density $n \simeq 10^{21}\,[\mathrm{cm^{-3}}]$ provided no evidence of superconductivity down to 2 [K] in either C_{V}, ρ, or *ac* susceptibility. Thus, the superconductivity observed by Bryan *et al.* (1999) may be due to small amounts of impurity phases such as Ga and Ba-Ge alloys with T_{sc}=1−10 [K] (Cohen *et al.*, 1967; Li *et al.*, 2003, 2004).

Good electrical transport and thermoelectric properties have been observed in the type-I clathrates $\mathcal{R}_8Ga_{16}Ge_{30}$ ($\mathcal{R}$= Ba, Sr, and Eu). The replacement of Ga for Ge produces a charge compensation for the divalent alkali-earth ion $\mathcal{R}^{2+}$. Adjusting the Ga/Ge ratio can tune the carrier density and improve the thermoelectric power factor $PF = S^2/\rho$ and the dimensionless figure of merit ZT. Electrical transport and thermoelectric properties for single crystals of SGG and β-EGG were examined by Sales *et al.* (2001). Both ρ and S showed metallic behavior because of the heavily doped level of electrons at $n \simeq 10^{21}\,[\mathrm{cm^{-3}}]$. The sharp drop in ρ for β-EGG below 35 [K] is characteristic of the loss of spin disorder scattering due to the long-range magnetic order of the Eu^{2+} magnetic moments. The room-temperature S of $-50\,[\mu\mathrm{V/K}]$ is typical for heavily doped n-type semiconductors. See Fig. 9. The Hall mobility μ_{H} of the carriers increases with decreasing temperature, which suggests that the scattering of carriers is dominated by acoustic phonons.

The thermoelectric properties for hot-pressed polycrystals of SGG have been reported by Nolas *et al.* (1998b);

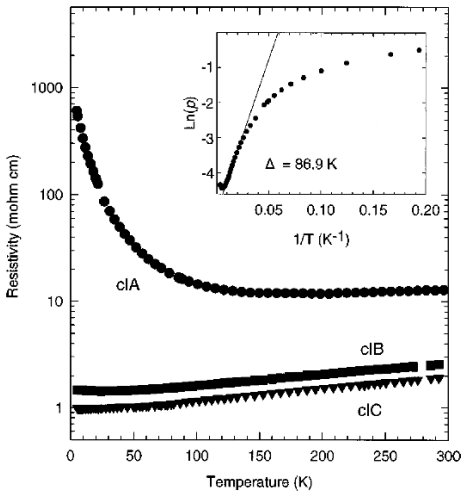

FIG. 10 Temperature dependences of electrical resistivity ρ for $Sr_8Ga_{16}Ge_{30}$ polycrystalline samples with various carrier density (See text). After the work of Nolas *et al.* (1998b).

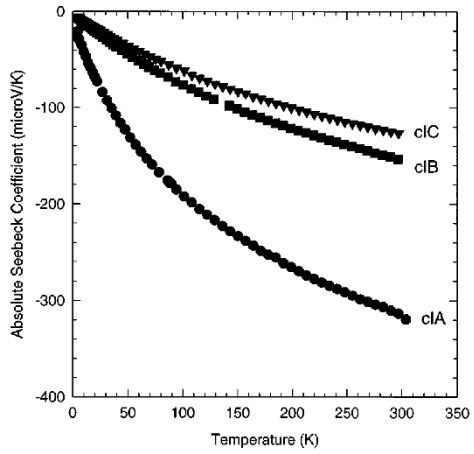

FIG. 11 Temperature dependences of the thermopower $S\,[\mu\mathrm{V/K}]$ for type-I $Sr_8Ga_{16}Ge_{30}$ polycrystalline samples with various carrier density (see text). After the work of Nolas *et al.* (1998b).

Nolas (2003). The values of the n in the article in 1998 were corrected in the review in 2003. The sample with $n \simeq 10^{19}\,[\mathrm{cm}^{-3}]$ allowed the measurement of the semiconducting ρ contribution below 100 [K], as shown in Fig. 10. The negative S decreases with increasing temperature and reaches a value of $-320\,[\mu\mathrm{V/K}]$ at 300 [K], as shown in Fig. 11. The sample with $n \simeq 10^{20}\,[\mathrm{cm}^{-3}]$ exhibited metallic behaviors in both ρ and S in the temperature range from 5 to 300 [K]. The thermal conductivity κ is approximately 1 [W/(mK)] and the value of ZT reaches 0.25 at 300 [K].

The value of the carrier density n in type-I SGG was tuned by adjusting the nominal composition in polycrystalline samples. Fujita *et al.* (2006) prepared the samples by arc melting the elements with the nominal ratio of

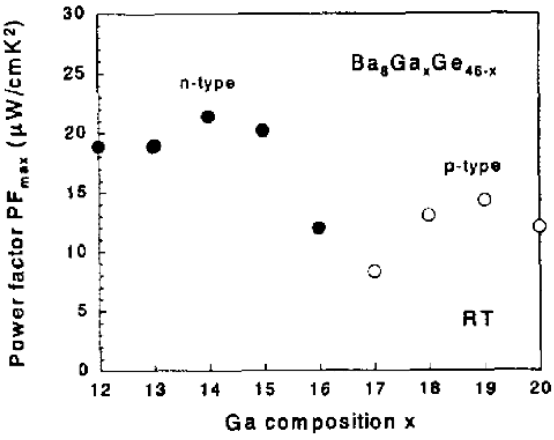

FIG. 12 Thermoelectric power factor at room temperature as a function of Ga composition x for n- and p-type $Ba_8Ga_xGe_{46-x}$ polycrystalline samples. Adopted from Anno *et al.* (2002).

$Sr:Ga:Ge{=}8:x:46{-}x$ ($x{=}13{-}20$). The ingot was powdered and sintered by the spark-plasma-sintering (SPS) technique. With increasing x, the actual Ga composition tended to increase, and the carrier density n decreased from 11.1 to $1.8{\times}10^{20}\,[\mathrm{cm}^{-3}]$. The effective mass m_e^* was almost constant at $3.1m_0$, and μ_H was $8{-}13\,[\mathrm{cm}^2/\mathrm{Vs}]$, at room temperature. The electrical conductivity σ and the negative S exhibited metallic behavior from 300 [K] up to 700 [K]; the metallic behavior turned into an intrinsic semidonducting one above 700−800 [K]. The tuning of the carrier density n to $5.6{\times}10^{20}\,[\mathrm{cm}^{-3}]$ maximized ZT of 0.62 at 800 [K].

Wang *et al.* (2009) have started with the nominal composition of $Sr:Ga:Ge{=}9.6:x:30$ ($x = 18{-}23$). The grounded polycrystalline sample was ultrasonically washed with diluted hydrochloric acid to remove the excess Ga. Dense samples were obtained by sintering the ground samples. The carrier density n decreased from $2.81{\times}10^{20}$ to $0.33{\times}10^{20}\,[\mathrm{cm}^{-3}]$ as the Ga/Ge ratio increased from 0.481 to 0.517. The samples with $n < 10^{20}\,[\mathrm{cm}^{-3}]$ showed a high S of $350{-}400\,[\mu\mathrm{V/K}]$ at 450 [K] and intrinsic semiconducting conduction above 450 K while those with higher n exhibited a metallic behavior up to 700 [K]. The value of ZT reached 0.85 at 650 [K] for the sample with the lowest Ga/Ge ratio of 0.481.

For β-$Eu_8Ga_{16+x}Ge_{30-x}$ (EGG), the carrier density n was controlled by changing the annealing temperature between 823 and 970 [K] (Bentien *et al.*, 2005b; Pacheco *et al.*, 2005). The samples for $-1.01 < x < -0.47$ had n between 0.43 and 1.53 e^- per unit cell. All samples showed a metallic behavior in ρ with a hump around 35 [K] attributable to the ferromagnetic transition. S exhibited metallic behavior and reached $-(75{-}160)\,[\mu\mathrm{V/K}]$ at 400 [K].

For SGG and β-EGG, no p-type conduction has

been observed yet. In contrast, the carrier types and density have been tuned in BGG (Anno *et al.*, 2002, 2003; Avila *et al.*, 2006a,b; Cederkrantz *et al.*, 2009; Tang *et al.*, 2010b). Anno *et al.* (2002) have tuned the carrier type by adjusting the initial composition of Ba : Ga : Ge=8 : x : 46−x (x =12−20). Polycrystalline samples were synthesized by the arc-melting and SPS. The carrier type changed from n-type (x=12−16) to p-type (x=17−20), which was confirmed by the change in the signs of S and $R_{\rm H}$. The PF at high temperatures had a maximum of 22 [μW/K^{2}cm] at x=14 for n-type and that of 15 [μW/K^{2}cm] at x=19 for p-type. See Fig. 12. κ was less than 2.5 [W/(mK)]. The estimated ZT value for n-type (x=15) and p-type (x=18) reached approximately 1.0 at 900 [K]. The tunable carrier type in BGG is advantageous for constructing a thermoelectric module using p- and n-type legs.

Martin *et al.* (2006, 2007) have performed transport experiments on polycrystalline Si-Ge type-I clathrates with the nominal composition $Ba_8Ga_{16}Si_xGe_{30-x}$ such that a constant Ga-to-group-IV element ratio is maintained but with increasing Si substitution 4< x <14. Electrical transport measurements on n-type specimens show a modest increase in the absolute Seebeck coefficient and a decrease in electrical resistivity with increasing Si content. Substitution of 20 at.% Si within the Ga-Ge lattice framework of the type I clathrate BGG results in thermoelectric performance enhancement. They have interpreted these observations as a modification in the band structure with Si substitution. The band modification has been confirmed by the XAFS study by Mansour *et al.* (2012).

Martin *et al.* (2008) have identified optimal carrier density n for n-type BGG. A polycrystalline sample with n=9.86×10^{20} [cm^{-3}] exhibited high ZT=0.8 at 953 [K]. The ZT value was comparable to the values for n-type BGG reported by Kuznetsov *et al.* (2000) (ZT=0.7 for polycrystalline sample at 700 [K]), by Christensen *et al.* (2006c) (ZT=0.9 for a Czochralski-grown single crystal at 1000 [K]) by Toberer *et al.* (2008) (ZT=0.8 for a flux-grown single crystal and ZT=0.74 for a polycrystalline sample at 1000 [K]), and by Hou *et al.* (2009) (ZT ∼0.8 for a Czochralski-grown crystal at 850 [K]). The highest ZT of 1.35 at 900 [K] was reported for an n-type crystal synthesized by the Czochralski method (Saramat *et al.*, 2006), but it has not been confirmed.

We mention the band calculations and x-ray photoemission spectroscopy studies on $\mathcal{R}_8M_{16}Z_{30}$ ($\mathcal{R}$ = Sr, Ba) (Blake *et al.*, 2001; Kono *et al.*, 2010; Madsen *et al.*, 2003; Nenghabi and Myles, 2008,b; Tang *et al.*, 2009, 2011a). Madsen *et al.* (2003) have pointed out that undoped SGG and BGG are semiconductors with band gaps of 0.71 and 0.89 [eV], respectively. Tang *et al.* (2009) have revealed that the valence band is constructed mainly from the Ga/Ge 4s and 4p wave functions with little contribution of the Sr/Ba atomic orbitals. However, the conduction band hybridizes with the unoccupied d states of the guest atom. These results indicate that electrical transport and thermoelectric properties of the n-type sample are expected to depend strongly on the guest atom while those of p-type clathrate compounds are relatively unaffected. Kono *et al.* (2010) have calculated the electronic structures and the thermoelectric properties for type-I and type-VIII $Ba_8Ga_{16}Sn_{30}$ (β- and α-BGS). The calculation has shown that these compounds are indirect semiconductors with band gaps of 0.51 [eV] and 0.32 [eV], respectively. The Seebeck coefficient of n-type β-BGS is higher than that of n-type α-BGS.

B. Phonon thermal conductivity

As mentioned in Sec. III, ternary type-I clathrates have received much attention as potential high-performance thermoelectric (TE) materials because of not only the good electronic properties but also the low $\kappa_{\rm ph}$ of $\simeq$1 [W/(mK)]. Nolas *et al.* (1998a,b) have reported glass-like temperature dependences of $\kappa_{\rm ph}$ for SGG polycrystalline samples. It was then regarded to satisfy the true "phonon-glass electron-crystal" (PGEC) concept. The nature of the THz-frequency vibrational states in structural glasses has been the subject of intensive and controversial debate for decades. This is due to the difficulty in identifying the microscopic structure of glasses. The microscopic structure of clathrate compounds are well defined, and this makes it possible to interpret the origin of glass-like thermal and dynamic properties generally observed in type-I clathrates containing off-center guest atoms.

Nolas *et al.* (1998a) and Cohn *et al.* (1999) have investigated the temperature dependence of the $\kappa_{\rm ph}$ down to 60 [mK] for a SGG polycrystalline sample. $\kappa_{\rm ph}$ varies as T^2 below 1 [K] and has a plateau around 10 [K], which is quite similar to the behavior of vitreous SiO_2 in the temperature dependence in addition to the magnitude, as shown in Fig. 13. The glass-like plateau in $\kappa_{\rm ph}(T)$ has been also observed for a single crystal of SGG. However, BGG showed a crystalline peak due to Umklapp process (Keppens *et al.*, 2000), which indicates the existence of translational symmetry in the sample. We should mention that the plateau in $\kappa_{\rm ph}(T)$ has been observed in gas hydrates in the same temperature region (English and Tse, 2010; Krivchikov *et al.*, 2005).

Sales *et al.* (2001) have reported a temperature dependence of heat transport for BGG, SGG, and β-EGG using single crystals with n-type carriers. The crystals were grown by slowly cooling molten stoichiometric mixtures of the elements. For SGG and β-EGG crystals, $\kappa_{\rm ph}$ exhibits a glass-like plateau in the temperature range 10-20 [K]. See Fig. 14. The room-temperature values of $\kappa_{\rm ph}$ for SGG and β-EGG are 1.0 and 0.6 [W/(mK)], respectively. In contrast, $\kappa_{\rm ph}$ for BGG shows a typical crystalline Umklapp peak at around 10 [K]. Nevertheless, the room-temperature $\kappa_{\rm ph}$ value is no more than 1.3 [W/(mK)].

The data of $\kappa_{\rm ph}$ on type-I (β-phase) and type-VIII (α-

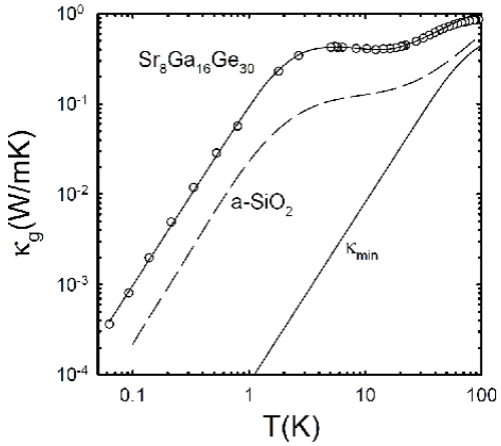

FIG. 13 Temperature dependences of phonon thermal conductivity $\kappa_{\rm ph}$ for polycrystalline samples of type-I $Sr_8Ga_{16}Ge_{30}$. The dashed line represents $\kappa_{\rm ph}$ for vitreous SiO_2. After Cohn *et al.* (1999).

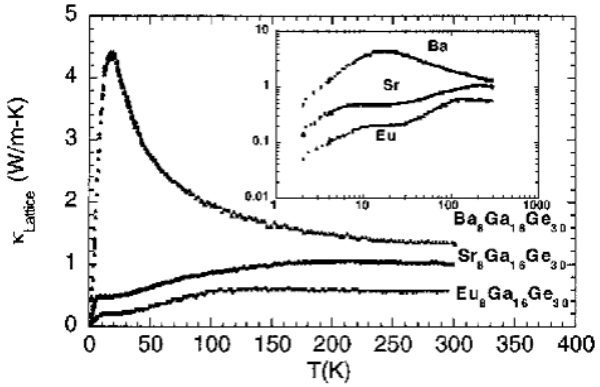

FIG. 14 Temperature dependences of phonon thermal conductivity $\kappa_{\rm ph}(T)$ for type-I $\mathcal{R}_8Ga_{16}Ge_{30}$ ($\mathcal{R}$ = Ba, Sr, Eu) single crystals. Adopted from Sales *et al.* (2001).

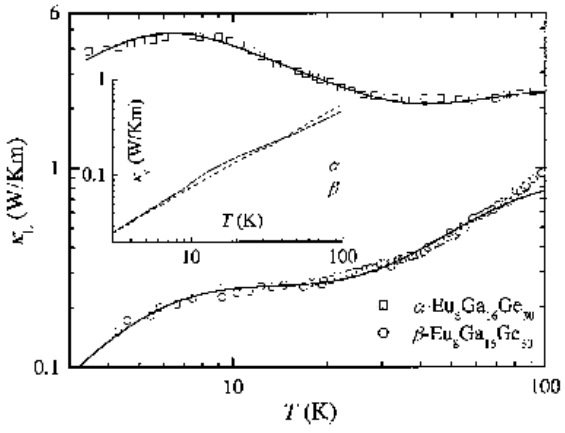

FIG. 15 Temperature dependences of phonon thermal conductivity $\kappa_{\rm ph}$ for type-I and type-VIII $Eu_8Ga_{16}Ge_{30}$ polycrystalline samples. After Paschen *et al.* (2001).

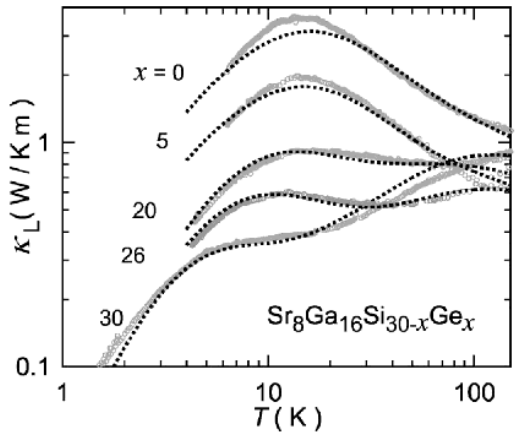

FIG. 16 Temperature dependences of phonon thermal conductivity $\kappa_{\rm ph}(T)$ vs. T on a log-log scale for type-I $Sr_8Ga_{16}Si_{30-x}Ge_x$ single crystals. After Suekuni *et al.* (2007).

phase) EGG by Paschen *et al.* (2001) are given in Fig. 15. In contrast to the plateau for the β-EGG sample, the crystalline Umklapp peak was observed around 5 [K] for a type-VIII sample. Type-I and VIII samples of EGG possess magnetic moments realizing ferromagnetic orderings at 36 and 10.5 [K], respectively.

Martin *et al.* (2006, 2007) have reported on the temperature dependence of $\kappa_{\rm ph}(T)$ of polycrystalline Si-Ge type-I clathrates with nominal composition of $Ba_8Ga_{16}Si_xGe_{30-x}$ in the temperature range 10-400 [K] with increasing Si substitution $4< x <14$.

Suekuni *et al.* (2007) have reported the variations of $\kappa_{\rm ph}$ on type-I $Sr_8Ga_{16}Si_{30-x}Ge_x$ ($0 \le x \le 30$) (SGSG) of single crystals. In these alloy series, the cage size is enlarged by the substitution of Ge for Si. The cage size expands by 8% and the guest vibrational energy decreases as x increases from 0 to 30. Thereby, the height of the peak in $\kappa_{\rm ph}$ at around 10−20 [K] was reduced and the temperature dependence of $\kappa_{\rm ph}(T)$ changed from crystal-like to glass-like as illustrated in Fig. 16. The drastic reduction in $\kappa_{\rm ph}$ suggests a strong interaction between acoustic phonons of cages and vibrational modes of Sr guests. A detailed theoretical interpretation on the above will be given in Sec. VII. $\kappa_{\rm ph}(T)$ for $x = 30$ varies as $T^{2-\delta}$ with a small factor δ <1 below 1 K (Umeo *et al.*, 2005), which confirms the data for the polycrystalline samples (Cohn *et al.*, 1999).

Some data for the thermal conductivity in polycrystalline SGG samples have displayed crystal-like peaks at 4-10 K (Uher *et al.*, 1999). These peaks may be due to metallic impurities. The samples were synthesized in a quartz tube or in a pyrolytic boron nitride (pBN) crucible placed inside a quartz tube, which were referred to as as-grown samples. The sample synthesized in the pBN was then crushed and sintered in a carbon die. For the as-grown samples, $\kappa_{\rm ph}$ shows crystalline behavior: $\kappa_{\rm ph} \propto 1/T$ and a large peak at around 4−10 [K]. On the

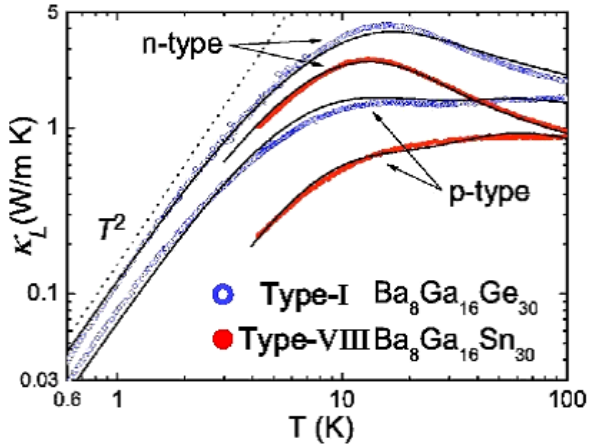

FIG. 17 (Color online) Temperature dependences of phonon thermal conductivity $\kappa_{\rm ph}$ for n- and p-type $Ba_8Ga_{16}Ge_{30}$ and type-VIII $Ba_8Ga_{16}Sn_{30}$ single crystals on a log-log scale. The data are adopted from the works of Avila *et al.* (2006b).

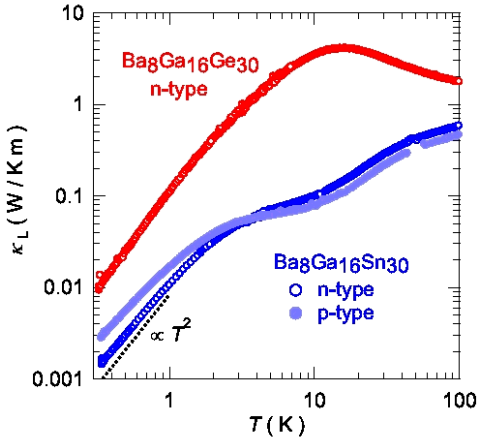

FIG. 18 (Color online) Temperature dependences of phonon thermal conductivity $\kappa_{\rm ph}(T)$ of n-type and p-type type-I $Ba_8Ga_{16}Ge_{30}$ and $Ba_8Ga_{16}Sn_{30}$ single crystals on a log-log scale. After Avila *et al.* (2006b, 2008); Suekuni *et al.* (2008a).

other hand, for the sintered sample, $\kappa_{\rm ph}$ shows a glass-like temperature dependence. Despite the similar value of the carrier density $n = 10^{21}$ [cm^{-3}], the behaviors of ρ and S seem to strongly depend on the crucible material. For samples synthesized in the quartz tube, ρ decreases to zero at helium temperatures. This is totally different from the data for single crystals with a similar carrier density of 10^{21} [cm^{-3}] (Sales *et al.*, 2001). The quite low ρ can be ascribed to the presence of highly-conducting metallic impurities, e.g., gallium. In fact, the S goes to zero at low temperatures, which is a result of a short circuit. Therefore, the crystal-like behavior in κ reported for some SGG polycrystalline samples is not intrinsic but is attributable to the metallic impurities.

For type-I BGG, a large difference in $\kappa_{\rm ph}(T)$ between the n- and p-type samples has been reported by different groups (Avila *et al.*, 2006a,b; Bentien *et al.*, 2004; Tang *et al.*, 2009). The single crystals were synthesized by the flux method using excess Ga. Avila *et al.* (2006a,b) grew the crystals with both p- and n-type carriers from nominal compositions of Ba:Ga:Ge=8:38:x, where x=30 for p-type and x=34 for n-type. $\kappa_{\rm ph}$ for the n-type samples showed a typical crystalline peak at 15 [K], which is totally suppressed for p-type samples, as shown in Fig. 17. $\kappa_{\rm ph}$ below 1 [K] for the p-type single crystal follows $\sim T^2$(Avila *et al.*, 2006b) or $\sim T^{1.5}$(Bentien *et al.*, 2006); that for n-type follows $\sim T^2$ (Avila *et al.*, 2006b). However, no difference was observed in either the crystal structure nor specific heat $C_{\rm V}(T \gtrsim 4\,[{\rm K}])$ for these compounds. Similar difference in $\kappa_{\rm ph}$ between p- and n-type samples was observed also in type-I $Ba_8Ni_{6-x}Ge_{40-x}$, $Ba_8Au_xSi_{46-x}$, and type-VIII $Ba_8Ga_{16}Sn_{30}$ (Avila *et al.*, 2006b; Aydemir *et al.*, 2011; Bentien *et al.*, 2006).

The Ba guest in type-I $Ba_8Ga_{16}Sn_{30}$ (β-BGS) has larger off-center displacement and lower guest vibration energy than that of BGG (Avila *et al.*, 2008; Suekuni *et al.*, 2008a). The carrier types of β-BGS are tunable as in BGG. $\kappa_{\rm ph}$ varies as $T^{2-\delta}$ below 1 [K] and exhibits a plateau around 4 [K] irrespective of the carrier types. See Fig. 18. The value of $\kappa_{\rm ph}$ below 10 [K] is the lowest among intermetallic clathrates. Because of the glass-like $\kappa_{\rm ph}$ and the Boson-peak like structure in the specific heat $C_{\rm V}$, β-BGS is regarded as a true phonon-glass material.

VI. SPECTROSCOPIES IN THZ FREQUENCY REGION

The excess densities of states realized as a hump in specific heats at around 10 [K] for type-I clathrate compounds have also been observed by various types of spectroscopies such as Raman scattering, infra-red absorption, and inelastic neutron scattering measurements. This Section describes in detail these observations.

A. Optical spectroscopies

1. Raman spectra and those assignments

The reflected light from crystals yields small shifts in initial frequency. This shift is called the Raman shift or scattering, which enables us investigate characteristic frequencies relevant to optical phonons in the vicinity of Γ-point ($\boldsymbol{q}$=0) in the Brillouin zone. This is due to the fact that the wave vector $\boldsymbol{k}$ of photons is negligibly small compared to that of $\boldsymbol{q}$ of optical phonon. It has been known that the Raman spectroscopy is a powerful method to access the dynamics relevant to the excess density of states.

Krishnan (1953) found during his Raman scattering experiments on silica glass a broad band in the vicinity of 30−120 [cm^{-1}], which markedly differs from the behavior of crystal quartz. Note that 1 [THz]=33.35 [cm^{-1}].

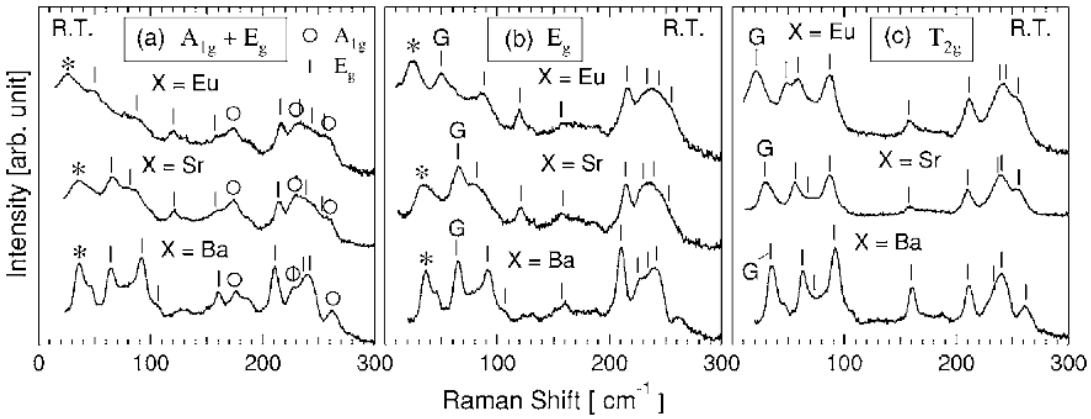

FIG. 19 Polarization dependence of Raman spectra for type-I $\mathcal{R}_8Ga_{16}Ge_{30}$ ($\mathcal{R}$ = Ba, Sr, Eu) at room temperature. "G" are the symmetry-allowed Raman active phonons, and bars and open circles denote the assigned peak. The peaks marked by $*$ are additional modes. After Takasu *et al.* (2006).

This band has its maximum intensity at the low frequency end and the intensity falls off continuously. The broad and intense band has been also observed in various types of topologically disordered amorphous materials or structural glasses by Raman scattering, inelastic neutron scattering and infrared absorption. It should be noted that Helen *et al.* (2000) have performed hyper-Raman scattering experiments to investigate the broad band in the THz region in silica glass. The relevant mode obtained by hyper-Raman scattering principally involves rotational motion of SiO_4 tetrahedra. This mode corresponds to the mode suggested by Buchenau *et al.* (1984, 1986) from the analysis of their inelastic neutron scattering data.

Type-I clathrates have three distinct cage sites 6*c*, 16*i*, and 24*k*. The guest(1) occupies the 2*a* sites in the dodecahedra, and the guest(2) does the 6*d* sites in the tetrakaidecahedra. There are 54 atoms per unit cell and thus 162 (3×54) phonon modes at the Γ-point. Group theory of lattice vibrations for type-I clathrates with a cubic primitive structure $Pm\bar{3}n$ indicates the number of Raman-active vibrational modes $3A_{1g}+7E_g+8T_{2g}$ relevant to the cage atoms. The group theory also ensures the existence of two guest(2) modes E_g and T_{2g} under the assumption that the guest(2) occupies the on-center 6*d* site. Because the vibrations of the guest(1) at the 2*a* site are *not* Raman active, all observed guest modes are attributed to the guest(2) atoms.

Raman scattering from a polycrystalline sample provides all active modes. The study of β-$\mathcal{R}_8Ga_{16}Ge_{30}$ ($\mathcal{R}$= Sr and Eu) has provided assignments of the guest(2) and cage modes (Nolas *et al.*, 2000b). However, they were unable to identify all of the modes due to the numerous Raman active modes.

Takasu *et al.* (2006) have given full assignments to the Raman active modes observed for type-I $\mathcal{R}_8Ga_{16}Ge_{30}$ ($\mathcal{R}$=Ba, Sr and Eu) by combining polarized Raman scattering measurements on single crystals with first principles calculations. Vibrational modes with each irreducible representation have been determined by polarization dependence measurements. The polarization geometry is represented by the notation (α, β), where α and β denote the polarization directions of incident and scattered light, respectively. Three geometries of (x, x), (x,y), and (x+y,x-y) were employed, where x and y correspond to the [100] and [010] crystal axes, respectively. The phonon with A_{1g} symmetry appears in (x,x), E_g in both (x,x) and (x+y,x-y), and T_{2g} in (x,y). The A_{1g} spectra have been obtained by subtracting the E_g spectra from the A_{1g}+E_g.

The Raman spectra of the A_{1g}+E_g, E_g, and T_{2g} modes are shown in Fig. 19 for the three compounds at room temperature (Takasu *et al.*, 2006). The modes above 70 [cm^{-1}] are fully assigned as cage modes in comparison with the energies obtained by experiments and calculations. For $\mathcal{R}$=Ba, the $E_g(1)$ mode at 64 [cm^{-1}] and $T_{2g}(1)$ at 34 [cm^{-1}], marked by gGh in Fig. 19, is assigned to the modes for Ba(2). The $E_g(1)$ mode concerns guest vibrations along the four-fold axis; and the $T_{2g}(1)$ concerns the vibrations in the plane perpendicular to the fourfold axis and along the [100] axis. The modes for Sr(2) and Eu(2) have been assigned by comparing the analogous spectral shape between $\mathcal{R}$=Ba, Sr, and Eu. The energy of the $T_{2g}(1)$ mode at room temperature decreased on going from Ba(2) (34 [cm^{-1}]), Sr(2) (30 [cm^{-1}]), and to Eu(2) (21 [cm^{-1}]). The energies for Ba(2) and Sr(2) agreed with those obtained from the analysis of specific heat data (Avila *et al.*, 2006b; Suekuni *et al.*, 2007).

Besides the assigned peaks, there are two additional modes, marked by asterisks in Fig. 19, in the low-energy region of the A_{1g}+E_g and E_g spectra (Takasu *et al.*, 2006). Particularly for $\mathcal{R}$=Eu, the good subtraction of the E_g from A_{1g}+E_g has allowed us to assign the additional modes to one A_{1g} and one E_g mode. These modes were identified as the vibrations of the guest(2).

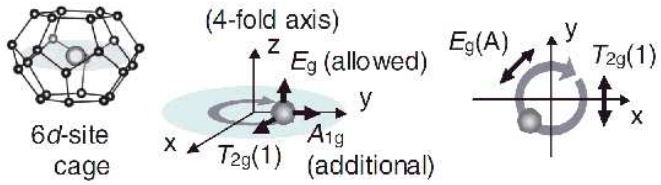

FIG. 20 c) Illustration of librational modes of the guest atom $\mathcal{R}(2)$. See the text for the notations of additional A_{1g} , E_g(A), and $T_{2g}(1)$. Adopted from Takasu *et al.* (2008).

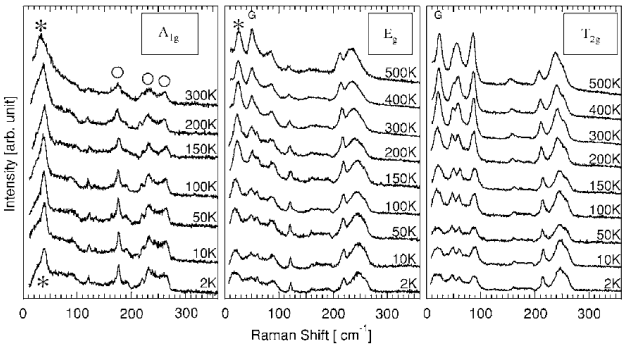

FIG. 21 Temperature dependences of Raman spectra for type-I $Eu_8Ga_{16}Ge_{30}$. After Takasu *et al.* (2006).

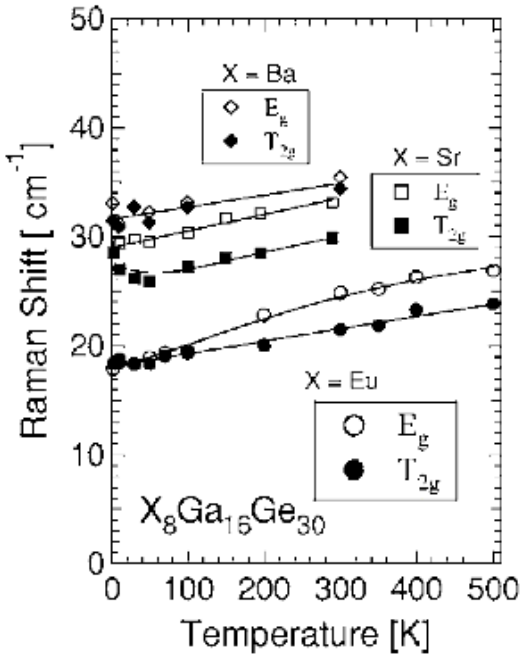

FIG. 22 Temperature dependences of mode energies of guest atoms, $T_{2g}(1)$ and E_g(A), for type-I $\mathcal{R}_8Ga_{16}Ge_{30}$ ($\mathcal{R}$ = Ba, Sr, Eu). After Takasu *et al.* (2006).

Neutron diffraction experiments have provided evidence that the nuclear density of the guest atom Eu(2) departs from the 6*d* site of cage-center to one of four off-center 24*k* sites along the [1,0,0] direction (Chakoumakos *et al.*, 2001; Sales *et al.*, 2001). This deviation lowers the site symmetry from $4\bar{2}m$ (6*d*) to *m* (24*k*). The lowered symmetry does not affect the $E_g(1)$ and $T_{2g}(1)$ modes, but the displacement along the [1,0,0] direction, corresponding to the A_{1g}(A) mode, becomes Raman active, as shown in Fig. 20 (Takasu *et al.*, 2008). The additional E_g(A) mode has been identified as the tangential fluctuation to [1,1,0]. Thus, the vibrations of the guest(2) have been described as rotational or librational modes,together with an additional A_{1g} mode.

2. Temperature, carrier-type, and pressure dependences of Raman spectra

Temperature dependences of the Raman spectra for the guest atom $\mathcal{R}$ = Eu are shown in Figs. 21 and 22 (Takasu *et al.*, 2006, 2007). The modes related to cages show no anomalous dependence on cooling from 500 [K] to 2 [K], in which temperature range their energy increases due to the thermal shrinkage effect. This is the same tendency for $\mathcal{R}$=Ba and Sr. However, it should be emphasized that the vibrational energies of the $T_{2g}(1)$ and E_g(A) on the guest(2) *decrease* on cooling. This anomalous softening can be primarily explained by the relevance of the anharmonic potential including a quartic term; $U(u) = k_0 + k_2u^2 + k_4u^4$, from which the mode frequency ω is expressed by $\omega^2 = \omega_0^2 + k_4\langle u^2\rangle$ under a self-consistent phonon approximation where ω_0 is the eigenfrequency of the harmonic term, k_4 the coefficient of the quartic anharmonic potential, and $\langle u^2\rangle \propto T$ is a mean-square atomic displacement of the guest(2), respectively. The quantity $\langle u^2\rangle$ explains the temperature dependence of ω^2 and Raman spectra relevant to the guest(2) on cooling.

For $\mathcal{R}$=Ba, the energy of $T_{2g}(1)$ coincides with that of E_g(A) at temperatures between 300 [K] and 2 [K], as shown in Fig. 22 (Takasu *et al.*, 2006). For the $\mathcal{R}$=Sr and Eu, the energy of $T_{2g}(1)$ is lower than that of E_g(A) at 300 [K]. This means that the potential minima are located toward the [100] direction which points from the high symmetry 6*d* site to the off-center 24*k* sites.

Vibrational properties of pseudo-ternary systems $\mathcal{R}_8Ga_{16}Si_{30-x}Ge_x$ ($\mathcal{R}$= Ba and Sr) have also been investigated in terms of the Raman spectroscopy (Takasu *et al.*, 2008). The vibrational energies of the guest(2) have decreased clearly with increasing Ge content x and cage size. For Ba samples of the end compositions $x = 0$ and $x = 30$ and the Sr compound with $x = 0$, the energy difference between $T_{2g}(1)$ and E_g(A) was small, indicating an isotropic potential at the guest(2) site for the these samples. For the Sr samples with x=20 and x=30, the difference becomes larger with increasing cage size, and thereby the energy of the $T_{2g}(1)$ was lower than that of the E_g(A). The results indicate that the potential anisotropy for Sr(2) between the [100] and [110] directions emerges with increasing

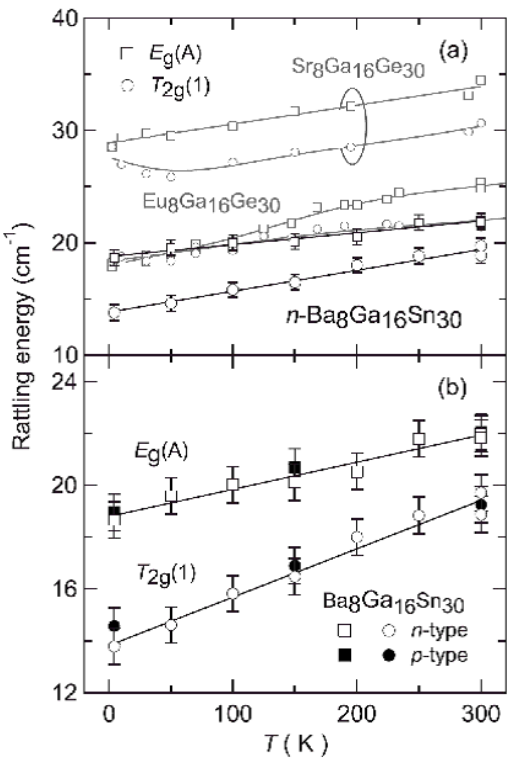

FIG. 23 Temperature dependences of the mode energies, $T_{2g}(1)$ and E_g(A), for n- and p-type of type-I $Ba_8Ga_{16}Sn_{30}$ and $\mathcal{R}_8Ga_{16}Ge_{30}$ ($\mathcal{R}$=Sr, Eu). Adopted from Takasu *et al.* (2006) and Suekuni *et al.* (2010).

the cage size.

Compared with $Ba_8Ga_{16}Ge_{30}$ (BGG), type-I $Ba_8Ga_{16}Sn_{30}$ has a larger cage, which results in a larger off-center deviation of Ba(2). The energy of $T_{2g}(1)$ is lower than that of the E_g(A) at temperatures between 300 [K] and 4 [K] (Suekuni *et al.*, 2010), indicating the strong anisotropy of the potential at the Ba(2) site. The energy of $T_{2g}(1)$ at 4 [K] in Fig 23 is 14 [cm^{-1}], which is lower than that in $\mathcal{R}_8Ga_{16}Ge_{30}$ for $\mathcal{R}$ = Ba (31 [cm^{-1}]), Sr (29 [cm^{-1}]), and Eu (18 [cm^{-1}]).

For BGG, carrier-type (n- and p-type) dependences of Raman spectra have been studied by Takasu *et al.* (2010). They have observed the additional E_g(A) mode independent of carrier types. For both n- and p-types, the decrease in the energies of $T_{2g}(1)$ and E_g(A) modes upon cooling provides information concerning the anharmonic potential for the guest Ba(2). The energy difference between $T_{2g}(1)$ and E_g(A) was larger in the p-type, and the energy of the $T_{2g}(1)$ was clearly lower than that of the E_g(A). Therefore, the potential anisotropy at the Ba(2) site is stronger in p-type. Furthermore, it has been clarified that the potential energy difference between the [100] and [110] directions is proportional to the off-center deviation of the guest(2) from the cage center in a series of type-I clathrates. The Raman intensity of cage vibrations at the 6c site for p-type is weaker than that for n-type, indicating that the vibration amplitude at the 6c site is smaller in the case of p-type. These experimental findings suggest that the 6c-site in p-type provides the guests with a larger space.

Raman scattering experiments under high pressure have provided important information on the structural stability of type-I clathrate compounds (Kume *et al.*, 2010; Shimizu *et al.*, 2009,b). The phase transition and the vibrational properties of BGG have been investigated at pressures up to 40 [GPa] at room temperature by Kume *et al.* (2010). They have demonstrated the occurrence of a first-order phase transition at 33 [GPa] by combining Raman scattering and synchrotron x-ray powder diffraction (XRD) experiments at high pressures. The Raman spectra showed anomalies at around 17 [GPa]. They have investigated the shift of vibrational frequency of the guest Ba as a function of the cage size. The results have indicated a linear relation between the vibrational frequency and the cage size.

The deviation of nearest-neighboring Ba(2) atoms create electric dipole fields (Takasu *et al.*, 2010). The T_{1u} and T_{2g} modes are correlated with the motion of the neighboring Ba(2) guests, and the corresponding dipole moment lies along its direction. The dipole fields of the T_{1u} and T_{2g} modes are directed opposite. In fact, the dipole interaction yields the energy shift: the energy of T_{1u} is larger by about 6 [cm^{-1}] than that of T_{2g}, indicating the existence of interacting dipoles between the neighboring terakaidecahedra.

3. Infrared spectroscopy in the terahertz (THz) frequency range

Terahertz (THz) frequency spectroscopy plays an important role for the investigation of the characteristics of vibrational modes not accessible by other optical spectroscopies such as Raman scattering. In this method, input and propagated electromagnetic pulse-shapes are measured. Fourier analysis of both pulses enables us to obtain the frequency-dependent absorption and dispersion of the observed spectra. Infrared-active phonon modes can be investigated in terms of this spectroscopy. THz time-domain spectroscopy (THz-TDS) has been successfully adopted for investigating vibrational properties of various kinds of clathrates. Ultrafast laser pulses generate short pulses of broadband THz radiation, which provide both high sensitivity and time-resolved phase information for the transmitted THz electric fields. Group theory of the lattice vibrations of type-I clathrates with cubic primitive structure $Pm\bar{3}n$ gives the infrared-active vibrational modes of ten T_{1u} for the cage atoms, one T_{1u} for the guest(1), and two T_{1u} for the guest(2) under the situation that guest(2) occupies the on-center 6d site.

THz-TDS studies on p-type $Ba_8Ga_{16}Ge_{30}$ single crystal with on-center guest atoms have been performed in the frequency range between 0.2 [THz] and 3.5 [THz] (Mori *et al.*, 2009). As shown in Fig. 24, peaks in conductivity spectra at ν_1=1.15 [THz] and ν_2=1.80 [THz] are identified with the guest(2) modes.

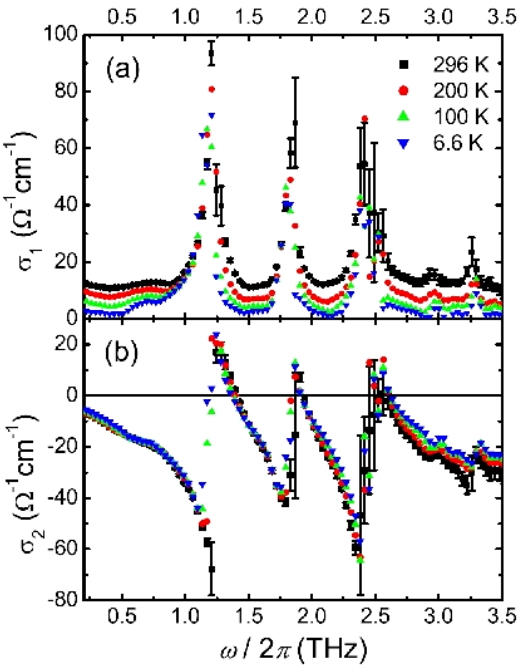

FIG. 24 (Color online) Temperature dependences of conductivity $\sigma(\omega)$=$\sigma_1(\omega)$ + $i\sigma_2(\omega)$ for type-I $Ba_8Ga_{16}Ge_{30}$. After Mori *et al.* (2009).

They have assigned these modes as vibrational modes of Ba(2) in the plane perpendicular to the fourfold axis and that along the [100] axis, respectively. The broad peak around 2.4 [THz] (ν_3 and ν_4) results from a hybridization between the cage mode and Ba(1) vibrations. Two peaks at higher frequencies are the cage modes.

The energies of ν_1 and ν_2 decrease by 4.2% with decreasing temperature from 300 [K] to 6.6 [K]. The decrease is attributed to the anharmonic potential at the Ba(2) site, as will be theoretically discussed in VII.A.2. For other modes, however, the mode energies slightly increased with decreasing temperature as a result of the effect of thermal shrinkage. The temperature dependence of each mode was consistent with the results of Raman scattering (Takasu *et al.*, 2006).

The vibrational modes for type-I $Ba_8Ga_{16}Sn_{30}$ single crystal with off-center guest atoms have been investigated in the frequency range between 0.3 and 3.0 [THz] (Mori *et al.*, 2011). As shown in Fig. 25, the mode with the lowest energy ν_1=0.72 [THz] at 296 [K] is assigned as the vibrations relevant to the off-center Ba(2) guest in the plane perpendicular to the fourfold axis. The observed peak was fitted by superposing two Lorentzian curves. The peak energy, defined as the peak position of the superposed curves, decreases by 7% with decreasing temperature down to 100 [K], and then *increases* with further decreasing temperature. Such anomalous peak-shape and temperature-dependence were not observed for type-I $Ba_8Ga_{16}Ge_{30}$

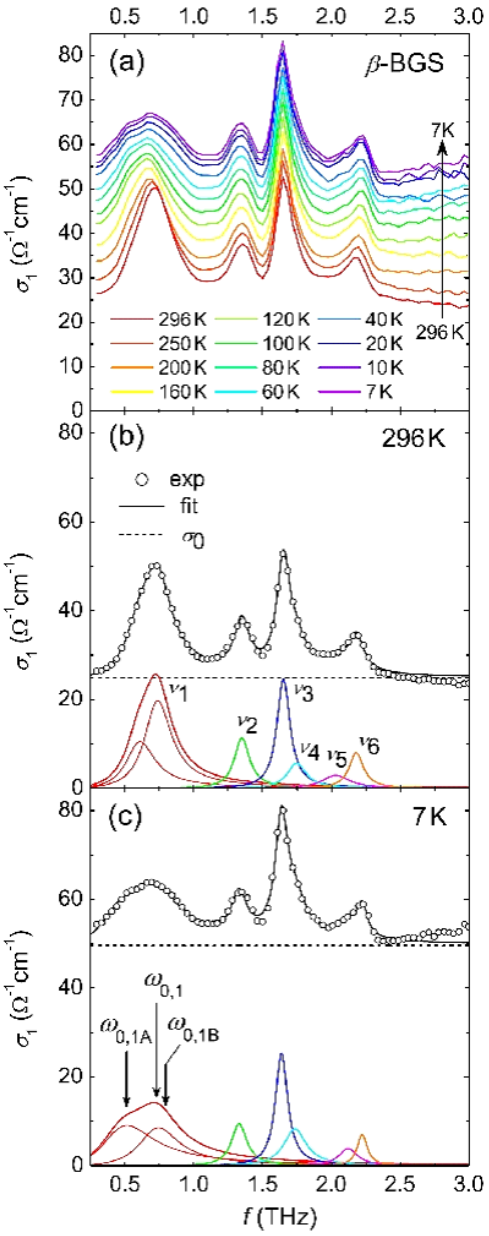

FIG. 25 (a) (Color online) Temperature dependences of real part of conductivities σ_1 for type-I $Ba_8Ga_{16}Sn_{30}$. (b) and (c) represent experimental data (open circles) and fitting results (solid lines) at 296 [K] and 7 [K], respectively (see text). After Mori *et al.* (2011).

containing on-center guest atoms. They have tried to explain the peak splitting at low temperatures assuming a one-dimensional double-well potential. The energy levels with quantum numbers n=0 and 1 are quasi-degenerate, whereas the n=2 and 3 levels are well separated due to the moderately deep potential well. At sufficiently low temperatures, the optical transitions occur mainly from n = 0 to 3 and from n=1 to 2 owing to a parity requirement of the wave functions. As a result, these two transitions result in double peaks. However, significant

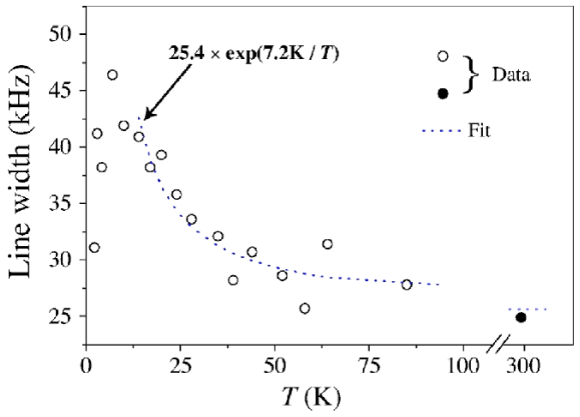

FIG. 26 ^{71}Ga NMR linewidth (square root of second moment) vs. temperature for type-I $Sr_8Ga_{16}Ge_{30}$. Adopted from Gou *et al.* (2005).

broadening of the spectra for the guest(2) towards low temperature was not reproduced by assuming this type of one-dimensional potential. The mechanism of this broadening at low temperatures will be discussed in VII.C.2.

NMR study provides important information on the motion of encaged guest atoms depending on temperature. Gou *et al.* (2005) have performed NMR studies for $Sr_8Ga_{16}Ge_{30}$ belonging to the category of an off-center system. They have measured ^{71}Ga NMR down to 1.9 [K]. The values of Knight shift and T_1 showed low density metallic behavior. There is a significant increase in linewidth above 4 [K] attributing to atomic motion, as shown in Fig. 26. They have estimated the relevant time scale of roughly $\tau \sim 10^{-5}$ [s] from the inverse of the linewidth. From the time scale of the narrowing of the NMR line, they have concluded that the reduced high-temperature width is due to motional narrowing. The point is that this is very slow compared with relevant vibrational frequencies of $\omega_{\rm ph}/2\pi \simeq 1$ [THz], and the relation $\omega_{\rm ph}\tau \gg 1$ holds. This indicates very slow hopping rates of Sr atoms between sites within the same cage. Another point is that the motion of guest atoms can be treated as vibrational.

Arcon *et al.* (2013) have performed ^{71}Ga NMR experiments on type-I SGG and BGG in order to extract the contributions from different Ga sites at randomly occupied Ga/Ge sites. They have claimed that the effect of weak covalent bonding should be taken into account in addition to ionic interactions.

B. Inelastic neutron scattering

Time-of-flight inelastic neutron scattering (INS) is a powerful technique for the investigation of vibrational states in clathrate compounds. In INS experiments, the energy $\hbar\omega$ and wavelength λ of incident neutrons can be taken as comparable to those of excited phonon energies and the length scale of lattice spacing, respectively. From this wavelength-energy relation, INS experiments have been proven to be unique for the study of the dynamic properties of materials on the atomic scale (Lovesey, 1984; Squires, 1978).

The quantity obtained by INS experiments is the dynamic structure factor $S(\boldsymbol{Q},\omega)$, which provides information projected onto plane-wave states since this is defined through the spatio-temporal Fourier transformation. When one projects exact eigenstates onto plane-wave states, a lifetime is obtained in frequency or wave vector space, where the width arises from that a plane-wave would experience. Thus, it is necessary to take into account this point for the interpretation of the energy width of local modes associated with $\mathcal{R}(2)$ guest atoms in cages.

1. Dynamic structure factor and the flat dispersion relation of phonons

Vibrational dynamics in the terahertz (THz) frequency range is the most important aspect for clarifying the glass-like phonon thermal conductivity $\kappa_{\rm ph}(T)$ in type-I clathrate compounds, because the upper limits of frequencies of acoustic branches appear in this frequency range. The THz frequency dynamics concerns the lowest two bands: acoustic and the lowest optic modes originating from networked cages and $\mathcal{R}(2)$ guest atoms.

The deformed vibrations of cages themselves manifest higher energy states than those in the THz frequency region. For this reason, it is sufficient to treat the rigid cage as having a mass M and an effective charge $-e^*_C$, and the $\mathcal{R}(2)$ guest atom with mass m and charge e^*_G. We define the position vector of the ℓ-th cage at time t as $\boldsymbol{R}_\ell + \boldsymbol{r}_\ell(t)$, where $\boldsymbol{R}_\ell$ is the equilibrium position of the ℓ-th cage center. The vector $\boldsymbol{r}_\ell(t)$ represents a small deviation from $\boldsymbol{R}_\ell$. The position of $\mathcal{R}(2)$ guest atom from the center of ℓ-th cage $\boldsymbol{R}_\ell$ is defined by the vector $\boldsymbol{U}_\ell + \boldsymbol{u}_\ell(t)$, where $\boldsymbol{U}_\ell$ is the equilibrium position of the $\mathcal{R}(2)$ guest atom with respect to $\boldsymbol{R}_\ell$, and $\boldsymbol{u}_\ell(t)$ is a small deviation from $\boldsymbol{U}_\ell$ at time t. Note that $\boldsymbol{U}_\ell \neq 0$ corresponds to the case of an *off-center* guest atom, while the *on-center* case becomes $\boldsymbol{U}_\ell = 0$. Figure 27 gives the definitions of the vectors $\boldsymbol{R}$, $\boldsymbol{r}_\ell(t)$, $\boldsymbol{U}_\ell$ and $\boldsymbol{u}_\ell(t)$.

The dynamic structure factor $S(\boldsymbol{Q},\omega)$ is proportional to the spatio-temporal Fourier transform of the density-density correlation function defined by

$$G(|\boldsymbol{r}-\boldsymbol{r}'|,t) = \langle \rho(\boldsymbol{r},t)\rho(\boldsymbol{r}',0)\rangle\,, \tag{31}$$

where $\rho(\boldsymbol{r},t)$ is the atomic number density at the time t, and the angular brackets denote an ensemble average at an equilibrium state. The variation of the atomic number density, e.g., induced by vibrations of $\mathcal{R}(2)$ guest atom , is defined as

$$\rho(\boldsymbol{r},t) = \sum_\ell \delta(\boldsymbol{D}_\ell + \boldsymbol{d}_\ell(t) - \boldsymbol{r}), \tag{32}$$

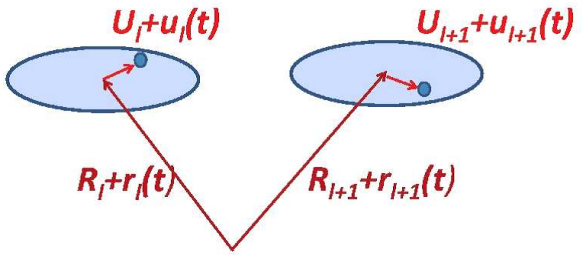

FIG. 27 (Color online) The definition of the position vector of the ℓ-th cage at time t as $\boldsymbol{R}_\ell + \boldsymbol{r}_\ell(t)$, where $\boldsymbol{R}_\ell$ is the equilibrium position of the ℓ-th cage center. The vector $\boldsymbol{r}_\ell(t)$ represents a small deviation from $\boldsymbol{R}_\ell$. The position of $\mathcal{R}(2)$ guest atom from the center of ℓ-th cage $\boldsymbol{R}_\ell$ is defined by the vector $\boldsymbol{U}_\ell + \boldsymbol{u}_\ell(t)$, where $\boldsymbol{U}_\ell$ is the equilibrium position of $\mathcal{R}(2)$ guest atom from $\boldsymbol{R}_\ell$, and $\boldsymbol{u}_\ell(t)$ is a small deviation from $\boldsymbol{U}_\ell$ at time t.

where the definitions $\boldsymbol{D}_\ell = \boldsymbol{R}_\ell + \boldsymbol{U}_\ell$ and $\boldsymbol{d}_\ell(t) = \boldsymbol{r}_\ell(t) + \boldsymbol{u}_\ell(t)$ apply. The $\boldsymbol{Q}$-component of the spatial Fourier transform of Eq. (32) becomes

$$\rho_{\boldsymbol{Q}}(t) = \sum_\ell \mathrm{e}^{-i\boldsymbol{Q}\cdot(\boldsymbol{D}_\ell + \boldsymbol{d}_\ell(t))}. \tag{33}$$

The dynamicstructure factor $S(\boldsymbol{Q},\omega)$ is proportional to the differential cross section for incident neutrons through the formula,

$$\frac{\mathrm{d}^2\sigma}{\mathrm{d}\Omega \mathrm{d}E} = \frac{k_\mathrm{f}}{k_\mathrm{i}}\frac{\bar{\sigma}}{4\pi}\mathrm{e}^{-\beta\hbar\omega/2} S\left(\boldsymbol{Q},\omega\right), \tag{34}$$

where k_i and k_f are the strength of the initial and final momenta of the neutrons. The change of momentum is given by $\hbar\boldsymbol{Q} = \hbar(\boldsymbol{k}_\mathrm{f} - \boldsymbol{k}_\mathrm{i})$, and $\hbar\omega = (\hbar^2/2m)(k_\mathrm{f}^2 - k_\mathrm{i}^2)$ is the change of energy of the incident neutron. $\bar{\sigma}$ is an arbitrarily chosen microscopic scattering cross section. The dynamic structure factor $S(\boldsymbol{Q},\omega)$ is expressed by the Fourier transform of Eq. (31) as

$$S(\boldsymbol{Q},\omega) = \frac{1}{2\pi\hbar N}\int_{-\infty}^{\infty}\mathrm{d}t \mathrm{e}^{-i\omega t} \times \sum_{\ell,\ell'}^{N} \bar{b}_\ell \bar{b}_{\ell'} \left\langle \mathrm{e}^{i\boldsymbol{Q}\cdot(\boldsymbol{D}_\ell + \boldsymbol{d}_\ell(t))} \mathrm{e}^{-i\boldsymbol{Q}\cdot(\boldsymbol{D}_{\ell'} + \boldsymbol{d}_{\ell'}(0))} \right\rangle, \tag{35}$$

where $\bar{b}_\ell$ is the neutron scattering length of atom ℓ, and N is its total number. The sum is taken over all atoms ℓ, ℓ' ($\ell \neq \ell'$) of the system. The expansion of Eq. (33) in terms of the small deviation $\boldsymbol{d}_\ell(t)$ yields the first-order density fluctuation,

$$\Delta\rho_{\boldsymbol{Q}}(t) = \sum_\lambda \Delta\rho_\lambda(\boldsymbol{Q},t) + O(d^2), \tag{36}$$

where the first term is expressed by

$$\Delta\rho_\lambda(\boldsymbol{Q},t) = -i\hbar\sum_{\lambda,\ell}\frac{\boldsymbol{Q}\cdot\boldsymbol{e}_\lambda}{\sqrt{2M_\ell\omega_\lambda}} \times \mathrm{e}^{-i\boldsymbol{Q}\cdot\boldsymbol{D}_\ell}\left(\phi_\lambda\left(\boldsymbol{D}_\ell\right)a_\lambda^\dagger(t) + \mathrm{h.c.}\right). \tag{37}$$

Here h.c. means the Hermitian conjugate, $\boldsymbol{e}_\lambda$ the polarization vector of the λ-mode, and ϕ_λ the associated eigenfunction, respectively. The $a_\lambda^\dagger(a_\lambda)$ is the creation (annihilation) operator of the phonon mode λ. M_ℓ means the mass of atoms in the ℓ-th cell. The substitution of Eq. (37) into Eq. (35) expanded up to the first order in $\boldsymbol{d}_\ell(t)$ yields the coherent inelastic term for the dynamic structure factor given by

$$S(\boldsymbol{Q},\omega) = \frac{n(\beta\omega+1)}{N\bar{\sigma}}\sum_\lambda 4\pi\delta(\omega-\omega_\lambda) \times \left|\sum_\ell \bar{b}_\ell \frac{(\boldsymbol{Q}\cdot\boldsymbol{e}_\lambda)\,\phi_\lambda\left(\boldsymbol{D}_\ell\right)}{\sqrt{2M_\ell\omega_\lambda}}\mathrm{e}^{-i\boldsymbol{Q}\cdot\boldsymbol{D}_\ell}\right|^2, \tag{38}$$

where $n(\beta\omega+1)$ is the Bose-Einstein (BE) distribution function with the definition $\beta = 1/k_\mathrm{B}T$.

Equation (38) indicates that $S(\boldsymbol{Q},\omega)$ becomes a flat dispersion relation independent of $\boldsymbol{Q}$ for a spatially localized mode ϕ_λ. This point is realized in the results of INS experiments on type-I clathrae compounds as given in VI.B.2 and VI.B.3. The phonon densities of states (PDOS) can be obtained from the INS measurements, though caution is needed in the case of multicomponent systems due to different scattering lengths $\bar{b}_\ell$ for different atomic species.

2. Inelastic neutron scattering experiments for on-center systems

INS measurements on polycrystalline powder samples of type-I $\mathcal{R}_8\mathrm{Ga}_{16}\mathrm{Ge}_{30}$ ($\mathcal{R}$=Ba and Sr) have been performed by Hermann *et al.* (2005) and Christensen *et al.* (2006b). Hermann *et al.* (2005) have investigated the phonon density of states (PDOS) in the THz frequency range associated with $\mathcal{R}(2)$ guest atoms in both $\mathcal{R}$=Ba and Sr. The case $\mathcal{R}$=Ba belongs to the category of quasi-on-center system showing the crystalline Umklapp process of phonon thermal conductivity $\kappa_\mathrm{ph}(T)$, while the $\mathcal{R}$=Sr belongs to off-center system yielding the glass-like plateau thermal conductivity at around 10 [K], as shown in Figs. 14 and 16. Christensen *et al.* (2006b) have observed the PDOS of three powder-samples of $\mathcal{R}$=Sr, and n- and p-type $\mathcal{R}$=Ba. See Fig. 28. These results (Christensen *et al.*, 2006b; Hermann *et al.*, 2005) involve information about both quasi-on-center and off-center systems, so we will discuss in detail these results in the next subsection VI.B.3 by focusing on the essential difference between the dynamics of on-center and off-center systems.

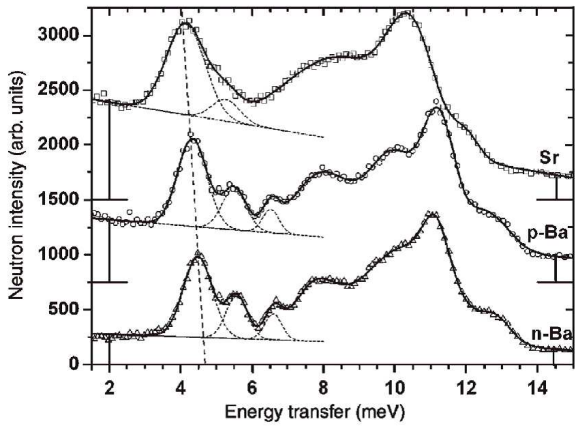

FIG. 28 Neutron scattering intensity corresponding to phonon densities of states (PDOS) for type-I n-$Sr_8Ga_{16}Ge_{30}$, p-$Ba_8Ga_{16}Ge_{30}$ and n-$Ba_8Ga_{16}Ge_{30}$. Gaussian fits have been shown for the first curves. After Christensen *et al.* (2006b).

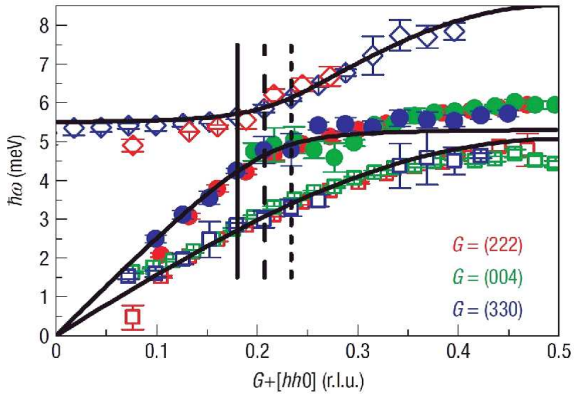

FIG. 29 (Color online) Phonon dispersion curves for quasi-on-center $Ba_8Ga_{16}Ge_{30}$ along [hh0] around the positions G= (222) (red), G= (004) (green) and G= (330) (blue). The error bars represent the standard deviation of the fitted energies. After Christensen *et al.* (2008).

Lee *et al.* (2007a) have carried out coherent INS experiments on a single crystal of $Ba_8Ga_{16}Ge_{30}$ belonging to a quasi-on-center system using triple-axis spectrometer. They obtained the phonon dispersion relations along the [100] direction in the THz frequency range. The results close to the Γ-point have proved the optical mode with T_u symmetry associated with the Ba(2) guest atom at E=4.5 [meV]. It is remarkable that the anti-crossing between the optic mode and the acoustic mode in the THz region was observed at around $\boldsymbol{q}$=(0.45,0,0) in the Brillouin zone, which indicates that the Ba(2) guest atoms play a crucial role for splitting out the acoustic modes attributable to the vibrations of networked cages.

Christensen *et al.* (2008) have observed the avoided crossing in $Ba_8Ga_{16}Ge_{30}$ containing quasi-on-center Ba(2) guest atom by using a 13 [g] single crystal. The dispersion curve of a (330) reflection along [110] direction exhibits the avoided crossing between longitudinal acoustic phonon and the optic mode attributing to the Ba(2) guest atom at h=0.225 of (3,3,0)+[h,h,0]. See Fig. 29. They have estimated the phonon life-time τ from the data of the scattered intensity of incident neutron. The τ of the phonons around the avoided crossing area is about 2 [ps], which is much longer than 0.2 [ps] obtained from the simple relation $\kappa_{ph}(T)=C_{ph}(T)v^2\tau/3$ using known values of the κ_{ph}, the specific heat $C_{ph}(T)$ of acoustic phonons, and the average phonon velocity v. This discrepancy indicates that this simple relation for $\kappa_{ph}(T)$ is not applicable in the region of flattened dispersion relations of acoustic phonons.

Christensen *et al.* (2009) have carried out INS experiments for powder samples of type-I $Ba_8\mathcal{Y}_xGe_{46-x}$ ($\mathcal{Y}_x$=Ni_6, Cu_6, Zn_8, Ga_{16}) under pressure of 9 [kbars]. The phonon thermal conductivities of these samples show the crystalline Umklapp peak at around 10 [K] except p-type $Ba_8Ga_{16}Ge_{30}$ (Bentien *et al.*, 2006). Christensen *et al.* (2009) have imposed chemical pressure by atomic substitution, and the physical pressure of 9 [Kbars] was applied using a clamp cell. The volume reduction induced by the physical pressure increases the energy of the modes associated with the guest atom. A softening of the mode energies was observed upon cooling the sample. Both p-type and n-type BGG showed a similar temperature dependence.

Koza *et al.* (2010) have performed INS experiments for $Ba_8Zn_xGe_{46-x-y}Ø_y$ with x=0, 2, 4, 6, 8 and y=3-3x/8, where Ø denotes a vacancy. They have studied the modulation of the eigenfrequency distribution of these compounds by progressively substituting Ge by Zn in addition to probing its dependence on temperature between 2 and 300 [K]. A number of peaks were shifted toward higher energies by about 1−2 [meV] as a result of the substitution. Measurements on temperature-dependence have demonstrated a hardening of the overall frequency distribution upon cooling. They observed a softening upon cooling of the lowest peak energy at 4.5−4.8 [meV] with a relative shift of 5% from 300 [K] too 2 [K], whose peak is attributable to the Ba(2) guest atom.

Euchner *et al.* (2012) have made a high-resolution INS study of the PDOS and the phonon dispersion relation on $Ba_8Ni_{6-x}Ge_{40+x}$. They have obtained evidence of spectral weight transfer between acoustic and optical phonons due to the strong hybridization. These data exclude an interpretation in terms of independent oscillators, e.g., the Einstein model or the soft potential model, since the relevance of hybridized modes between the Ba(2) guest atom and network cages are evident. The phonon life times are at least an order of magnitude larger than those estimated from $\kappa_{ph}(T)$.

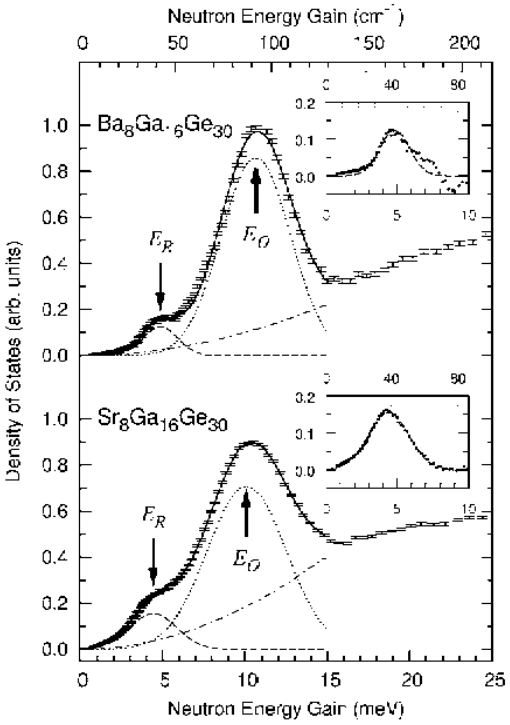

FIG. 30 The phonon densities of states (PDOS) of type-I $Ba_8Ga_{16}Ge_{30}$ and $Sr_8Ga_{16}Ge_{30}$ obtained from INS measurements. The dashed line is the contribution of the modes associated with Ba(2) guest atoms and Sr(2), the dotted-dashed line is the parabolic Debye contribution, and the dotted line is a Gaussian fit to the optical phonon density of states below 15 [meV]. Because both the neutron scattering lengths of Ba and Sr are different, the measured PDOS have been arbitrarily scaled. Insets: The Gaussian peaks at E_R associated with Ba(2) and Sr(2). Deviations in the inset for type-I $Ba_8Ga_{16}Ge_{30}$ are related to the Ba(1) mode. After Hermann *et al.* (2005).

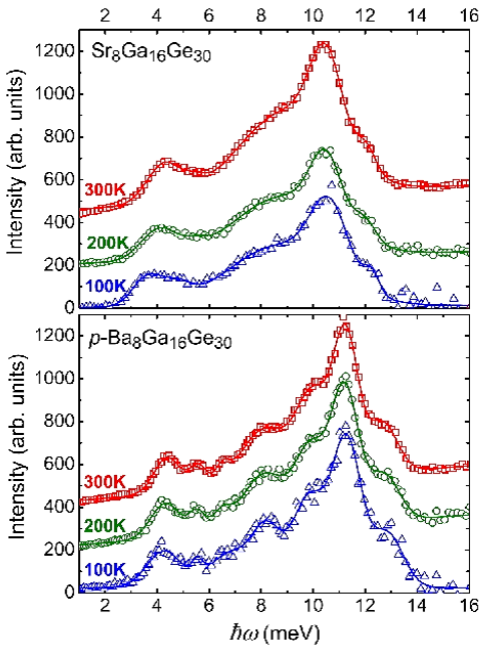

FIG. 31 (Color online) Inelastic neutron scattering (INS) data as a function of temperature 300, 200, and 100 [K] for type-I $Sr_8Ga_{16}Ge_{30}$ and p-type $Ba_8Ga_{16}Ge_{30}$. These are given by the squares, circles, and triangles, respectively. After Christensen *et al.* (2009).

3. Inelastic neutron scattering experiments on off-center systems

Hermann *et al.* (2005) have carried out INS measurements on the PDOS at room temperature on 2.81 and 1.34 [g] samples of polycrystalline samples of type-I $Ba_8Ga_{16}Ge_{30}$ (BGG) and $Sr_8Ga_{16}Ge_{30}$ (SGG). Figure 30 shows weighted PDOS for BGG and SGG, which were extracted from the INS data by integrating the scattering over a 2θ range of 30°-130° and with a subsequent subtraction of the background (Hermann *et al.*, 2005). The observation has confirmed that the local mode due to the $\mathcal{R}(2)$ guest atom is independent of the integration range. The local modes of both Ba(2) and Sr(2) guest atoms have exhibited a linewidth that exceeds the instrumental resolution. These results have indicated a damping of these local modes due to the interactions with network cages. The observed linewidth for Sr(2) local modes is larger than that for the Ba(2) local mode, which indicates a more pronounced interaction of the Sr guests with network cages.

Type-I $Eu_8Ga_{16}Ge_{30}$ (β-EGG) belongs to the category of off-center systems showing a plateau in $\kappa_{\rm ph}(T)$ as in the case of SGG. However, INS experiments on β-EGG was not possible because Eu(2) has a very large neutron absorption cross section (Hermann *et al.*, 2005). But nuclear inelastic scattering (NIS) measurements are available to obtain the PDOS associated with the Eu(2) guest atom. This technique utilizes the high brilliance of synchrotron radiation to obtain an element specific PDOS similar to Moessbauer absorption spectroscopy (Hermann *et al.*, 2006). The NIS has the advantage, different from INS experiments, that the nuclear fluorescence yields an ideal averaging over the entire Brillouin zone. Because of the resonant nature of the NIS technique, the determination of the PDOS in β-EGG provides clear evidence that the Eu(2) guest atom neither interacts nor participates in any high energy vibrational modes. Furthermore, the microscopic determination of the PDOS in terms of NIS measurements suggests the presence of low-lying local modes associated with Eu(2) guest atoms in β-EGG (Hermann *et al.*, 2005).

Lee *et al.* (2008) have performed coherent INS experiments to investigate phonon dispersion relations for SGG belonging to off-center systems. They have observed that the optic $T_{\rm u}$ mode of Sr(2) appears around 4.0 [meV]. Compared with the results of the low-lying

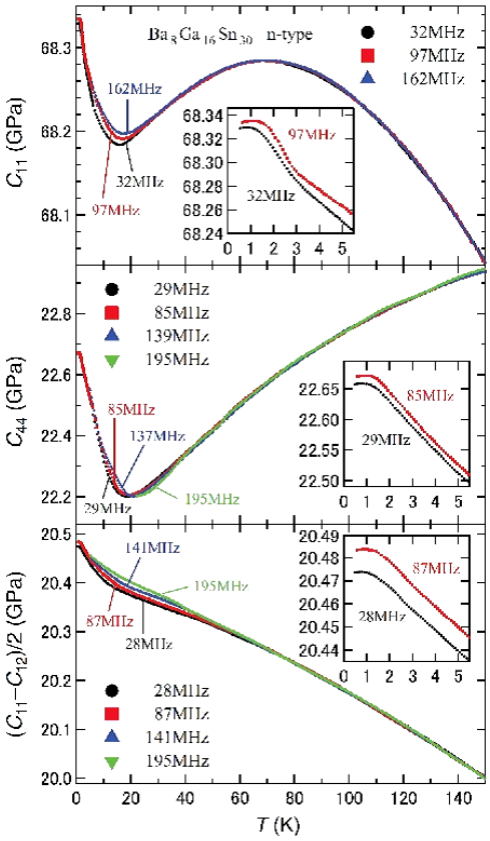

FIG. 32 (Color online) Temperature dependences of elastic stiffness constants C_{11}, C_{44}, and $(C_{11}-C_{12})/2$ in n-type type-I $Ba_8Ga_{16}Sn_{30}$. The insets represent the data in an expanded scale below 5 [K]. After Ishii *et al.* (2012).

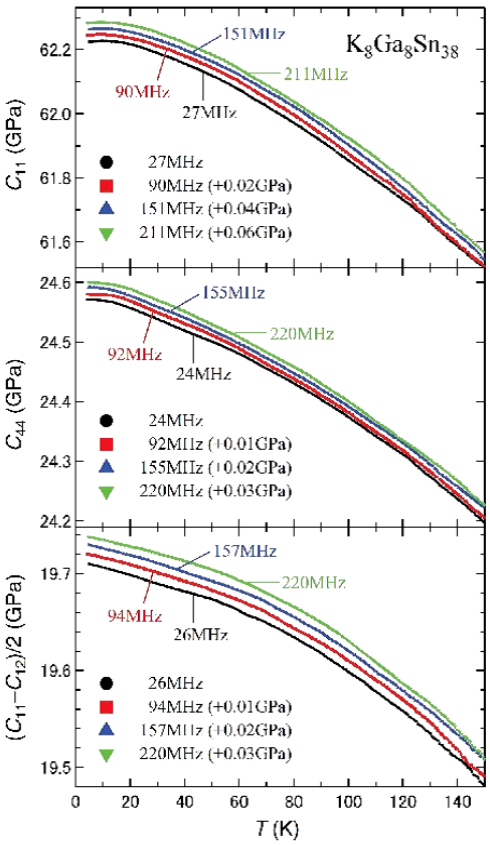

FIG. 33 (Color online) Temperature dependences of elastic stiffness constants C_{11}, C_{44}, and $(C_{11}-C_{12})/2$ in type-I $K_8Ga_8Sn_{38}$. After Ishii *et al.* (2012).

modes in BGG containing on-center Ba(2) guest atoms by Lee *et al.* (2007a), the avoided-crossing due to the Sr(2) guest atom is less clear (Lee *et al.*, 2008).

Christensen *et al.* (2009) have carried out INS experiments on powder samples of SGG and p-type BGG at temperatures of 100 [K], 200 [K], 300 [K], which are shown with squares, circles, and triangles, respectively in Fig. 31. It should be noted that, with decreasing temperature the *width* of the peak around 5 [meV] increases. These behaviors coincide with the results of infra-red absorption by Mori *et al.* (2009, 2011). The physical origin of this anomalous broadening will be discussed in the next section VII.

Here we should mention interesting works on clathrate hydrates in terms of incoherent INS (Baumert *et al.*, 2003; Gutt *et al.*, 2002; Tse *et al.*, 2001) and nuclear resonant IXS (Klug *et al.*, 2011) on the avoided crossing between low-lying optical modes and acoustic phonons. This was clearly demonstrated as the strong coupling between the local vibrations of guest molecules and water-framework vibrations.

Ishii *et al.* (2012) have performed ultrasonic measurements on type-I $Ba_8Ga_{16}Sn_{30}$ (β-BGS) and $K_8Ga_8Sn_{38}$ (KGS) single crystals. They have investigated the elastic softening of the elastic stiffness constant C_{44} relevant to the strain component e_{xy}, which show the softening of C_{44} up to 20 [K] for β-BGS. No charge-carrier dependence is observed between n-type and p-type β-BGS. For KGS, however, such tendencies have not been found, as shown in Figs. 32 and 33 (Ishii *et al.*, 2006, 2012). These are the evidence that local vibrations of Ba(2) atom in β-BGS strongly couple with transverse ultrasonic waves. The significant softening on the bulk modulus in β-BGS contrasts to the continuous hardening in KGS.

VII. PHONON DISPERSION RELATIONS

A. Theoretical aspects of THz frequency dynamics of type-I clathrate compounds

1. Molecular dynamics calculations

Molecular dynamics (MD) calculations have been done for clathrate hydrates with encaged guest atoms or molecules (Baumert *et al.*, 2003; English and Tse, 2009, 2011; Inoue *et al.*, 1996a; Tse *et al.*, 1997). It has been pointed out (Tse *et al.*, 1997) that the avoided crossing

arises from the coupling between local vibrations of guest atoms and acoustic phonons of network cages. Myles *et al.* (2007) have performed MD calculations on the dispersion relations of acoustic and optic phonons of type-I $Ba_8Ga_{16}Ge_{30}$ and $Ba_8Ga_{16}Si_5Ge_{25}$. Their calculation is based on first-principle density functional theory (DFT) using a plane-wave basis and the pseudo-potential method. Acoustic modes of both materials lie below $30-35\,[\mathrm{cm}^{-1}]$ ($=3.7-4.3\,[\mathrm{meV}]$), and most of optic modes show flat dispersion. However, the optic modes of type-I $Ba_8Ga_{16}Ge_{30}$ in the range $100-190\,[\mathrm{cm}^{-1}]$ ($=12.4-23.6\,[\mathrm{meV}]$) and of type-I $Ba_8Ga_{16}Si_5Ge_{25}$ in the range $110-175\,[\mathrm{cm}^{-1}]$ ($=13.6-21.7\,[\mathrm{meV}]$) display significant dispersion. The DFT calculations were made on the total energy and electric structures for type-I $Ba_8Ga_{16}Sn_{30}$ under hydrodynamic pressure (Li *et al.*, 2012).

Koza *et al.* (2010) carried out the lattice-dynamical calculations in order to interpret the PDOS obtained from INS measurements for $Ba_8Zn_6Ge_{40}$ and Ba_8Ge_{43} belonging to quasi-on-center systems. In both compounds, eigenmodes relevant to the Ba guest are primarily located in the energy regime below 14 [meV]. The low-energy modes at 3.10 [meV] are mainly due to Ba(2) cations and Ba(1) cations contribute to the modes at 8.14 [meV]. The partial contributions of the host lattice constituents Ge and Zn indicate larger amplitudes in the energy range of Ba(1) than in that of Ba(2) eigenfrequencies. They have pointed out that the suppression of the acoustic bandwidth is accomplished not only by the hybridization of Ba with Ge dynamics, but also by the lowest energy eigenstates at the Brillouin-zone boundary.

Johnsen *et al.* (2010) have carried out DFT calculations for $Ba_8\mathcal{T}_6Ge_{40}$ ($\mathcal{T}$=Cu, Ag, and Au) to explain the atomic dynamics probed by their INS experiments. The DFT calculations were in good agreement with the PDOS data of INS concerning low-energy phonon-modes of *n*-type Cu compounds, but showed discrepancies for *p*-type Ag and Au compounds with glass-like thermal conductivities.

Euchner *et al.* (2012) have performed first-principle DFT calculations on the phonon dispersion relations of the following three cases: type-I $Ba_8Ge_{40}Ni_6$, Ge_{46} framework without guest atoms, and Ge diamond structure. They have made a rescaling of the energy axis to achieve an agreement with experimental data for $Ba_8Ge_{40}Ni_6$. The rescaling parameter of 1.4 is relatively large, indicating an underestimated Ba-Ge interaction within their DFT approach. They have calculated the participation ratio (PR) characterizing the local or extended natures of eigenmodes, in which the value of PR close to unity means extended modes with simultaneous displacements of relevant atoms. Those of PR close to zero indicate the local modes associated with local vibrations of the Ba(2) guest atom. The flat branches at $6-8\,[\mathrm{meV}]$ in $Ba_8Ge_{40}Ni_6$ were identified as the modes associated with the Ba(2) guest atom.

The constraints of the limited size in *ab initio* calculations make it difficult to treat the effect of disorder of the atomic configuration, whereas the system of quasi-on-center Ba-Ge-Ni is possible to create structures with different Ni content. These are $Ba_8Ge_{40}Ni_6$ and $Ba_8Ge_{42}Ni_4$, which have different occupation of Ni at the 6*c* position. This is the only site that exhibits disorder in Ba-Ge-Ni clathrate structure. Since the 6*c* position is located in the large 24-atom trapezohedron, the Ni content yields distortions of the cages. Euchner *et al.* (2012) have claimed that the disorder distribution of Ni and Ge yields a broadening of the guest modes.

Matsumoto *et al.* (2009) have theoretically investigated the effect of a quadratic anharmonic potential to explain the temperature dependence of the optical conductivities (Mori *et al.*, 2009, 2011). They have calculated unequally spaced energy-levels of a one-dimensional single well and of double-well potentials. The dipole interaction of the guest atoms with electric fields was assumed to induce transitions among vibrational states with unequally spaced energies. They have calculated the natural line broadening and the shift of the peak frequency. In the case of a single-well potential, a softening of the peak frequency and an asymmetric narrowing of the line width with decreasing temperature were explained as a shift in the spectral weight to lower-level transitions. However, the calculated results for one-dimensional double wells showed that the spectral width of the lowest mode decrease with deceasing temperature. This is in conflict with the experimental results showing the reverse effect by Mori *et al.* (2011), This discrepancy indicates that this type of isolated potential for guest atoms is unsatisfactory for describing the experimental results.

Safarik *et al.* (2012) have theoretically investigated the error arising from the use of the harmonic Debye-Waller factor to explain strong anharmonic vibrations of off-center Eu(2) guest atoms in type-I $Eu_8Ga_{16}Ge_{30}$ by assuming a one-dimensional anharmonic potential. They have assessed the error in the values and temperature dependence of the thermal average square displacement for Eu(2) guest atoms. The harmonic approximation led at most to a $\sim 25\%$ error.

To summarize, MD calculations are powerful for gaining insight on the characteristics of vibrational properties of on-center systems with translational-invariance symmetry. It is obvious that MD calculations are not efficient for off-center systems without translational symmetry. However, the results of MD calculations definitely exclude an interpretation of the Boson-peak like hump of the PDOS at around 0.5 [THz] observed for off-center systems from adiabatic isolated-oscillator pictures such as the Einstein model or the soft potential model, since the hybridized modes between $\mathcal{R}(2)$ guest atoms and network cages are crucial.

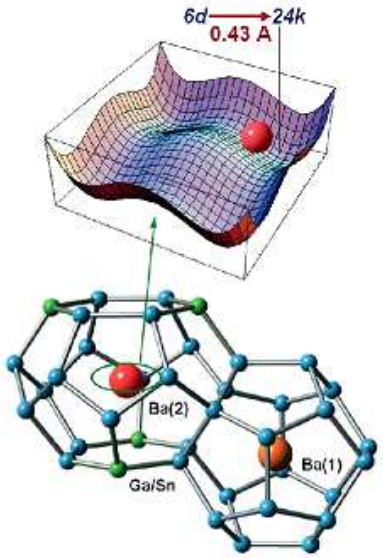

FIG. 34 (Color online) Schematic illustration of the anharmonic potential for the $\mathcal{R}(2)$ guest atom in over-sized cages in type-I clathrate compounds. After Avila *et al.* (2008).

2. Anharmonic potential expressed in terms of the relative coordinate

In this subsection, we describe the THz frequency dynamics by constructing a model from simple and general points of views. This type of the model enables us grasp the essential points of physics involved. The atomic configuration of type-I clathrate compounds with off-center guest atoms has been given by means of diffraction measurements (Bentien *et al.*, 2005; Christensen *et al.*, 2006a, 2009; Nolas *et al.*, 2000) and extended x-ray absorption fine-structure (EXAFS) studies (Baumbach *et al.*, 2005; Jiang *et al.*, 2008).

As described in Sec. III, $\mathcal{R}(2)$ guest atoms in these compounds take on- or off-center position in 14 hedrons depending on the ratio of cage size and atomic radius of guest atom. For example, the guest atoms in 14 hedron in type-I $Ba_8Ga_{16}Sn_{30}$ (β-BGS) take the off-center position at $|\boldsymbol{U}_\ell| = 0.43\,[\text{Å}]$ from the center of the tetradecahedral cage (Suekuni *et al.*, 2008a). Note that the amplitude of $\mathcal{R}(2)$ guest atoms are of the order of $0.05\,[\text{Å}]$, which is sufficiently small compared with the $|\boldsymbol{U}_\ell|$. The deviation $|\boldsymbol{U}_\ell| = 0.43\,[\text{Å}]$ is 7.4% of the nearest-neighbor distance $d = 5.84\,[\text{Å}]$ between Ba^{2+} atoms. Hence, the potential function for off-center guest atoms is shaped like the sheared bottom of a wine bottle. For example, four sites of $24k$ off-center positions are schematically illustrated in Fig. 34 (Avila *et al.*, 2008).

The THz frequency dynamics is the most important part for elucidating peculiar thermal and dynamic properties of off-center systems. This frequency range is mainly concerned with the acoustic and the lowest optic bands. For this situation, we focus on the dynamics of cages and $\mathcal{R}(2)$ guest atoms. Cages are treated to possess total mass M with effective charge $-e_C^*$, and guest atoms do mass m with charge e_G^*. The position vector of the ℓ-th cage at time t was defined in section VI.B.1 as $\boldsymbol{R}_\ell + \boldsymbol{r}_\ell(t)$, where $\boldsymbol{R}_\ell$ is the equilibrium position of the ℓ-th cage center. The vector $\boldsymbol{r}_\ell(t)$ represents a small deviation from $\boldsymbol{R}_\ell$. The position of an $\mathcal{R}(2)$ guest atom is defined by the vector $\boldsymbol{U}_\ell + \boldsymbol{u}_\ell(t)$, where $\boldsymbol{U}_\ell$ is the position of an $\mathcal{R}(2)$ guest atom from $\boldsymbol{R}_\ell$, and $\boldsymbol{u}_\ell(t)$ is a small deviation from $\boldsymbol{U}_\ell$ at time t. Note that $\boldsymbol{U}_\ell \neq 0$ corresponds to the case of an off-center guest atom, whereas the on-center case becomes $\boldsymbol{U}_\ell = 0$. This clarifies the difference between on-center and off-center systems on the same theoretical basis. The definition of coordinates is given in Fig. 27.

Nakayama and Kaneshita (2011) have employed the following form of the anharmonic potential, which is applicable to both the off-center and the on-center systems. This is expressed in terms of "relative displacement" $\boldsymbol{w}_\ell(t) = \boldsymbol{u}_\ell(t) - \boldsymbol{r}_\ell(t)$ as

$$V_{\text{anh}} = \sum_\ell \left[\frac{\xi}{2} |\,\boldsymbol{U}_\ell + \boldsymbol{w}_\ell(t)|^2 + \frac{\eta}{4} |\,\boldsymbol{U}_\ell + \boldsymbol{w}_\ell(t)|^4 \right], \quad (39)$$

where the parameter ξ takes a positive or negative value, and $\eta > 0$. This type of potential expressed by the relative coordinate $\boldsymbol{w}_\ell(t)$ allows us to legitimately treat the THz frequency dynamics of hybridized modes consisting of guest atoms and network cages beyond the adiabatic approximation.

The potential V_{anh} of Eq. (39) involves two types of anharmonic potentials depending on positive or negative ξ, namely wine-glass or wine-bottle type potential. Thus, Eq. (39) makes it possible to treat in a unified way both on-center and off-center systems.

3. Spontaneous symmetry breaking of off-center systems

For the case of off-center systems, the parameter set $\xi < 0$ and $\eta > 0$ in Eq. (39) yields a potential like the bottom of wine-bottle, in which the minimum becomes $V_{\text{anh,min}} = -\xi^2/(4\eta)$ at $|\,\boldsymbol{U}_\ell|^2 = -\xi/\eta$. The non-zero $\boldsymbol{U}_\ell$ enables to rewrite the potential of Eq. (39) as

$$V_{\text{anh}} = \frac{\xi}{2} \sum_\ell |\,\boldsymbol{U}_\ell + \boldsymbol{w}_\ell(t)|^2 \left[1 - \frac{|\,\boldsymbol{U}_\ell + \boldsymbol{w}_\ell(t)|^2}{2|\,\boldsymbol{U}_\ell|^2} \right]. \quad (40)$$

We describe the vibrations around the equilibrium position of off-center guest atoms by the following complex number,

$$W_\ell = \mathrm{e}^{i(\theta_\ell + \delta\theta_\ell(t)/\sqrt{2})} \left[U_0 + \frac{h_\ell(t)}{\sqrt{2}} \right], \quad (41)$$

where W_ℓ represents the vector $\boldsymbol{U}_\ell + \boldsymbol{w}_\ell$. The equilibrium position of the $\mathcal{R}(2)$ guest atom from the center of the cage is given by $U_0 \mathrm{e}^{i\theta_\ell}$, which indicates that the potential of Eq. (40) preserves the *local* gauge symmetry.

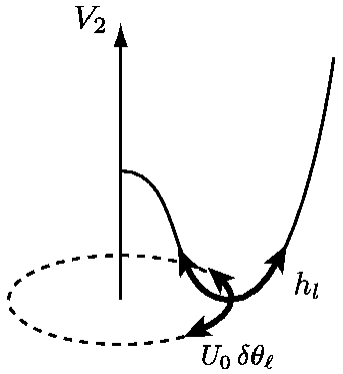

FIG. 35 Illustration showing the emergence of two degrees of freedom of motion; stretching $h_\ell(t)$ and libration $U_0\delta\theta_\ell(t)$.

The phase factor can be considered as a dynamical variable representing the guest position trapped in one of our hindering potentials caused by local symmetry breaking. The variable $h_\ell(t)$ in Eq. (41) represents a small fluctuation along the radial direction from the randomly oriented angle θ_ℓ. Figure 35 depicts two parameters representing these two modes. It is straightforward to include another degree of freedom $\delta\varphi_\ell(t)$ perpendicular to the plane introduced in Eq. (41).

The reformed potential function with respect to small quantities $h_\ell(t)$ and $\delta\theta_\ell(t)$ is given from Eq. (40) for $|\boldsymbol{w}_\ell| < |\boldsymbol{U}_\ell|$, as

$$V_{\rm anh} = \frac{1}{2}\sum_\ell (\tilde{\xi}_s h_\ell^2 + \tilde{\xi}_\theta U_0^2 \delta\theta_\ell^2), \tag{42}$$

where the effective force constants $\tilde{\xi}_s$ and $\tilde{\xi}_\theta$ in Eq. (42) are introduced to redefine ξ in Eq. (40) in order to express the differences between angular motion and stretching motion. In addition, these force constants involve the effect of the random orientation of $\{U_\ell\}$ and anharmonicity through the following definitions,

$$\tilde{\xi}_s = -\xi_s\left(\frac{1+\left\langle h_\ell^2\right\rangle/U_0^2}{2}\right), \quad \tilde{\xi}_\theta = -\xi_\theta\left(\frac{1+\left\langle \delta\theta_\ell^2\right\rangle}{2}\right), \tag{43}$$

where the angular brackets in the parentheses represent a thermal average on the anharmonic term in Eq. (40), which should be proportional to T at higher temperatures.

B. Equations of motion

1. Effect of charge fluctuation

The relative displacements $\{\boldsymbol{w}_\ell\}$ from the center of the cage induce electric dipoles for both of the on-center and the off-center systems as in the case of ionic crystals (Fano, 1960). The total potential energy due to the inter-site dipole-dipole interaction is expressed as

$$V_{\rm dip} = \sum_{\ell,m}\frac{e_G^{*2}}{2R_{\ell m}^3}[\boldsymbol{w}_\ell\cdot\boldsymbol{w}_m - 3(\boldsymbol{w}_\ell\cdot\hat{\boldsymbol{R}}_{\ell m})(\boldsymbol{w}_m\cdot\hat{\boldsymbol{R}}_{\ell m})], \tag{44}$$

where the dipole $\boldsymbol{p}_\ell$ is defined by $\boldsymbol{p}_\ell = e_G^*\boldsymbol{w}_\ell$, and $\hat{\boldsymbol{R}}_{\ell m}$ is a unit vector in the direction of the vector $\boldsymbol{r}_{\ell m} = \boldsymbol{r}_\ell - \boldsymbol{r}_m$. The Fourier transformed expression of Eq.(44) under the random phase approximation is obtained as (Cohen and Keffer, 1955)

$$V_{\rm dip} = \frac{(e^*)^2}{4}\sum_{\ell,\boldsymbol{k},\mu}|\boldsymbol{q}_{\boldsymbol{k}\mu}|^2 {\rm e}^{-i\boldsymbol{k}\cdot\boldsymbol{r}_{0\ell}}\frac{1-3(\hat{\boldsymbol{q}}_{\boldsymbol{k}\mu}\cdot\hat{\boldsymbol{R}}_{0\ell})^2}{R_{0\ell}^3} + {\rm c.c.}, \tag{45}$$

where $\boldsymbol{q}_{\boldsymbol{k}\mu}$ means the Fourier transform of $\boldsymbol{w}_\ell$ relevant to the mode μ, and c.c. indicates the complex conjugate of the first term.

Equation (45) can be expressed, with using the Lorentz sums, as

$$V_{\rm dip} = \frac{m\omega_{\rm p}^2}{2}\sum_{\boldsymbol{k}\mu}|\boldsymbol{q}_{\boldsymbol{k}\mu}|^2 L_\mu, \tag{46}$$

where $L_\mu = (\hat{\boldsymbol{q}}_{\boldsymbol{k}\mu}\cdot\hat{\boldsymbol{k}})^2 - 1/3$ for small $\boldsymbol{k}$ for a cubic lattice, $\omega_{\rm p}^2 = 4\pi n_{\rm C}(e_{\rm G}^*)^2/m$ is the squared plasma frequency of guest atoms with mass m, and charge $e_{\rm G}^*$ in cgs esu units and $n_{\rm C}$=$1/a^3$ is the number density of charges. We should note that $L_\parallel$=2/3 for longitudinal modes and $L_\perp$=$-1/3$ for transverse modes, respectively (Cohen and Keffer, 1955).

2. Fourier-transformed representation of equations of motion

Each cage is elastically connected with nearest neighbor cages. We denote the coupling strength by the harmonic force constants $f_\parallel$ and $f_\perp$, which represent longitudinal (dilation) and transverse (shear) modes. With these quantities, the potential energy is expressed by

$$V_{\rm lat} = \sum_{\ell,\mu}\frac{f_\mu}{2}|\boldsymbol{r}_{\ell,\mu} - \boldsymbol{r}_{\ell+1,\mu}|^2, \tag{47}$$

where μ denotes the species of the three modes: $\parallel$, $\perp$, and $\perp'$.

Network cages compose a cubic lattice (Baumbach *et al.*, 2005; Bentien *et al.*, 2005; Christensen *et al.*, 2006a; Nolas *et al.*, 2000), which is invariant under translation by any lattice vector. This enables us make the Fourier transformation of the potential function given by

$$V_{\rm lat} = 2\sum_{\boldsymbol{k},\mu} f_\mu |\boldsymbol{Q}_{\boldsymbol{k}\mu}|^2 \sin^2\left(\frac{\boldsymbol{k}\cdot\boldsymbol{a}}{2}\right), \tag{48}$$

where $\boldsymbol{a}$ is a lattice vector. The Fourier transformation of the anharmonic potential expressed by the relative coordinate $\boldsymbol{w}_\ell$ is made as

$$\bar{V}_{\rm anh} = \frac{1}{2}\sum_{\boldsymbol{k},\mu}\bar{\xi}_\mu|\boldsymbol{q}_{\boldsymbol{k}\mu}|^2, \tag{49}$$

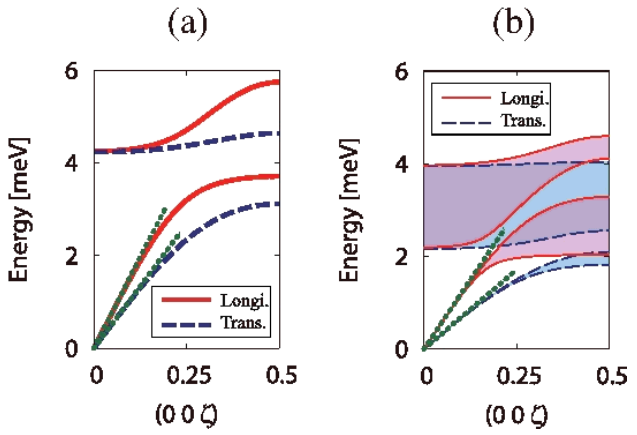

FIG. 36 (Color online) (a) Phonon dispersion curves along the [001] direction for BGG on-center systems. Dispersion relations for longitudinal modes are plotted with solid lines and for transverse modes with dashed lines. Dotted linear lines from the origin represent the long-wave limit of the acoustic dispersion relations. The degeneracy of optic modes at the Γ-point is observed at 4.2 [meV] arising from the on-centered symmetric potential. (b) Phonon dispersion curves along the [001] direction for β-BGS off-center systems. Dispersion relations for longitudinal (transverse) modes are illustrated by the region bounded by solid (dashed) lines. Dotted linear lines from the origin again represent the long-wave limit of acoustic dispersion relations. Note that optic modes observed at the Γ-point are not separated at 2.2 [meV] and 4.1 [meV]. Adopted from Nakayama and Kaneshita (2011).

where $\bar{\xi}$ represents the force constants of the both on-center and off-center systems.

The nature of the force constants $\bar{\xi}_\mu$ in Eq. (49) are quite different for on-center and off-center systems. The crucial difference is that $\tilde{\xi}_\mu$ for off-center systems involves both the librational ($\tilde{\xi}_\theta$) and the radial ($\tilde{\xi}_s$) degrees of freedom, while $\hat{\xi}$ for on-center systems *is isotropic*, and independent of the mode μ, whether longitudinal or transverse. The equations of motion for two variables $\boldsymbol{q}_{k\mu}, \boldsymbol{Q}_{k\mu}$ are obtained by replacing $\bar{\xi}_\mu \to \hat{\xi}$ in Eq. (50). On-center systems impose the condition $\xi > 0$, $\eta > 0$ in Eq. (39). This yields the equilibrium position of on-center guest atoms $\boldsymbol{U}_\ell(t) = 0$. In this case, the force constant $\bar{\xi}$ becomes $\hat{\xi} = \xi + \eta\langle|\boldsymbol{w}_\ell(t)|^2\rangle/2$ by taking account of the thermal average of the anharmonic terms.

The equations of motion for two variables $\boldsymbol{q}_{k\mu}, \boldsymbol{Q}_{k\mu}$ with $\mu = \parallel, \perp$ are obtained from the Euler-Lagrange equation as

$$m\omega_{k\mu}^2(\boldsymbol{q}_{k\mu} + \boldsymbol{Q}_{k\mu}) = (\bar{\xi}_\mu + m\omega_{\rm p}^2 L_\mu)\boldsymbol{q}_{k\mu}, \qquad (50)$$

$$(m+M)\omega_{k\mu}^2 \boldsymbol{Q}_{k\mu} = 4f_\mu \sin^2\left(\tfrac{k\cdot a}{2}\right)\boldsymbol{Q}_{k\mu} - m\omega_{k\mu}^2 \boldsymbol{q}_{k\mu} \qquad (51)$$

Here, the above equations of motion are applicable to both cases of on-center or off-center system. It is straightforward to introduce the effect of random orientation of off-center guest atoms by taking $\bar{\xi}_\mu \to \bar{\xi}$ ($\tilde{\xi}_\theta \le \bar{\xi}_\mu \le \tilde{\xi}_s$).

C. Phonon dispersion relations for off-center and on-center systems in the THz frequency region

1. On-center System

The force constants $f_\parallel, f_\perp$ in Eq. (47) for $Ba_8Ga_{16}Ge_{30}$ (BGG) for an on-center system are obtained using the sound velocities $v_\parallel = 4,096$ [m/sec] and $v_\perp = 2,795$ [m/sec] (Christensen *et al.*, 2008). These yield $f_\parallel = 26.4$ [N/m] and $f_\perp = 12.3$ [N/m] with using $M = 7.04m$ and $a = 10.78$ [Å]. The force constant $\hat{\xi}$ for n-type BGG on-center systems is obtained at 2 [K] in the same manner as for the data of Raman scattering $\omega_0/2\pi = 32\,[\mathrm{cm}^{-1}]$ ($= 0.96$ [THz]) (Suekuni *et al.*, 2010; Takasu *et al.*, 2006) as $\hat{\xi} = 8.23$ [N/m]. Equation (50) involves the squared plasma frequency $\omega_{\rm p}^2$ arising from the fluctuation of charged guest atoms defined in Eq. (46). The magnitude of the plasma frequency should be $\omega_{\rm p}/2\pi \cong 0.09$ [THz] using the mass (m=137 [u]) and the charge of Ba^{2+} ($e_G^* = 2e$) by taking the number density $n_{\rm C}$=$0.628\times10^{27}\,[\mathrm{m}^{-3}]$ and the relative electric susceptibility $\epsilon_r/\epsilon_0 \cong 10$, the same as that of Si crystal.

Nakayama and Kaneshita (2011) have calculated analytically the dispersion relations for BGG on-center systems from Eqs. (50) and (51) using the force constants mentioned above, as is shown in Fig. 36(a). The acoustic phonon dispersions in Fig. 36(a) for BGG are flattened below $\omega_{0\mu}$ for both transverse and longitudinal modes. The eigenfrequencies of optic modes at the Γ-point are degenerate, reflecting that the isotropic force constant $\hat{\xi}$ is independent of the mode μ.

The experimental data on the dispersion relations in terms of coherent inelastic neutron scattering are available for n-type BGG on-center systems (Christensen *et al.*, 2008; Lee *et al.*, 2007a). The calculated results shown in Fig. 36(a) using the smallest number of parameters of f_μ and $\hat{\xi}$ recover well the inelastic neutron scattering data for BGG (Christensen *et al.*, 2008; Lee *et al.*, 2007a).

2. Off-center system

Equations (50) and (51) describe the hybridization between the vibrations of cages and the off-center $\mathcal{R}(2)$ guest atoms in addition to the effect of the random orientation of off-center guest atoms on the spectral width of the phonon dispersion relations. The hybridization occurs as a result of the coupling between *parallel* components of displacements regardless of the transverse ($\perp$) or longitudinal ($\parallel$) modes. Figures 37(a) and (b) illustrate the physical meaning of this coupling mechanism. For example, consider the case in which longitudinal acoustic phonons with polarization vector parallel to the y-axis are incident along y-axis when the $\mathcal{R}(2)$ guest atom takes the far-side position as depicted in Fig. 37(a). These longitudinal acoustic phonons dominantly couple with the stretching component $h_\ell(t)$ paral-

lel to the polarization vector. Provided that the $\mathcal{R}(2)$ guest atom sits on the right side along the x-axis as shown in Fig. 37(b), the longitudinal acoustic phonons incident along the y-axis couple with the libration component $U_0\delta\theta_\ell$, which is parallel to the polarization vector of the acoustic phonons. Thus, the coupling constant continuously spans from the librational one $\tilde{\xi}_\theta$ to the stretching one $\tilde{\xi}_s$. The same arguments hold for the coupling of transverse acoustic phonons. These cause the broadening of the spectral width through the distribution of force constants $\tilde{\xi}_\theta \leq \tilde{\xi}_\mu \leq \tilde{\xi}_s$ with the definition $\mu = \perp$ or $\parallel$ (Nakayama and Kaneshita, 2011).

The force constants $f_\parallel, f_\perp$ in Eq. (51) can be obtained from the sound velocities $v_\parallel$=3,369 [m/sec] and $v_\perp$=1,936 [m/sec] for type-I $Ba_8Ga_{16}Sn_{30}$ (β-BGS) of off-center systems measured by Suekuni *et al.* (2008a) using the relation $v_\mu = a\sqrt{f_\mu/(m+M)}$, which provide $f_\parallel$=18.1 [N/m] and $f_\perp$=5.77 [N/m] by employing masses m=136 [u] for the Ba^{2+} atom and M=8.55m for the cage, and the lattice spacing between unit cell a=11.68 [Å].

The force constants $\tilde{\xi}_\mu$ in Eq. (42) can be determined from the data of optical spectroscopy since the spectra for optic modes provide the information at $\boldsymbol{k}$=0, namely, at the Γ-point. Taking $\boldsymbol{k} \to 0$ in Eq. (51) and combining it with Eq. (50), the squared eigenfrequency for optic modes is given by

$$\omega_{0\mu}^2 = \frac{\tilde{\xi}_\mu + m\omega_{\rm p}^2 L_\mu}{m}\left(1+\frac{m}{M}\right), \qquad (52)$$

where μ denotes the longitudinal or transverse polarization of optic modes. The electrostatic interaction $V_{\rm dip}$ for off-center systems becomes the same as in the case of on-center BGG.

The force constant $\tilde{\xi}_\mu$ in Eq. (52) for β-BGS off-center systems is obtained from the data of Raman scattering (Takasu *et al.*, 2006, 2010) and far-infrared spectroscopy (Mori *et al.*, 2009, 2011). Mori *et al.* (2009, 2011) have observed infrared active spectra at 7 [K], with the lowest-lying peak at 0.71 [THz], and with a line-width broadening of 0.57 [THz] for β-BGS off-center systems by means of THz time-domain spectroscopy. This spectrum should be assigned to the librational mode of off-center rattling guest-ions, which couples with the transverse acoustic mode.

The spectrum of the $A_{1\rm g}$ stretching mode coupled with the longitudinal mode is not observed for β-BGS off-center systems owing to technical reasons (Suekuni *et al.*, 2010; Takasu *et al.*, 2006). For other type of off-center systems, e.g., SGG, the spectra at 2 [K] are obtained at 48 [cm^{-1}], and the spectrum at 36 [cm^{-1}] for β-EGG off-center systems for the $A_{1\rm g}$ mode (Suekuni *et al.*, 2010; Takasu *et al.*, 2006). By extrapolating these data, the eigenfrequency of the A_{1g} mode of β-BGS is estimated as $\omega_0/2\pi$ = 30 [cm^{-1}] (= 0.9 [THz]), from which the force constant $\tilde{\xi}_\parallel$ associated with longitudinal optic mode can be evaluated. These assignments lead to $\tilde{\xi}_\parallel$=7.32(1± 0.25) [N/m] and

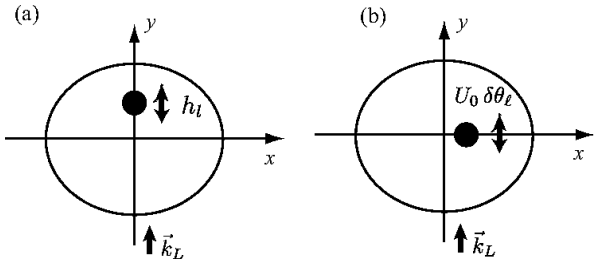

FIG. 37 Illustration showing the coupling mechanism between acoustic phonons and $\mathcal{R}(2)$ guest atoms. The figure (a) is the case that the off-center guest atom takes the far-side position for incident longitudinal ($\parallel$) acoustic phonons with the wave vector $\boldsymbol{k}_{\rm ph}$, and (b) shows $\mathcal{R}(2)$ guest atom sits perpendicular position to the same longitudinal acoustic phonons. The coupling becomes effective to parallel components of relevant displacements regardless of the transverse or longitudinal modes.

$\tilde{\xi}_\perp$=2.21(1±0.25) [N/m], taking the plasma frequency $\omega_{\rm p}/2\pi$=0.09 [THz] from Eq. (52). The contribution from this plasma frequency is only 10% at the Γ-point.

The calculated dispersion relations for β-BGS off-center systems are given in Fig. 36(b). It is remarkable, see in Fig. 36(b), that the spectral width becomes broader and gapless in the region of avoided crossing. This is attributable to the random orientation of guest atoms.

Experimental far-infrared spectroscopy data at low temperatures (Mori *et al.*, 2009, 2011) for off-center systems provide interesting line-width broadening features. The spectral width of about 0.57 [THz] of the lowest-lying infrared active optic modes 0.71 [THz] at 7 [K] decreases with *increasing* temperature. This feature contradicts the assumption that the anharmonicity of the potential Eq. (39) is a key element for interpreting the origin of the line-width broadening (Matsumoto *et al.*, 2009). These experimental results (Mori *et al.*, 2009, 2011) suggest that the random configuration of $\boldsymbol{U}_\ell$ yields the broadening of optical spectra at low temperatures.

Thermal-averaged squared-displacements, $\langle h_\ell^2\rangle$ and $\langle\delta\theta_\ell^2\rangle$, are proportional to temperature T. Raman scattering (Suekuni *et al.*, 2010; Takasu *et al.*, 2006, 2010) and far infrared spectroscopy (Mori *et al.*, 2009, 2011) experiments have shown that the spectral energies belonging to the lowest band monotonically decrease with decreasing temperature T. These observations can be interpreted by means of thermal-averaged anharmonic terms given by $\langle h_\ell^2\rangle$ and $\langle\delta\theta_\ell^2\rangle$ given in Eqs. (42) and (43), which are proportional to temperature T under a self-consistent phonon approximation.

Equations (50) and (51) yield the frequency range of the avoided crossing given by

$$\delta\omega_{c\mu} \cong \left[\frac{m}{M}\left(\frac{\bar{\xi}_\mu}{m}+\omega_{\rm p}^2 L_\mu\right)\right]^{1/2} \cong \omega_{0\mu}\sqrt{\frac{m}{M}}, \qquad (53)$$

where the last relation gives a small contribution arising from the plasma frequency compared with the first term

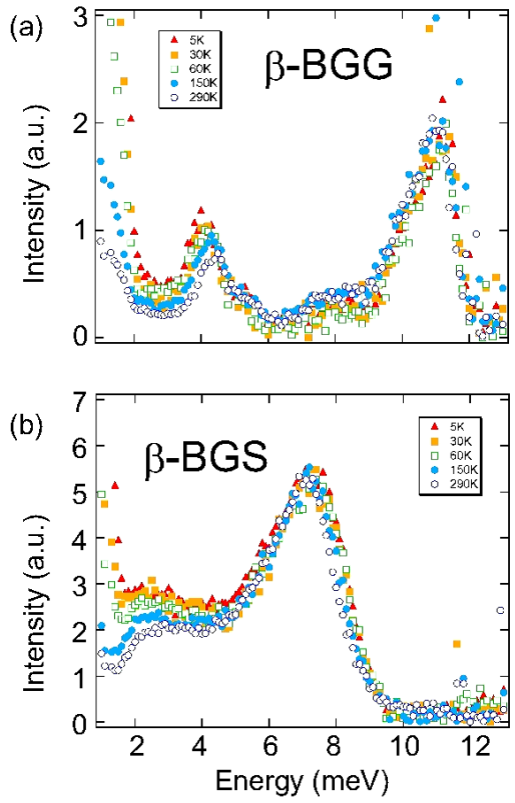

FIG. 38 (Color online) Phonon densities of states for both of type-I $Ba_8Ga_{16}Ge_{30}$ (BGG) (a) and $Ba_8Ga_{16}Sn_{30}$ (β-BGS) (b) obtained by means of coherent INS experiments in the temperature range from 5 [K] to 290 [K]. The data provide integrated densities of states from 0.4 to 0.7 [$\AA^{-1}$] in $\boldsymbol{k}$-space. See text for the assignments of the spectra. After Nakamura and Arai (2010).

in the parenthesis. This relation is valid since the contribution from the plasma frequency is only 10% of $\omega_{0\perp}$ for β-BGS. Equation (53) indicates that the frequency $\delta\omega_{c\mu}$ at avoided crossing is governed by the quantities $\omega_{0\mu}$ and the square root of mass ratio $\sqrt{m/M}$. The frequency $\delta\omega_{c\mu}$ for off-center systems is much smaller than the case of on-center systems due to the inequality $\bar{\xi}_\mu < \hat{\xi}$.

3. Comparison of calculated dispersion relations to INS experiments

Coherent INS measurements for both BGG and β-BGS were performed in the temperature range from 5 [K] to 290 [K] using the cold neutron disk-chopper spectrometer AMATERAS installed in Materials and Life Science Experimental Facility (MLF), Japan Proton Accelerator Research Complex (J-PARC) (Nakamura and Arai, 2010). The results integrated in the range from 0.4 [$\AA^{-1}$] to 0.7 [$\AA^{-1}$] are given in Fig. 38 (a) for BGG and Fig. 38 (b) for β-BGS. These data provide important information on the THz frequency dynamics of clathrate compounds.

First, for the data of quasi-on-center BGG, Fig. 38(a) shows three sharp peaks at 4.0, 7.5 and 11 [meV]. The assignments of these spectra can be made in comparison with optical spectroscopies described in Sec. VI.A. The lower peaks at 4.0 [meV] and 7.5 [meV] have been observed in both Raman scattering (Takasu *et al.*, 2006) and infra-red spectroscopies (Mori *et al.*, 2009). These have been assigned as T_{2g} and E_g modes attributable to Ba(2) guest atoms encapsulated in 14 hedrons. The higher spectrum at 11 [meV] corresponds to Ba(1) guest atoms in 12 hedrons. The lower peak at around 4.0 [meV] varies considerably with T from 5 [K] to 290 [K], while two higher peaks do not show such a strong temperature dependence. The strong dependence on temperature manifests the relevance of the "wine-glass" type anharmonic potential employed in Eq. (39) for Ba(2) guest atoms in BGG. Calculated results for dispersion relations for BGG are given in Fig. 36 (a).

Figure 38 (b) on off-center β-BGS shows two peaks at 2−4 [meV] and 7 [meV]. The lower hump arises from the vibrations of Ba(2) guest atoms in the 14 hedron, and the peak at 7 [meV] is attributable to Ba(1) guest atoms in the 12 hedrons. There is no clear gap between 2 and 4 [meV], which is distinctly different from the result for BGG given in Fig. 38 (a). The data in Fig. 38 (b) indicate that the lower-energy side of the hump at around 2 [meV] is appreciably affected by temperature compared with the higher-energy side at around 4 [meV].

The calculations given in Fig. 36 (b) have clarified that the lower side is concerned with the hybridization between libration vibrations of guest atoms and the transverse acoustic modes from networked cages. At the same time, the higher-energy side of the hump results from the hybridization between the stretching vibrations of guest atoms and the longitudinal acoustic phonons. Thus, the INS data indicate that the libration motion of Ba(2) guest atoms in β-BGS experience much stronger anharmonicity compared with that of the stretching motion. This is consistent with the view that the thermal-averaged anharmonic term $\langle\delta\theta_\ell^2\rangle$ in Eq. (43) is large enough compared with the stretching term $\langle h_\ell^2\rangle$. This is a reasonable interpretation for the observations on INS experiments by Nakamura and Arai (2010) for BGG and β-BGS.

To conclude this subsection, we emphasize that the observed densities of states given in Fig. 38 recover the calculations on BGG and β-BGS shown in Fig. 36, very well. In particular, the gapless density of states given in Fig. 38 (b) for β-BGS is well reproduced in Fig. 36(b).

4. The origin of Boson-peak like excess density of states

Since the specific heats of type-I clathrate compounds containing off-center guest atoms, for example, β-BGS or SGG, exhibit a hump at around

$T \simeq 4\,[\mathrm{K}]$, the corresponding modes have been observed by Raman scattering (Kume *et al.*, 2010; Suekuni *et al.*, 2010; Takasu *et al.*, 2006, 2010) and infra-red measurements (Mori *et al.*, 2009, 2011).

The relation between the phonon specific heat $C_{\rm ph}(T)$ and the phonon density of states $D(\omega)$ is expressed by the formula,

$$C_{\rm ph}(T) = \frac{-1}{k_{\rm B}T^2} \sum_{\mu} \left[\int_0^{\infty} \frac{\partial n_{\rm B}(\beta\hbar\omega)}{\partial\beta} \hbar\omega_\mu D\left(\omega_\mu\right) d\omega_\mu \right] \quad (54)$$

where $n_{\rm B}$ is the Bose-Einstein distribution function and the inverse temperature is defined by $\beta = 1/k_{\rm B}T$. The density of states $D(\omega)$ can be obtained in principle by inverting Eq.(54) using the observed data of $C_{\rm ph}(T)$, though this procedure involves an uncertainty. However, specific heat measurements are not affected by the mode-selection rule on excited modes as in the case of optical spectroscopies, in which active modes are distinguished by infrared absorption, Raman scattering, and hyper-Raman scattering experiments. Optical spectroscopies provide information close to the Γ-point. These are different from humps observed in specific heats that represent averaging over a wide sector of $\boldsymbol{k}$-space.

The characteristic frequency of guest atoms in cages is much smaller than the Debye frequency $\omega_{\rm D}$ expressing the upper limit of propagating acoustic phonons of the network cages without guest atoms. The coupling of guest atoms and cages yields the hybridization of dispersion curves and creates the flat and broad band. This is the origin of the Boson-peak like mode observed in type-I clathrae compounds containing off-center guest atoms. Thus, the flat band with broad spectra at around 0.5 [THz] shown in Fig. 36(b) is the origin of the Boson-peak like excess density of states.

VIII. GLASS-LIKE SPECIFIC HEATS BELOW 1 [K]

A. Low temperature specific heats and two-level tunneling states

1. Two-level tunneling model

In off-center type-I clathrate compounds, the disorder is introduced by randomly oriented guest atoms. This is the origin of glass-like specific heats observed for off-center systems at low temperatures. At $T \lesssim 1\,[\mathrm{K}]$, a quantum mechanical description is needed to describe the states contributing to T-linear specific heats. For structural glasses, it has been postulated that an atom or a group of atoms can occupy one of two potential minima (Anderson *et al.*, 1972; Phillips, 1972). See the reviews by Hunklinger and Raychaudhuri (1986) and Phillips (1987). Each tunneling state can be simply represented by assuming a double-well potential shown in Fig. 39, where the abscissa gives the position of the tunneling element in multi-dimensional configuration space.

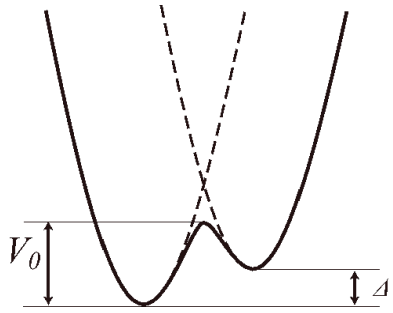

FIG. 39 Schematic illustration of double well potential representing the two-level tunneling state.

This tunneling model provides a good phenomenological basis on which various observations can be consistently explained. It should be emphasized that the idea of double-well potential is based on the adiabatic approximation. This is acceptable since the wavelengths of excited acoustic phonons below 1 [K] are sufficiently larger than the scale of tunneling elements. The THz frequency dynamics attributable to the hybridization between local vibrations of guest atoms and acoustic phonons due to network cages should take into account the non-adiabatic aspect, as been described in Sec. VII.

We choose a basis set of (φ_1, φ_2) of the appropriate potential V_1 and V_2 belonging to ground energies (E_1, E_2). By taking the zero of energy as the mean of E_1 and E_2, the Hamiltonian matrix becomes

$$\mathcal{H} = \frac{1}{2} \begin{pmatrix} -\epsilon & \Delta \\ \Delta & \epsilon \end{pmatrix}, \quad (55)$$

where the tunnel splitting Δ due to the overlap of the wavefunctions is given by

$$\Delta = 2\,\langle \varphi_1 | H | \varphi_2 \rangle\,. \quad (56)$$

The overlap integral Δ generally involves an exponential decay given by

$$\Delta = \hbar\Omega \mathrm{e}^{-\lambda} = \hbar\Omega \mathrm{e}^{-\ell\sqrt{2mV_0}/\hbar}, \quad (57)$$

where $\hbar\Omega$ is approximately equal to $(E_1 + E_2)/2$, while ℓ and V_0 are the separation and the barrier height between the two wells, and m is the mass of the tunneling element. Typical values of the tunneling parameter λ can be estimated from the requirement that Δ must be approximately equal to $k_{\rm B}T$ if the tunneling states dominantly contribute to thermal properties at a temperature T. This requires, for example, $\Delta \cong 1\,[\mathrm{K}]$ at 1 [K], which gives approximately 5 for λ with $\hbar\Omega$ equal to 100 [K].

For off-center guest atoms, the overlapping integral Δ is due to the angular rotation of off-center guest atoms given by

$$\Delta = \hbar\Omega\, \mathrm{e}^{-\sqrt{2IV_0}\delta\theta/\hbar}, \quad (58)$$

where the moment of inertia $I = 25.4\,[\mathrm{u\AA}^2]$ for β-BGS. The zero-point energy scale $\hbar\Omega$ of the guest atom trapped

in one of four local-potential minima is estimated, from the uncertainty principle, to be $\hbar\Omega \approx 4.6\,[\mathrm{K}]$ for an actual spatial size $\approx (0.3\,[\mathrm{\AA}])^3$ for β-BGS. This energy scale $\hbar\Omega \approx 4.6\,[\mathrm{K}](=4\,[\mathrm{meV}])$ is comparable with that of the Boson-peak like hump in β-BGS observed from specific heats and spectroscopic measurements.

The Hamiltonian matrix of Eq. (55) provides eigenvalues

$$E = \pm\frac{1}{2}\left(\epsilon^2 + \Delta^2\right)^{1/2}. \tag{59}$$

The distribution function of ϵ must be an even function because both the positive and negative values of ϵ are equally likely. The range of energy variation of ϵ is determined by the thermal energy where atoms or molecules become free from the constraint of neighboring atoms. In structural glasses, this corresponds to the glass-transition temperature T_{g}. The glass-transition temperature obeys the Tammann's rule of the form $T_{\mathrm{g}} \cong 2T_{\mathrm{melt}}/3\,[\mathrm{K}]$. Thus, the distribution function $f(\epsilon, \Delta)$ is a reasonably slowly varying function on ϵ in the range of interest $10\,\mathrm{mK} < \epsilon/k_{\mathrm{B}} < 1\,[\mathrm{K}]$, so that $f(\epsilon, \Delta)$ can be taken as independent of ϵ. Because of the exponential dependence of Δ on λ, only a relatively small range of λ is sampled for a large range of Δ.

We should remark here that ϵ expresses the asymmetry energy of *two-level* systems, i.e., the thermal activation energy needed for the rearrangement of local microscopic structures in the regime $\epsilon/k_{\mathrm{B}} \gg 1\,[\mathrm{K}]$. Thus, ϵ does not manifest the energies of the excess density of states related to the Boson peak observed at $3-10\,[\mathrm{K}]$ for structural glasses.

2. Specific heats below 1 [K]

By introducing the density of states $n(E)$ per volume per energy, the specific heat at low temperatures is given by

$$C_{\mathrm{tun}}(T) = \frac{1}{4k_{\mathrm{B}}T^2}\int_0^{\Delta_0/2} n(E)E^2\,\mathrm{sech}^2\left(\frac{\beta E}{2}\right)dE, \tag{60}$$

where $\beta = (k_{\mathrm{B}}T)^{-1}$. The form of the distribution function $n(E)$ is not known *a priori*, but $n(E)$ should be a continuous function in the temperature regime $T \ll \Delta_0/k_{\mathrm{B}}$ where Δ_0 is the upper bound of E.

If we employ a simpler view that the states are distributed uniformly from -$\Delta_0/2$ to $\Delta_0/2$ such as $n(E) = \bar{N}/\Delta_0$, where $\bar{N}$ is the number density of tunneling sates per volume, Eq. (60) yields at $T \ll \Delta_0/k_{\mathrm{B}}$,

$$C_{\mathrm{tun}} \cong \frac{\pi^2\bar{N}}{3\Delta_0}k_{\mathrm{B}}^2 T. \tag{61}$$

Above 1 [K], the part of the asymmetry energy ϵ in Eq. (59) is a dominant term in Eq. (61). In this case, using observed values of specific heats of silica glass of $C_{\mathrm{tun}} \cong 2.5\times10^{-4}\,[\mathrm{mJ\,cm^{-3}K^{-1}}]$ at $T = 0.1$ [K] and the upper bound of $\Delta_0 \cong T_{\mathrm{g}} \cong 500\,[\mathrm{K}]$ in Eq. (61), the number density of tunneling states is estimated as $\bar{N} \cong 10^{20}\,[\mathrm{cm^{-3}}]$.

We can estimate the number density of tunneling states $\bar{N}$ by taking the upper bound as $\Delta_0 \cong 500\,[\mathrm{K}]$ in Eq. (61) as $\bar{N} \cong 1.1\times10^{17}\,[\mathrm{cm^{-3}}]$. Therefore, in silica glass only 10^{-5} states per SiO_2 element contribute to tunneling states.

The structural glasses are in non-equilibrium states, so that observed specific heats should vary logarithmically with the measuring time, implying the relaxation in a multi-valley potential in configuration space (Anderson *et al.*, 1972; Phillips, 1972). Here, we do not enter into the details of this interesting phenomenon. The readers can find the expression of specific heats involving relaxation time τ in articles by Hunklinger and Raychaudhuri (1986) and Phillips (1987).

The two-level tunneling model provides a good phenomenological picture of observed universal phenomena. However, it is difficult to identify the tunneling entity in glasses due to its structural complexity. Compared with structural glasses, type-I clathrate compounds containing off-center guest atoms are microscopically well defined, and it is possible to understand the tunneling entity on an atomic scale. This is the major goal of the next sections.

3. Failure of the noninteracting picture for tunneling elements

One of the important features of type-I clathrate compounds found in experiments (Avila *et al.*, 2006a,b; Bentien *et al.*, 2004, 2005; Cohn *et al.*, 1999; Nolas *et al.*, 1995, 1996, 1998a,b,b,c, 2000, 2001a; Sales *et al.*, 1996; Sales, 1998; Sales *et al.*, 2001; Suekuni *et al.*, 2007, 2008a,b, 2010; Xu *et al.*, 2010) is that guest atoms take either the on-center or off-center position depending on the size of cages or, equivalently, the ionic radii of guest atoms.

A typical deviation r_0=0.43 [Å] in β-BGS has been obtained from diffraction experiments (Avila *et al.*, 2006b, 2008). p-type BGG is slightly off-center by 0.15 Å (Christensen *et al.*, 2006a; Jiang *et al.*, 2008). In this connection, it should be noted that n-type BGG shows crystal-like thermal conductivity, while p-type behaves with glass-like thermal properties (Avila *et al.*, 2006a,a, 2008). This is one piece of evidence that the long-range dipole-interaction plays a crucial role in type-I clathrates, since the Coulomb interaction between the cages and the guest cation Ba^{2+} in BGG is shielded in n-type electron-rich BGG, while the dipole interaction in p-type becomes relevant even for small dipole moments. The network configuration consisting of off-center guest atoms is schematically illustrated in Fig. 40.

At first glance, individual off-center guest atoms seem to independently contribute to glass-like thermal properties at low temperatures. This naive view misleads

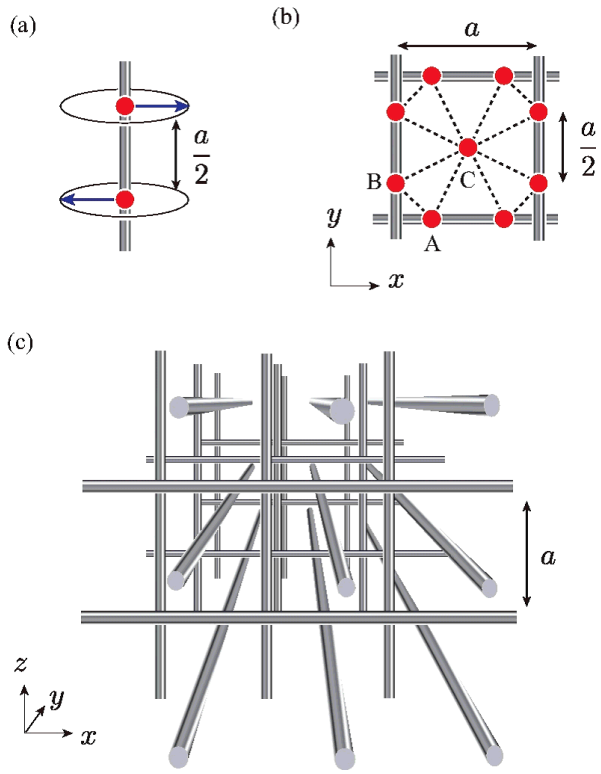

FIG. 40 (Color online) Schematic illustration of the configuration of the guest atoms in the over-sized cages in β-BGS. The four-fold inversion axes are directed along x, y, z. (a) The deviation from the on-center position (filled circles) induces the electric dipoles (arrows). Here two nearest dipoles are depicted. The electric dipoles rotate in the plane perpendicular to the axis linking the nearest dipoles. (b) The configuration of the on-center positions of the guest atoms. The filled circles represent the positions of off-center guest atoms, around which the electric dipoles are induced. The sites A, B, and C in (a) are seated on the chains parallel to x, y, and z, respectively: $A = (a/4, 0, a/4)$, $B = (0, a/4, 3a/4)$, $C = (a/2, a/2, a/2)$. The distance between the next-nearest neighbors (dashed lines) is $\sqrt{3/8}\,a$. Note that these three dipoles constitute an *equilateral triangle* and easily generate a frustrated situation. (c) The 3D configuration of the dipole chains are illustrated.

in that it suggests an isolated *non-interacting* picture could explain the observed glass-like behaviors. Such a *non-interacting* picture does *not* reproduce the observed temperature dependence as well as the magnitudes of the specific heats for type-I clathrate compounds with off-center guest atoms at 1 [K] and below (Nakayama and Kaneshita, 2008). In fact, as will be discussed in the next section, the tunneling between the nearby potential minima in configuration space generated by a combination of interacting dipoles is crucial for interpreting glass-like thermal properties at low temperatures.

In an isolated non-interacting picture, the problem is reduced to the state of a single cage where $\mathcal{R}(2)$ guest atoms experience a *hindering* potential $V_{\rm h}(\theta)$ along the azimuthal direction (Nolas *et al.*, 2001a; Sales *et al.*, 2001). The barrier height of the hindering potential $V_{\rm h}$ between nearby potential wells is estimated to be of the order of 10 [K]. Actually, first principles calculations have shown $V_{\rm h}$ to be $\cong$20 [K] for $Sr^{2+}(2)$ guest atoms in SGG (Madsen and Santi, 2005).

Since the separation of neighboring wells is small, for example, $\pi U_0/2$=0.67 [Å] in β-BGS, $\mathcal{R}(2)$ guest atom to tunnel to a nearby potential minimum at lower temperatures $T \ll V_{\rm h}$, where the off-center guest atom executes zero-point motion at one of the four wells with an energy $\hbar\Omega$.

The tunneling splitting Δ due to the angular rotation of off-center guest atoms is given by

$$\Delta = \hbar\Omega\, {\rm e}^{-\sqrt{2IV_{\rm h}}\delta\theta/\hbar}, \tag{62}$$

where $\delta\theta \le \pi/2$ is the angle between two nearby minima. Since the zero-point energy $\hbar\Omega$ of the guest atom is estimated to be $\hbar\Omega \approx 4.6$ [K] for β-BGS, we can estimate the most probable lower-bound as $\Delta_{\rm min} = 0.03$ [K] by using the hindering potential height $V_{\rm h}(\theta) \approx 10$ [K] and the moment of the inertia of dipoles $I = 25.4$ [uÅ^2] for β-BGS into Eq. (62).

The lower bound of the integral in Eq. (60) should be $\Delta_{\rm min}/2$. Introducing the dimensionless variable x defined by $x = E/(2k_{\rm B}T)$, the function $x^2\,{\rm sech}^2(x)$ in the integrand of Eq. (60) has a maximum at around $x = 1$. The contribution to the integral of the product of $x^2\,{\rm sech}^2(x)$ and $n(2xk_{\rm B}T)$ should become sharply smaller at temperatures below $T \lesssim \Delta_{\rm min}/k_{\rm B} \approx 0.03$ [K], but the experimental data of specific heats for type-I clathrate compounds do not show this tendency.

Furthermore, the isolated *non-interacting* picture is based on the idea that *every* off-center guest atom contributes to the specific heat. Taking the distribution function $n(E) = \bar{N}/\Delta_0$ with $\Delta_0 \approx V_{\rm h} \approx 20$ [K] and $\bar{N}$ =6, where 6 is the number of guest atoms in a unit cell of β-BGS, Eq. (61) becomes

$$C_{\rm tun} \cong 1.0 \times 10^4\, T \ \ [{\rm mJ\,mol^{-1}\,K^{-1}}], \tag{63}$$

which is two orders of magnitude larger than the observed value for β-BGS $C_{\rm tun} \cong 30\,T$ [mJ mol^{-1} K^{-1}] (Suekuni *et al.*, 2008a,b). Thus, the *non-interacting* picture based on the assumption that every off-center guest-ion would independently contribute to the tunneling states yields the specific heat $C_{\rm tun}(T)$ of two orders of magnitude *larger* than the observed values at 1 [K], in conflict with observations. It is therefore not reasonable to employ the non-interacting picture to explain glass-like properties of type-I clathrate compounds observed at $T \lesssim 1$ [K] (Nakayama and Kaneshita, 2008).

B. Interacting-dipoles in type-I clathrate compounds

1. Multi-valley potentials in configuration space

In type-I clathrate compounds with divalent guest ions, the deviation of the guest ion from the center of the cage induces an *electric dipole moment* due to the difference of the charges between the guest atom with the charge +2e and the ion with the charge -e constituting cages. The strength of the electric dipole moment can be estimated to be p=4.1 Debye in the case of β-BGS with the deviation U_0=0.43 [Å] from the center. The deviation is about 7.2% of the distance between the neighboring 14-hedrons ($a/2$=5.84 [Å], where a is the lattice constant). Thus, the cages with off-center guest atoms intrinsically possess electric dipoles, and that it is crucial to take into account these characteristics. See Fig. 41.

Bentien *et al.* (2005) have pointed out, from crystallographic studies (Bentien *et al.*, 2000, 2002) and thermal conductivity measurements (Bentien *et al.*, 2004), that the Ba(2) guest can be off-center in p-type $Ba_8Ga_{16}Ge_{30}$. Avila *et al.* (2006b) have found that p-type BGG shows crystal-like thermal conductivity, while n-type behaves as glass-like. This indicates that the long-range interaction between divalent guest atoms becomes relevant owing to anti-shielding by doped holes in p-type, while n-type BGG takes the opposite tendency. p-type BGG are slightly off-center by 0.15 [Å] (Christensen *et al.*, 2006a; Jiang *et al.*, 2008) with much smaller dipole moments compared with the case of β-BGS. This is one piece of evidence that the long-range dipole-interaction is crucial for interpreting the thermal properties of type-I clathrates since the Coulomb interaction between cation guest-ion Ba^{++} in BGG is shielded in n-type electron-rich BGG, while the dipole-dipole interaction in p-type becomes relevant even for small dipole moments.

In type-I clathrate compounds, off-center guest atoms are in 14-hedron cages, and its nearest-neighbor off-center guest atoms are located in the next two 14-hedron cages, which share the *same* four-fold inversion axis. The four-fold inversion axes are directed along the x, y, z axes due to the cubic symmetry of β-BGS as illustrated in Fig. 40(a). The key for yielding glass-like behavior is that these dipoles constitute an equilateral-triangle structure among next-nearest neighbor dipoles, as depicted in Fig. 40(b). This configuration generates a frustrated situation necessary to the emergence of glass-like behavior below 1 [K].

To make our argument clear, let us consider two electric dipoles $\boldsymbol{p}_\ell$ and $\boldsymbol{p}_m$ separated by a distance $|\boldsymbol{R}_{\ell m}|$. The dipolar interaction is given by the following form,

$$V_{\ell m} = \frac{1}{4\pi\varepsilon_r |\boldsymbol{R}_{\ell m}|^3}\Big[\boldsymbol{p}_\ell\cdot\boldsymbol{p}_m - 3(\boldsymbol{p}_\ell\cdot\hat{\boldsymbol{R}}_{\ell m})(\boldsymbol{p}_m\cdot\hat{\boldsymbol{R}}_{\ell m})\Big] \quad (64)$$

where ε_r is the dielectric constant of the clathrate, and $\hat{\boldsymbol{R}}_{\ell m} = \boldsymbol{R}_{\ell m}/|\boldsymbol{R}_{\ell m}|$ is a unit vector. The potential function for two coupled dipoles $\boldsymbol{p}_1$ and $\boldsymbol{p}_2$ along an axis becomes $V_{12} = V_{\rm h}(\theta_1) + V_{\rm h}(\theta_2) + W_{12}(\theta_1,\theta_2)$ with

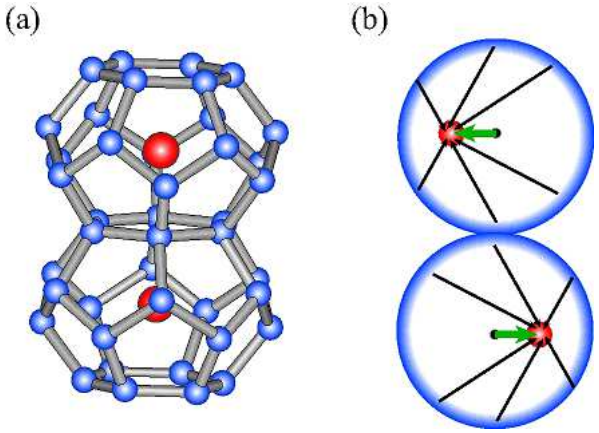

FIG. 41 (Color online) (a) Illustration of two 14-hedrons cages along z-direction consisting of anions and guest cations. (b) The cage (outer circle) and the symmetry-broken off-center guest atom compose an effective electric dipole moment (thick arrow), which is the vector sum of each dipole (thin arrow).

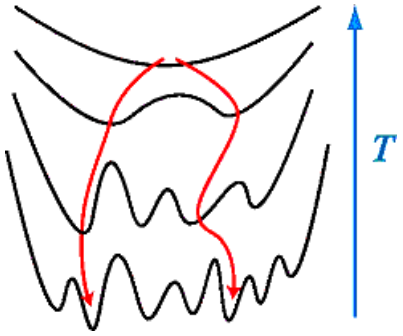

FIG. 42 (Color online) Schematic illustration of free-energy landscape representing non-equilibrium states.

$W_{12} = p^2\cos(\theta_1-\theta_2)/(4\pi\varepsilon_r R_{12}^3)$, where two global minima (maxima) in (θ_1,θ_2) configuration space appear at $|\theta_1-\theta_2| = \pi$ (2π) since the dominant term for a nearest-neighbor pair is the first term in Eq. (64). This configuration acts as a new hindering potential in addition to the four-fold inversion symmetric potential $V_{\rm h}$. This argument can be straightforwardly extended to the case of multiple pairs providing many potential minima in configuration space $\mathcal{P} = (\theta_1,\theta_2,\theta_3,\cdots)$, where the potential function is $V_{123\ldots} = \sum V_{\rm h}(\theta_\ell) + \sum V_{\ell m}$.

The energy scale of the dipole-dipole interactions between nearest neighbors is given by its maximum value,

$$J_1 = \frac{p^2}{4\pi\varepsilon_r R_1^3}, \quad (65)$$

where R_1 is the distance between the nearest neighbors. The actual distance between nearest-neighbor guest atoms in β-BGS is R_1=$a/2$=5.84 [Å]. The characteristic energy scale for nearest-neighbor coupling is then estimated as $J_1 \cong 6\varepsilon_r/\varepsilon_0$ [K]. Taking into account

the dielectric constant for semiconductors in the range $5 \lesssim \varepsilon_r/\varepsilon_0 \lesssim 20$, it turns out that $\mathcal{R}(2)$ guest atoms experience strong electric fields. The energy-scale of the dipole-dipole interaction is estimated to be of the order of a few 10 [K]. They are no longer regarded as isolated dipoles. Combining four-fold inversion symmetry of dipoles with the frustrated situation due to the equilateral triangle (See Fig. 40(b)), many local minima are created in a hierarchical potential map in configuration space $\mathcal{P}$, where tunneling should occur in a multi-valley potential in configuration space with simultaneous local structural rearrangements of an appropriate number of guest atoms. See the illutration of multi-valley potential depicted in Fig. 42.

2. Explicit form of specific heats below 1 K

The range of the energy distribution $n(E)$ can be determined from the energy at which the dipoles become free from the constraint of neighboring dipoles. The maximum coupling strength from neighbor dipoles $\Delta_0 \cong z_1 J_1 + z_2 J_2 \cong 6J_1$ with configuration numbers $z_1 = 2$ and $z_2 = 8$ ($J_3 \ll J_1, J_2$). We introduce the ratio between the number of tunneling states $\bar{N}$ and the total number of off-center guest atoms N given by $\eta = \bar{N}/N < 1$. Since $\bar{N}/J_1 = 3\pi\varepsilon_r\eta/p^2$ using $R_1 = a/2$ into Eq. (65), Eq. (61) becomes the simple form

$$C_{\rm tun} \cong \frac{6\pi^3\varepsilon_r\eta}{p^2} k_{\rm B}^2 T. \tag{66}$$

Equation (66) predicts larger specific heats for smaller dipole moments p, but η vanishes with $p \to 0$ (Nakayama and Kaneshita, 2008).

A carrier-type dependence on $C_{\rm tun}(T)$ has been observed by Suekuni *et al.* (2008a) for n- and p-type β-BGS with deviations $U_0 = 0.434$ and 0.439 [Å], respectively. The observed $C_{\rm tun}(T)$ below 1 [K] for n-type β-BGS is a few percent larger than that of the p-type, as shown in Fig. 18. This accords with the prediction of Eq. (66).

The comparison of Eq. (66) with the observed magnitude of a specific heat $C_{\rm tun}(T) \cong 30T$ [mJ mol^{-1} K^{-1}] below 1 [K] for β-BGS (Suekuni *et al.*, 2008a,b) provides important information on the tunneling states. Taking $\varepsilon_r \cong 10\varepsilon_0$, η becomes $\cong 0.06$ from $C_{\rm tun}(T) \cong 50(\varepsilon_r/\varepsilon_0)\eta T$ [mJ mol^{-1} K^{-1}]. This indicates that only 6% of the off-center guest ions contribute to the specific heats *on average*. This implies that the averaged number of dipoles simultaneously rearranged by tunneling is $1/\eta \cong 20$.

The formulation of the specific heat from Eq. (66) is based on the tunneling states caused by the dipole-dipole interaction; then $C_{\rm tun}(T)$ vanishes when the dipole-dipole interaction becomes irrelevant. This is a reason why the specific heats of on-center clathrate compounds show the Debye specific heat at low temperatures.

3. Tunneling states in alkali-halide crystals containing CN^- ions

The previous subsection has highlighted the role of off-center dipoles in type-I clathrate compounds. In this connection, we should mention low temperature thermal properties of alkali-halide crystals containing CN^- ions which provide good examples showing the relevance of long-range dipole-dipole interactions. The alkali-halide mixed crystals have served as a model for the exploration of the low-energy excitations characteristic to structural glasses (De Yoreo *et al.*, 1986; Loidl *et al.*, 1988; Narayanamurti and Pohl, 1970; Topp and Pohl, 2002; Winterlich *et al.*, 1995). The low temperature thermal properties of $(KBr)_{1-x}(KCN)_x$ single crystals in the range of $0.25 \le x \le 0.70$ have investigated by De Yoreo *et al.* (1986) and Topp and Pohl (2002).

Although $(KBr)_{1-x}(KCN)_x$ is crystalline, it is disordered in two ways. The CN^- ions and the Br^- ions are randomly distributed over the anion sub-lattice. This disorder by itself is unlikely to produce emergence of a glass-like behavior since mixed crystals such as KBr:KI involves the same disorder, but does not show glass-like behavior (Nathan *et al.*, 1976). In the case of KBr:KCN, the CN^- molecules are disordered with respect to their orientations in the cubic lattice.

The observed specific heats are well described by the relation given in Eq. (28). For x=0.25, 0.50, and 0.70, the values of the small factor δ giving the best fit for the long-time data are δ=0.03, 0.00, and 0.08, respectively. The observed values of specific heats below 1 [K] for the case of x=0.25 yields the number density of $\bar{N} \cong 10^{17}$ [cm^{-3}]. This is the evidence that all of CN^- elements do not contribute to tunneling states, similar to the case in off-center clathrate compounds described in the previous section. The role of long-range interactions between elastic dipoles randomly distributed in crystals have been theoretically investigated (Grannan *et al.*, 1990a,b; Randeria and Sethna, 1988).

We should mention the INS experiments performed for the KCN:CN system by Walton *et al.* (1974). They have observed at 5 [K] a clear anti-crossing of the acoustic phonon dispersion relation between 0.4 and 0.5 [THz] corresponding to T_{1u} and T_{2u} modes of a CN^- molecule in a KCl crystal doped with 6×10^{19} CN^- [cm^{-3}]. However, the anti-crossing was not observed at room temperature. The strong dependence of INS intensities on temperature indicates that the coupling between acoustic phonons and libration modes of CN^- depend on the state of the CN^- molecule, namely, the libration modes are well characterized at low temperatures compared with those at room temperature.

IX. UNDERLYING MECHANISMS OF GLASS-LIKE THERMAL CONDUCTIVITIES

The reduction of phonon thermal conductivities $\kappa_{\rm ph}(T)$ is the key element to increase the dimension-

less figure of merit ZT according to the "phonon-glass electron-crystal" concept (Slack, 1995). Berman (1949) discovered in structural glasses the unexpected anomaly of $\kappa_{\rm ph}(T)$. He measured $\kappa_{\rm ph}(T)$ of several samples of silica glass in the temperature range 2.2−90 [K] and found the plateau behavior in the temperature range 5−10 [K] with a magnitude several orders of magnitude smaller than that of crystal silica. However, these properties attracted little attention until the work of Zeller and Pohl (1971), who discovered three characteristic temperature regions; (i) $\kappa_{\rm ph}(T) \propto T^{2-\delta}$ below 1 [K], (ii) the plateau region of $\kappa_{\rm ph}(T)$ at around 5−10 [K], and (iii) $\kappa_{\rm ph}(T)$ show the T-linear rise subsequent to the plateau region above 10 [K]. The same features of $\kappa_{\rm ph}(T)$ have been found for a variety of glasses and amorphous materials (Freeman and Anderson, 1986; Zeller and Pohl, 1971).

Nolas *et al.* (1998b) have pointed out that the $\kappa_{\rm ph}(T)$ of off-center SGG polycrystalline samples behaves like those of structural glasses. The same characteristics have been observed for other type-I clathrate compounds containing off-center guest atoms (Avila *et al.*, 2006a,b; Bentien *et al.*, 2004, 2005; Cohn *et al.*, 1999; Nolas *et al.*, 1995, 1996, 1998a,b,b,c, 2000, 2001a; Sales *et al.*, 1996; Sales, 1998; Sales *et al.*, 2001; Suekuni *et al.*, 2007, 2008a,b, 2010; Xu *et al.*, 2010), where the temperature dependence and the magnitude of $\kappa_{\rm ph}(T)$ are almost identical to those of structural glasses; these are the power law of $\kappa_{\rm ph}(T) \propto T^{2-\delta}$ in the temperature below $T \simeq 1$ [K], the plateau-temperature region at T=1−10 [K], and the subsequent rise of $\kappa_{\rm ph}(T)$ proportional to T at the high-temperature end of the plateau.

This section describes theoretical interpretations taking into account the quantum mechanical aspects of these unique behaviors observed in type-I clathrate compounds belonging to off-center systems.

A. Thermal conductivities below 1 K

$\kappa_{\rm ph}(T)$ can be evaluated on the assumption that heat is carried by acoustic phonons obeying linear-dispersion relations. This is expressed by

$$\kappa_{\rm ph}\left(T\right) = \frac{1}{3}\sum_{\mu}\int_0^{\omega_{c\mu}} \hbar\omega_\mu \frac{\partial n_{\rm B}}{\partial T} v_\mu^2 \tau_\mu\left(T,\omega\right) D(\omega_\mu) {\rm d}\omega_\mu, \tag{67}$$

where $n_{\rm B}$ is the Bose-Einstein distribution function, and $D(\omega_\mu)$, $v_\mu = \partial\omega_\mu(k)/\partial k$ and τ_μ are the Debye density of states, the group velocity, and the life-time of acoustic phonons of the mode μ, respectively. Note that the Matthiessen's rule for the life-time $1/\tau_\mu = \sum_i 1/\tau_i$ should hold for independent scattering process i.

The cut-off frequency $\omega_{c\mu}$ means the cross-over frequency from linear dispersion to flat dispersion of acoustic phonons of the mode μ, at which the group velocity v_μ of acoustic phonons of the mode μ almost vanishes. At temperatures below 1 [K], this cut-off frequency becomes irrelevant, whereas this frequency becomes crucial above 1 [K].

For type-I clathrates with off-center guest atoms at $T \lesssim 1$ [K], dominant scattering arises from the interaction between tunneling states and thermally excited acoustic phonons. The scattering rate of a phonon of the mode μ due to the interaction with a tunneling state is given by (Phillips, 1987)

$$\frac{1}{\tau_\mu(\omega)} = \sum_E \frac{\pi g_\mu^2 \omega_\mu}{\rho v_\mu^2}\left(\frac{\Delta}{E}\right)^2 \tanh\left(\frac{\beta\hbar\omega}{2}\right)\delta\left(\hbar\omega - E\right), \tag{68}$$

where g_μ is the deformation coupling constant and ρ the mass density ($\rho = 6.01\times10^3$ [kg m^{-3}] for β-BGS). The averaging procedure by the distribution function $f(\varepsilon,\lambda)$ defined in VIII.A.1 can be simplified by replacing $\sum_E \delta(\hbar\omega - E) \to \int n(E){\rm d}E$ as in the case of Eq. (60). The dominant tunneling process occurs at $\Delta \cong E$, then Eq. (68) provides

$$\frac{1}{\tau_\mu(T,\omega)} = \frac{\pi^2 g_\mu^2 \omega_\mu}{2\rho v_\mu^2}\left(\frac{\varepsilon_r\eta}{p^2}\right)\tanh\left(\frac{\beta\hbar\omega}{2}\right), \tag{69}$$

where the density of states is taken as $\bar{N}/\Delta_0 \cong \pi\varepsilon_r\eta/2p^2$ due to the interacting-dipole picture given in Sec. VIII.B.2. By combining the above scattering rate with Eq. (67), $\kappa_{\rm tun}(T)$ becomes

$$\kappa_{\rm tun}(T) \cong \frac{\rho k_{\rm B}^3 v_{\rm s}}{2\pi^2\hbar^2 g^2(\varepsilon_r\eta/p^2)}T^2, \tag{70}$$

where the velocity $v_{\rm s}$ and the deformation coupling constant g refer to the average values for the three modes of acoustic phonons. A more convenient form involving the specific heat $C_{\rm tun}$ is obtained as

$$\kappa_{\rm tun}(T) \cong \left(\frac{3\pi\rho v_{\rm s}\eta k_{\rm B}^3}{\hbar^2 C_{\rm tun}/T}\right)\left(\frac{T}{g/k_{\rm B}}\right)^2. \tag{71}$$

This relation suggests that thermal conductivities $\kappa_{\rm tun}(T) \propto T^{2-\delta}$ with small factor δ reflecting $C_{\rm tun}(T) \propto T^{1+\delta}$ (Kaneshita and Nakayama, 2009). The small factor δ originates from the distribution function $f(\epsilon,\lambda)$ as iscussed in Sec. VIII.B.2. Equation (71) predicts that the magnitude of $\kappa_{\rm tun}(T)$ should be proportional to the inverse of $C_{\rm tun}(T)$, namely, $\kappa_{\rm tun}(T) \to$ small when $C_{\rm tun}(T) \to$ large. This relation holds for $\kappa_{\rm tun}(T)$ of n- and p-type β-BGS as observed in Figs. 7 and 18.

We employ the following physical parameters of β-BGS. The average value of v_μ is $v_{\rm s}$=2.3×10^3 $\left[{\rm m\,s^{-1}}\right]$ from the actual values of velocities, $v_{C_{11}}$=3369 $\left[{\rm m\,s^{-1}}\right]$, $v_{C_{11}-C_{12}}$=1969 $\left[{\rm m\,s^{-1}}\right]$, and $v_{C_{44}}$=1844 $\left[{\rm m\,s^{-1}}\right]$. These yield

$$\kappa_{\rm tun}(T) = 2.0\times10^5\left(\frac{T}{g/k_{\rm B}}\right)^2 \left[{\rm W\,K^{-1}\,m^{-1}}\right]. \tag{72}$$

Using the experimental data of $\kappa_{\rm tun}(T) \cong 0.02T^2$ $\left[{\rm W\,K^{-1}\,m^{-1}}\right]$ for β-BGS (Suekuni *et al.*, 2008a), the deformation coupling g

is estimated as $g \simeq 0.3\,[\mathrm{eV}]$. This is a reasonable value because the deformation coupling constants g in glasses are in the range of $0.1-1\,[\mathrm{eV}]$ (Anderson *et al.*, 1972; Phillips, 1972).

B. Plateau region of thermal conductivities at around 5 K

For off-center type-I clathrate compounds, some mechanisms have been proposed to explain $\kappa_{\rm ph}(T)$ in the plateau temperature region (Bridges and Downward, 2004; Dong *et al.*, 2001; English and Tse, 2009; Hermann *et al.*, 2005). Bridges and Downward (2004) argued a mechanism for plateau thermal conductivities of off-center clathrate compounds. Hermann *et al.* (2005) have considered the role of Einstein oscillators in filled skutterudites in view of explaining their lattice dynamics. Dong *et al.* (2001) have performed molecular dynamics (MD) calculations for $\kappa_{\rm ph}(T)$ on clathrate compounds with and without guest atoms in cages. The addition of guest atoms in cages produced a reduction of phonon thermal conductivity. English and Tse (2009) have investigated the mechanism for $\kappa_{\rm ph}(T)$ in methane hydrate, which shows the same plateau temperature region as the case of off-center clathrate compounds. These works have employed MD calculations combined with the linear response formula for $\kappa_{\rm ph}(T)$, not taking into account quantum aspects such as the annihilation or creation of acoustic phonons *via* anharmonic interactions. The importance of the three-phonon process, Umklapp process, was first pointed by Peierls (1929) to explain the peak of $\kappa_{\rm ph}$ observed at about $10\,[\mathrm{K}]$ for crystals. MD calculations at the present stage cannot reproduce these *quantum* processes. This is the most difficult task in MD calculations on heat transport simulations.

1. Umklapp process for on-center systems

Type-I clathrate compounds belonging to on-center systems possess the symmetry of translational invariance. This implies that the wave vector $\boldsymbol{k}$ of acoustic phonons carrying heat are well defined in the whole Brillouin zone. Acoustic phonons are scattered mainly by two mechanisms: Rayleigh elastic scattering due to imperfections and the anharmonic phonon-phonon inelastic scattering. The Rayleigh scattering due to the static imperfections proportional to $1/\tau_{\rm R}(\omega) \propto \omega^4$ does not become the dominant scattering mechanism in type-I clathrate compounds. This is because the wavelength of excited phonons is much larger than the scale of imperfections. So, we should have the situation $v_\mu \tau_\mu(T,\omega) > L$ at low temperatures, where L is the size of the crystalline part. This leads to $\kappa_{\rm ph}(T) \propto C_{\rm ph} \propto T^3$ for on-center type-I clathrate compounds.

With increasing temperature above 1 [K], the wave vectors of thermally excited phonons approaches the middle of the Brillouin zone, and the Umklapp process starts to contribute to the decrease of $\kappa_{\rm ph}(T)$ at around $T \sim 10\,[\mathrm{K}]$. See Figs. 14 and 16.

Coherent INS data for on-center BGG given in Fig. 29 show that the avoided crossings for transverse acoustic phonons occur at $|\boldsymbol{k}| \gtrsim |\boldsymbol{G}|/4$ with the reciprocal lattice vector $\boldsymbol{G}$. This allows the Umklapp process $\boldsymbol{k}_1 + \boldsymbol{k}_2 = \boldsymbol{k}_3 + \boldsymbol{G}$ for acoustic phonons which simultaneously satisfy energy conservation law for anharmonic three-phonon processes. These crystalline features of $\kappa_{\rm ph}(T)$ are clearly manifested in experimental data of on-center clathrate compounds shown in Figs. 14 and 16.

At high temperatures $T \geq \hbar\omega_{c\mu}/k_{\rm B}$, the number of excited phonons are proportional to T. The scattering probability $1/\tau_\mu$ due to ahnharmonic interactions of acoustic phonons of the mode μ is proportional to the number of excited phonons $\propto T$ resulting in the mean free path $\ell_\mu = v_\mu \tau_\mu \propto 1/T$. Since the average velocity v_μ^2 in Eq. (67) should be independent of T, $\kappa_{\rm ph}(T) \propto T^{-1}$ as observed in Figs. 14 and 16.

2. Plateau temperature region of off-center systems

$\kappa_{\rm ph}(T)$ of type-I clathrate compounds containing off-center guest atoms take the universal form as described in Sec. V.B. The energy range of the plateau region in $\kappa_{\rm ph}(T)$ overlaps with that of the Boson-peak like excess density of states in off-center type-I clathrate compounds in the THz frequency region. The physical origin of the plateau temperature region should be interpreted in reference to this excess density of states.

The upper cut-off frequency $\omega_{c\mu}$ of the integral in the general formula for $\kappa_{\rm ph}(T)$ in Eq. (67) represents the cross-over frequency from the linear dispersion relation to the flat dispersion relation of acoustic phonons, where the group velocity of acoustic phonons of the mode μ vanishes. The frequency $\omega_{c\mu}$ behaves as a mobility edge for acoustic phonons. Thus, the cross-over frequency $\omega_{c\mu}$ is crucial to reveal the plateau behavior of $\kappa_{\rm ph}(T)$.

Transverse acoustic phonons with two degrees of freedom of the modes mainly contribute to phonon thermal transport. The dispersion relations of β-BGS theoretically calculated in Fig. 36(b) show a wide flat region for the acoustic branch of transverse phonons arising from the coupling with the low-lying librational modes (Nakayama and Kaneshita, 2011). The calculated results given in Fig. 36(b) definitely show that the avoided crossing starts at the region below $|\boldsymbol{k}| \cong |\boldsymbol{G}|/4$. This result indicates that acoustic phonons carrying heat are limited to those with the wave number $|\boldsymbol{k}| \lesssim |\boldsymbol{G}|/4$. This leads to the plateau temperature region of $\kappa_{\rm ph}(T)$ similar to the case of the Dulong-Petit limit of the Debye specific heats, i.e., $\kappa_{\rm ph}(T)$=constant. Namely, conventional heat transport occurs via already excited phonons yielding a saturation in $\kappa_{\rm ph}(T)$, which is referred to as the plateau.

The cross-over frequency $\omega_{c\mu}$ is obtained by subtract-

ing the frequency $\delta\omega_{c\mu}$ given by Eq. (53) as $\omega_{c\mu} = \omega_{0\mu} - \delta\omega_{c\mu}$. The use of Eq. (51) leads to

$$\omega_{c\mu} \cong \omega_{0\mu}\left(1 - \sqrt{\frac{m}{M}}\right). \tag{73}$$

The peak frequency of the thermal distribution at the temperature T becomes $\hbar\omega_{c\mu} \cong 3.83 k_{\rm B} T$, taking into account the Stefan shift. Then, the relation between the lowest optic eigenfrequency $\omega_{0\perp}$ and the onset temperature $T_{\rm p}$ of the plateau becomes, from Eq. (73)

$$T_{\rm p} \cong \hbar\omega_{0\perp}\frac{\left(1 - \sqrt{m/M}\right)}{3.83 k_{\rm B}}. \tag{74}$$

The above relation between $T_{\rm p}$ of $\kappa_{\rm ph}(T)$ and $\hbar\omega_{c\mu}$ of the phonon dispersion relation holds for type-I clathrates with off-center rattling guest atoms.

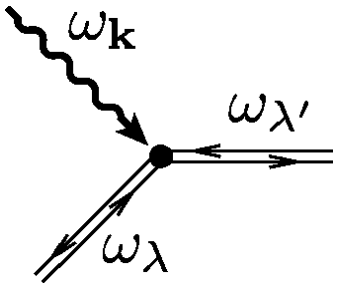

FIG. 43 Diagram illustrating a first-order process of local-mode hopping. The local mode (double lines) interacts with the acoustic phonon (wavy line) with the eigenfrequency $\omega_{\boldsymbol{k}}$, hopping from the initial state with ω_λ to the final with $\omega_{\lambda'}$, where $\omega_{\lambda'} > \omega_\lambda > \omega_{\boldsymbol{k}}$. The set of arrowheads in the opposite directions on the double lines indicate that the local modes consist of the superposition of plane waves with opposite directions.

C. T-linear rise above the plateau temperature region

1. Thermal transport due to the hopping of local modes associated with guest atoms

At the temperature regime $T \gtrsim 10\,[\rm K]$ above the plateau, the $\kappa_{\rm ph}(T)$ of off-center type-I clathrate compounds exhibit the empirical law $\kappa_{\rm ph}(T) = \kappa_{\rm plateau} + \kappa_{\rm add}$, where $\kappa_{\rm add} = \alpha T$ (Avila *et al.*, 2006a, 2008; Bentien *et al.*, 2005; Cohn *et al.*, 1999; Nolas *et al.*, 2000, 2001a; Sales *et al.*, 2001; Suekuni *et al.*, 2007, 2008a). The prefactors α become $\alpha = 0.009\,[\rm W\,K^{-2}\,m^{-1}]$ for n-type and $\alpha = 0.007\,[\rm W\,K^{-2}\,m^{-1}]$ for p-type β-BGS (Avila *et al.*, 2006a, 2008; Suekuni *et al.*, 2007, 2008a). Of importance is that $\kappa_{\rm ph}(T)$ vanishes when extrapolating the temperature $T \to 0$, as seen from Fig. 14. It implies that a new *additional* heat-transport channel opens up above the plateau temperature region. This feature, termed $\kappa_{\rm add}(T)$, at high temperatures is the same as those of structural glasses or amorphous materials (Freeman and Anderson, 1986; Stephens, 1973; Zeller and Pohl, 1971). This is remarkably different from the cases of on-center type-I clathrate compounds, which behave as $\kappa_{\rm ph}(T) \propto 1/T$ above $T \gtrsim 10\,[\rm K]$.

The plateau temperature regions of $\kappa_{\rm ph}(T)$ are also observed for silica aerogels (Bernasconi *et al.*, 1992). In silica aerogels, there are two types of phonons, low-energy extended acoustic phonons and high-energy localized phonons separated at the cross-over frequency $\omega_{\rm c}$. Alexander *et al.* (1986) have proposed a hopping mechanism of localized modes to explain the T-linear dependence of $\kappa_{\rm add}(T)$ of silica aerogels. Jagannathan *et al.* (1989) and Nakayama and Orbach (1999a,b) have introduced this mechanism to explain the T-linear rise of $\kappa_{\rm add}(T)$ above the plateau in structural glasses. Hashimoto and Shimizu (2011) have demonstrated for silica glass the hopping of local modes associated with the Boson peak. They have employed transient saturation spectroscopy for $^{167}{\rm Er}^{3+}$ ions doped in a silica glass fiber in the range $2.5-30\,[\rm K]$, a temperature range taken above the plateau region. The result is consistent with the idea that local modes carry heat by their hopping assisted by acoustic phonons.

Here we present a simple explanation for the hopping mechanism contributing to $\kappa_{\rm ph}(T)$ in the temperature regime above the plateau. The formula of Eq. (67) for the thermal conductivity based on the propagation of extended acoustic phonons is not applicable to the hopping mechanism. At such high temperatures, the additional channel of heat transfer is opened up via the diffusion of local modes associated with guest atoms, where the hopping of local modes occurs via the anharmonic interaction with extended acoustic phonons as shown in Fig. 43.

The thermal conductivity due to the phonon-assisted hopping is given by (Alexander *et al.*, 1986)

$$\kappa_{\rm hop}(T) = \sum_\lambda C_\lambda(T)\frac{R_\lambda^2}{3\tau_\lambda(T)}, \tag{75}$$

where R_λ is the hopping distance of the local mode λ and R_λ^2/τ_λ is the thermal diffusivity due to the local mode hopping. The decay rate $1/\tau_\lambda(T)$ is caused by the interaction with acoustic phonons, and C_λ the specific heat associated with the local mode λ. In the higher temperature regime above the plateau region $T \geq \hbar\omega_{c\mu}/3.83 k_{\rm B}$, the specific heat C_λ follows the Dulong-Petit relation in the form $C_\lambda = k_{\rm B}/V$, where V is the volume of the system. Substituting this relation into Eq. (75), we have the thermal conductivity formula given by

$$\kappa_{\rm hop} \cong \frac{k_{\rm B}}{3V}\sum_\lambda \frac{R_\lambda^2}{\tau_\lambda(T)}, \tag{76}$$

where the sum over λ means the integral on ω_λ is defined by

$$\sum_\lambda \to \sum_\mu \int_{\omega_{c\mu}}^{\omega_{c\mu}+\Delta\omega_\lambda} d\omega_\lambda N_{\rm ex}(\omega_\lambda). \tag{77}$$

Here $N_{\rm ex}$ is the excess density of states and $\Delta\omega_\lambda$ is its bandwidth. The decay rate $1/\tau_\lambda(T)$ is proportional to the Bose-Einstein distribution function $n_{\rm B}(T)$ of acoustic phonons of the form $n_{\rm B} \cong k_{\rm B}T/\hbar\omega_{c\mu}$ in the high temperature regime $T \gtrsim \hbar\omega_{c\mu}/3.83k_{\rm B}$. These procedures give rise to the following simple relation for $\kappa_{\rm hop}(T)$,

$$\kappa_{\rm hop}(T) \simeq \frac{Nk_{\rm B}^2}{V}\frac{R(\omega_{c\mu})^2 T}{\hbar\omega_{c\mu}\tau(\omega_{c\mu})}, \tag{78}$$

where the factor 3 is canceled out by taking into account the contribution from the three acoustic phonon modes. We can estimate from Eq. (78) the actual value of the hopping contribution to $\kappa_{\rm hop}(T)$ above the plateau region by the following arguments.

With increasing temperature above $T \gtrsim \hbar\omega_{c\mu}/3.83k_{\rm B}$, acoustic phonons are hybridized with vibrations of guest atoms manifesting the Ioffe-Regel limit $kR(\omega_{c\mu}) \cong 1$, or equivalently, $\omega_{c\mu}\tau(\omega_{c\mu}) \cong 1$ (A. F. Ioffe and Regel, 1960). This is the limit in which a quantum mechanical treatment is applicable. The average hopping distance $R(\omega_{c\mu})$ is surely the distance between the nearest neighbor off-center guest atoms of the order of 1 [nm]. Thus, the hybridized local mode λ associated with the guest atoms in cages should satisfy the condition $\omega_{c\mu}\tau(\omega_{c\mu}) \cong 1$. Substituting these relations into Eq. (78) together with the number density of the local mode λ of $N/V = 1/R(\omega_{c\mu})^3$, we have

$$\kappa_{\rm hop} \simeq 0.002\,[{\rm WK^{-1}m^{-1}}]. \tag{79}$$

The estimated value agrees well with the observed prefactor α for off-center type-I clathrate compounds, reflecting that the T-linear rise above the plateau region is a universal phenomena.

The quantitative microscopic calculations on $\kappa_{\rm hop}$ should be made by taking into account the anharmonic interaction Hamiltonian between the acoustic phonon with the wave vector $\boldsymbol{k}$ and the local modes $|\lambda\rangle$, $|\lambda'\rangle$, which is expressed as follows:

$$H_{\rm hop} = C_{\rm eff}\sum_{\boldsymbol{k},\lambda,\lambda'}(A_{\mathbf{k},\lambda,\lambda'}\, c_\lambda^\dagger c_{\lambda'} b_{\mathbf{k}} + {\rm h.c.}), \tag{80}$$

where the operators $b_{\boldsymbol{k}}^\dagger$ and $c_\lambda^\dagger$ ($b_{\boldsymbol{k}}$ and c_λ) are the creation (annihilation) operators for an acoustic phonon and a local mode, respectively. $H_{\rm hop}$ is proportional to the dilatation of cages due to incoming acoustic phonons. The explicit form of the coupling constant $A_{\mathbf{k},\lambda,\lambda'}$ in Eq. (80) is given by (Kaneshita and Nakayama, 2009; Nakayama and Orbach, 1999a,b)

$$A_{\mathbf{k},\lambda,\lambda'} = \sqrt{\frac{1}{V}}\left(\frac{\hbar}{2\rho}\right)^{3/2}\sqrt{\frac{\omega_{\mathbf{k}}}{\omega_\lambda\omega_{\lambda'}}}\left(\frac{I}{v_\mu \ell_\lambda \ell_{\lambda'}}\right), \tag{81}$$

where ρ is the mass density. The localization length ℓ_λ is the size of cages containing guest atoms, which is comparable with the hopping distance of the local mode λ. The factor I in Eq. (81) is the overlap integral between local modes represented by

$$I \cong \left(\frac{16}{\pi}\right){\rm e}^{-R_\lambda/\ell_\lambda + {\rm i}\mathbf{k}\cdot\mathbf{R}_\lambda}, \tag{82}$$

where the local mode decays exponentially. As seen above, the explicit form of the local mode is not necessary, but only the order of R_λ and ℓ_λ.

For the process $|\boldsymbol{k};\lambda\rangle \to |\lambda'\rangle$ illustrated in Fig. 43, first-order perturbation theory provides the hopping life-time of the local mode λ at temperatures $k_BT \gg \hbar\omega_{c\mu}$ of the form

$$\begin{aligned}\frac{1}{\tau_\lambda(T)} &= \frac{2\pi}{\hbar^2}\sum_{\lambda,\lambda'} \mid A_{\boldsymbol{k},\lambda,\lambda'} \mid^2 \\ &\times\ [1 + n(\omega_{\boldsymbol{k}}) + n(\omega_{\lambda'})]\,\delta\left(\omega_{\boldsymbol{k}} - \omega_{\lambda'} + \omega_\lambda\right).\end{aligned} \tag{83}$$

The substitution of Eq. (83) into Eq. (76) yields the hopping contribution to the thermal conductivity given by

$$\kappa_{\rm hop}(T) = \frac{12^2 C_{\rm eff}^2 k_{\rm B}^2 T}{\pi^4\rho^3 v_s^5 \ell_\lambda^5}, \tag{84}$$

where the mass density ρ=6.01×10^3 [kg m^{-3}] is for β-BGS, $\ell_\lambda \simeq 1$ [nm] and $1/v_s^5$ is the average of $1/v_\mu^5$ taking $\cong$3.6 ×10^{-17} [m^{-5} s^5] for β-BGS. Since the magnitude and temperature dependence of the thermal conductivities above the plateau temperature region of off-center type-I clathrate compounds are almost identical to those of structural glasses, it is appropriate to take the coupling constant $C_{\rm eff}$ of structural glasses, which provides $C_{\rm eff}$=−2.0×10^{12} [N m^{-2}] (Kaneshita and Nakayama, 2009; Nakayama and Orbach, 1999a,b). As a result, the thermal conductivity for β-BGS becomes $\kappa_{\rm ph}(T) \cong 0.003T\,[{\rm W\,K^{-1}\,m^{-1}}]$ above the plateau $T \geq 10$ [K]. This coincides well with the experimental values of β-BGS (Avila *et al.*, 2006a, 2008; Suekuni *et al.*, 2007, 2008a).

2. Overall interpretation of glass-like thermal conductivities

The analyses described from Sec. VIII to Sec. VII lead to the following interpretation on $\kappa_{\rm ph}(T)$ of off-center type-I clathrate compounds. These are summarized as follows; (i) two-level tunneling states generated by *interacting* electric dipoles explain the observed $\kappa_{\rm ph}(T) \propto T^{2-\delta}$ with a small value of δ below 1 [K], (ii) the plateau region, $\kappa_{\rm ph}(T)$ = constant, is a direct consequence of the *flattening* of acoustic modes due to the hybridization with local vibrations of off-center guest atoms, and (iii) the subsequent T-linear rise above the plateau originates from the hopping of local modes assisted by acoustic modes of networked cages.

There is an additional complication at much higher temperatures, as shown in Fig. (14) and (18), where the T-linear rise in $\kappa_{\rm ph}(T)$ does not continue, but $\kappa_{\rm ph}(T)$

shows a curling over above $T \simeq 100$[K]. This temperature regime is important for practical application of type-I clathrates to efficient thermoelectric materials. In this regime, quenching of phonon-assisted hopping occurs via the breakdown of three-phonon anharmonic scattering (Simons, 1964). The hysteresis becomes larger in adjusting to an instantaneous thermal equilibrium distribution, which leads to a curling over of $\kappa_{\rm ph}(T)$ attributable to the hydrodynamic or Akhieser limit (Akhieser, 1939a). Thus, the key aspects of thermal conductivities of type-I clathrate compounds containing off-center guest atoms can be completely understood over the entire temperature range in a consistent way.

X. SUMMARY AND CONCLUSIONS

This article has reviewed the development of research on phonon-glass electron-crystal (PGEC) thermoelectric materials, in particular, focusing on experimental and theoretical aspects of type-I clathrate compounds. After the PGEC concept was coined by Slack (1995), much efforts have been spent in exploring efficient thermoelectric materials. As a candidate for PGEC materials, Slack (1995) have promoted clathrate compounds encapsulating guest atoms in cages. Type-I clathrate compounds manifest the PGEC concept when the size mismatch is large enough between the guest ion and the tetrakaidecahedoral cage. Thereby, the guest atoms take off-center positions in the tetrakaidecahedron.

The microscopic structure of type-I clathrate compounds have been clarified by means of the following experimental techniques: x-ray diffraction, neutron diffraction, resonant x-ray diffraction, and extended x-ray absorption fine structure spectroscopy. These have been described in detail in Sec. III. Specific heat measurements on type-I clathrate compounds with off-center guest atoms have revealed the existence of the Boson-peak like excess density of states over the Debye phonons at around several Kelvin. The characteristic temperatures θ of guest atom $\mathcal{R}(2)$ have been estimated from the peaks in the plot of $C_{\rm V}(T)/T^3$ vs. T. These results have been summarized in Table I. In addition, the T-linear specific heats identical to those of glasses have been experimentally verified below about 1 [K], as described Sec. IV.

The excess densities of states over the Debye phonons have been also found by means of spectroscopic measurements: infrared absorption, Raman scattering, Mössbauer spectroscopy, and inelastic neutron scattering. Optical spectroscopies have made possible the identification of the relevant modes contributing to the excess densities of states. Raman scattering and infrared absorption experiments for type-I clathrate compounds containing off-center guest atoms have revealed the relevance of the $\rm T_{2g}$ mode and the $\rm E_g$ mode to the excess densities of states. These modes do not exist in the case of type-I clathrate compounds with on-center guest atoms. It is remarkable that the line widths of these modes increase on cooling and the spectral energies shift lower, which provide opposite behaviors to those expected for usual crystalline materials. This key observation has been confirmed by INS experiments as well (Nakamura and Arai, 2010). These experiments and theoretical interpretation have been described in detail in Sec. VI and Sec. VII.

Furthermore, thermal conductivity measurements display glass-like behaviors characterized as follows: T^2-dependence at temperatures below 1 [K], the plateau at temperatures of several [K], and the T-linear dependence above the plateau at around 10 [K]. Surprisingly enough, these temperature dependences as well as the magnitudes are identical to those of structural glasses in the whole temperature range. We have described relevant experiments in Sec. V, emphasizing that off-center guest atoms play a key role for the emergence of glass-like thermal and dynamical properties.

Concerning the efficiency of the thermopower, type-I $\rm Ba_8Ga_{16}Sn_{30}$ manifests low thermal conductivities in addition to high absolute values of the Seebeck coefficients S of 300 [μV/K] for both p- and n-type crystals at 300 [K]. The electrical resistivity ρ at room temperature is in the range $20-40\times10^{-3}$ [Ωcm], which is several times larger than that expected for efficient thermoelectric materials. This large ρ is caused by low-carrier densities of 10^{19} [$\rm cm^{-3}$] and low carrier mobilities $20-40$ [$\rm cm^2$/Vs]. As a result, the dimensionless figure of merit $ZT = S^2T/\rho\kappa_{\rm tot}$ does not reach the desired value of 1.0, but exhibit maxima of 0.58 and 0.50 at around 450 [K] for the p- and n-type samples, respectively. It is necessary to decrease the resistivity by doping carriers in order to realize the "electron-crystal" concept.

Type-VIII $\rm Ba_8Ga_{16}Sn_{30}$ is a possible candidate for an efficient thermoelectric material. The Ba guest atoms in distorted dodecahedron vibrate with the atomic displacement parameter (ADP) three times larger than those of cage atoms. These anisotropic and anharmonic vibrations depress $\kappa_{\rm ph}$ at higher temperatures above 100 [K]. The actual values of $\kappa_{\rm ph}$ take the value 0.7 [W/(mK)] at above 100 [K], as shown in Fig. 17. These values are higher than that $\kappa_{\rm ph}$=0.4 [W/(mK)] of β-BGS, but they are still lower than those of thermoelectric materials based on Bi-Te. The carrier density can be tuned by substituting various types of elements for the cage atoms Ga and Sn. For Cu substitution, ZT for p-type and n-type samples increase to 0.9 at 480 [K] and 1.45 at 520 [K], respectively. These values exceed those of the Pb-Te based materials at the same temperature. Therefore, type-VIII $\rm Ba_8Ga_{16}Sn_{30}$ without toxic elements is regarded as a human-friendly thermoelectric material with operation temperatures around $400-600$ [K]. At higher temperatures, Si- and Ge-based clathrates have better structural stability than Sn-based clathrates. Thermoelectric modules composed of similar clathrates based on Sn, Ge, and Si may have a conversion efficiency higher than 10% in the wide temperature range from 300 [K] to 1200 [K].

Finally, we should emphasize that the theoretical understanding of glass-like behaviors of $\kappa_{\rm ph}$ of off-center clathrate compounds has benefited very much from accumulated research on structural glasses. However, in structural glasses, it is difficult to identify relevant entities or elements due to their complex microscopic structures (Nakayama, 2002). This is the main reason why the arguments on the origin of the Boson peak have continued for decades. This being said, it is clear that off-center guest atoms in type-I clathrate compounds are a key ingredient for emerging glass-like behavior. This has made it possible to provide clear theoretical interpretation of glass-like thermal and dynamic properties for these compounds.

To sum up, the subjects described in this review involve interesting phenomena not only for the physics itself but also for the exploration of renewable-energy materials. We hope that this review will serve as a basis for further development of clathrate-related efficient thermoelectric materials.

XI. ACKNOWLEDGMENTS

We are most grateful to M. A. Avila, T. Kume, T. Mori, Y. Takasu, and N. Toyota for many valuable discussions and useful suggestions. We thank H. Fukuoka, T. Hasegawa, I. Ishii, C.H. Lee, T. Suzuki, K. Tanigaki, H. Tou, M. Udagawa, K. Umeo, J. Xu, and S. Yamanaka for fruitful discussions. Special thanks are to M. Nakamura and M. Arai for supplying the INS data of type-I clathrates prior to publication. We are grateful to O. B. Wright for a critical reading of the manuscript. T. N. wishes to acknowledge with gratitude the support and hospitality of Max-Planck Institute for the Physics of Complex Systems during his stay in 2012-13. This work was partially supported by a NEDO Grant No. 09002139-0 and Grant-in-Aid for Scientific Research from the Ministry of Education, Culture, Sports, Science and Technology (MEXT) of Japan, Grants Numbers 18204032, 19051011, 20102004, 22013018, 22540404, and 22740225.

References

Akai, K., G. Zhao, K. Koga, K. Oshiro, and M. Matsuura, 2005, in *Proceedings of the 24th International Conference on Thermoelectrics*, (IEEE, New York), pp. 230-233.

Akai, K., T. Uemura, K. Kishimoto, T. Tanaka, H. Kurisu, S. Yamamoto, T. Koyanagi, K. Koga, H. Anno, and M. Matsuura, 2009, J. Electron. Mater. **38**, 1412.

Akhieser, A., 1939, J. Phys. **1**, 277.

Alexander, S., O. Entin-Wohlman, and R. Orbach, 1986, Phys. Rev. B **34**, 2726.

Anderson, O. L., 1959, J. Phys. Chem. Solids **12**, 41.

Anderson, P. W., B. I. Halperin, and C. M. Varma, 1972, Phil. Mag. **25**, 1.

Anno, H., M. Hokazono, M. Kawamura, J. Nagao, and K. Matsubara, 2002, in *Proceedings of the 21st International Conference on Thermoelectrics*, (IEEE, New York) , pp. 77-80.

Anno, H., M. Hokazono, M. Kawamura, and K. Matsubara, 2003, in *Proceedings of the 22nd International Conference on Thermoelectrics*, (IEEE, New York) , pp. 121-126.

Anno, H., H. Yamada, T. Nakabayashi, M. Hokazono, and R. Shirataki, 2012, J. Solid State Chem. **193**, 94.

Arcon, D., A. Zorko, P. Jeglic, J. Xu, J. Tang, Y. Tanabe, S Hegri, and K. Tanigaki, 2013, J. Phys. Soc. Jpn **82**, 014703.

Ashcroft, N. W. and N. D. Mermin, 1976, in *Solid State Physics*, (Thomson Learning, London), Chap.16.

Avila, M. A., K. Suekuni, K. Umeo, and T. Takabatake, 2006, Physica B **383**, 124.

Avila, M. A., K. Suekuni, K. Umeo, H. Fukuoka, S. Yamanaka, and T. Takabatake, 2006, Phys. Rev. B **74**, 125109.

Avila, M. A., K. Suekuni, K. Umeo, H. Fukuoka, S. Yamanaka, and T. Takabatake, 2008, Appl. Phys. Lett. **92**, 041901.

Aydemir, U., C. Candolfi, A. Ormeci, Y. Oztan, M. Baitinger, N. Oeschler, F. Steglich, and Yu. Grin, 2011, Phys. Rev. B **84**, 195137.

Baumbach, R., F. Bridges, L. Downward, D. Cao, P. Chesler, and B. Sales, 2005, Phys. Rev. B **71**, 024202.

Baumert, J., C. Gutt, V. P. Shpakov, J. S. Tse, M. Krisch, M. Mueller, H. Requardt, D. D. Klug, S. Janssen, and W. Press, 2003, Phys. Rev. B **68**, 174301.

Beekman, M. and G. S. Nolas, 2008, J. Mater. Chem. **18**, 842.

Beekman, M., W. Schnelle, H. Borrmann, M. Baitinger, Y. Grin, and G. S. Nolas, 2010, Phys. Rev. Lett. **104**, 018301.

Bentien, A., A. E. C. Palmqvist, J. D. Bryan, S. Latturner, G. D. Stucky, L. Furenlid, and B. B. Iversen, 2000, Angew. Chem. Int. Ed. **39**, 3613.

Bentien, A., B. B. Iversen, J. D. Bryan, G. D. Stucky, A. E. C. Palmqvist, A. j. Schlutz, and R. W. Henning, 2002, J. Appl. Phys. **91**, 5694.

Bentien, A., M. Christensen, J. D. Bryan, A. Sanchez, S. Paschen, F. Steglich, G. D. Stucky, and B. B. Iversen, 2004, Phys. Rev. B **69**, 045107.

Bentien, A., E. Nishibori, S. Paschen, and B. B. Iversen, 2005, Phys. Rev. B. **71**, 144107.

Bentien, A., V. Pacheco, S. Paschen, Y. Grin, and F. Steglich, 2005, Phys. Rev. B **71**, 165206.

Bentien, A., S. Johnsen, and Bo B. Iversen, 2006, Phys. Rev. B **73**, 094301.

Berman, R., 1949, Phys. Rev. **76**, 315.

Bernal, J. D. and R. H. Fowler, 1933, J. Chem. Phys. **1**, 515.

Bernasconi, A., T. Sleator, D. Posselt, J. K. Kjems, and H. R. Ott, 1992, Phys. Rev. B **45**, 10363.

Blake, N. P., L. Møllnitz, G. Kresse, and H. Metiu, 1999, J. Chem. Phys. **111**, 3133.

Blake, N. P., J. D. Bryan, S. Latturner, L. Møllnitz, G. D. Stucky, and H. Metiu, 2001, J. Chem. Phys. **114**, 10063.

Bobev, S. and S. C. Sevov, 2000, J. Solid State Chem. **153**, 92.

Bobev, S. and S. C. Sevov, 2001, J. Am. Chem. Soc. **123**, 3389.

Bridges, F. and L. Downward, 2004, Phys. Rev. B **70**, 140201(R).

Bryan, J. D., V. I. Srdanov, G. D. Stucky, and D. Schmidt, 1999, Phys. Rev. B **60**, 3064.

Buchenau, U., N. Nücker, and A. J. Dianoux, 1984, Phys. Rev. Lett. **53**, 2316.

Buchenau, U., M. Prager, N. Nücker, A. J. Dianoux, N. Ahmad, and W. A. Phillips, 1986, Phys. Rev. B **34**, 5665.

Bustarret, E., C. Marcenat, P. Achatz, J. Kačmarčik, F. Lévy, A. Huxley, L. Ortéga, E. Bourgeois, X. Blase, D. Débarre, and J. Boulmer, 2006, Nature **444**, 465.

Callen, H. B., 1948, Phys. Rev. **73**, 1349.

Callen, H. B., 1952, Phys. Rev. **85**, 16.

Carrillo-Cabrera, W., J. Curda, H. G. von Schnering, S. Paschen, and Yu. Grin, 2000, Z. Kristallogr. - New Cryst. Struct. **215**, 207.

Carrillo-Cabrera, W., R. Cardoso Gil, V. -H. Tran, and Yu. Grin, 2002, Z. Kristallogr. - New Cryst. Struct. **217**, 181.

Cederkrantz, D., A. Saramat, G. J. Snyder, and A. E. C. Palmqvist, 2009, J. Appl. Phys. **106**, 074509.

Chakoumakos, B. C., B. C. Sales, D. Mandrus, and V. Keppens, 1999, Acta Cryst. B **55**, 341.

Chakoumakos, B. C., B. C. Sales, D. G. Mandrus, and G. S. Nolas, 2000, J. Alloys Compd. **296**, 80.

Chakoumakos, B. C., B. C. Sales, and D. G. Mandrus, 2001, J. Alloys Compd. **322**, 127.

Chari, M. S. R. and M. V. N. Chari, 1989, Phys. Lett. A. **136**, 149.

Chari, M. S. R. and M. V. N. Chari, 1990, J. Phys.: Condens. Matter **2**, 631.

Chen, G., M. S. Dresselhaus, G. Dresselhaus, J. P. Fleurial, and T. Caillat, 2003, Int. Mater. Rev. **48**, 45.

Christensen, M., N. Lock, J. Overgaard, and B. B. Iversen, 2006, J. Am. Chem. Soc. **128**, 15657.

Christensen, M., F. Juranyi, and B. B. Iversen, 2006, Physica B **385-386**, 505.

Christensen, M., G. J. Snyder, and B. B. Iversen, 2006, in *Proceedings of the 25th International Conference on Thermoelectrics*, (IEEE, New York) , pp. 40-43.

Christensen, M. and B. B. Iversen, 2007, Chem. Mater. **19**, 4896.

Christensen, M., A. B. Abrahamsen, N. B. Christensen, F. Juranyi, N. H. Andersen, K. Lefmann, J. Andreasson C. R. H. Bahl, and B. B. Iversen, 2008, Nature Materials **7**, 811.

Christensen, M., S. Johnsen, F. Juranyi, and B. B. Iversen, 2009, J. Appl. Phys. **105**, 073508.

Christensen, M., S. Johnsen, and B. B. Iversen, 2010, Dalton Trans. **39**, 978.

Claussen, W. F., 1951, J. Chem. Phys. **19**, 259.

Claussen, W. F., 1951, J. Chem. Phys. **19**, 1425.

Claussen, W. F., 1951, J. Chem. Phys. **19**, 662.

Cohen, R. W., B. Abeles, and G. S. Weisbarth, 1967, Phys. Rev. Lett. **18**, 336.

Cohen, M. H. and F. Keffer, 1955, Phys. Rev. **99**, 1128.

Cohn, J. L., G. S. Nolas, V. Fessatidis, T. H. Metcalf, and G. A. Slack, 1999, Phys. Rev. Lett. **82**, 779.

Condron, C. L., J. Martin, G. S. Nolas, P. M. B. Piccoli, A. J. Schultz, and S. M. Kauzlarich, 2006, Inorg. Chem. **45**, 9381.

Cutler, M. and N. F. Mott, 1969, Phys. Rev. **181**, 1336.

Davidson, D. W., 1973, in *A Water: A Comprehensive Treatise*, edited by F. Franks (Plenum Press, New York), **2**.

Davy, H., 1811, Phil. Trans. R. Soc. Lond. **101**, 1.

Davy, H., 1811, Phil. Trans. R. Soc. Lond. **101**, 155.

De Yoreo, J. J., W. Knaak, M. Meissner, and R. O. Pohl, 1986, Phys. Rev. B **34**, 8828.

Dong, J., O F. Sankey, and C. W. Myles, 2001, Phys. Rev. Lett. **86**, 2361.

Dresselhaus, M. S. and I. L. Thomas, 2001, Nature **414**, 332.

Dresselhaus, M. S., G. Chen, M. Y. Tang, R. G. Yang, H. Lee, D. Z. Wang, Z. F. Ren, J. -P. Fleurial, and P. Gogna, 2007, Adv. Mater. **19**, 1043.

Eisenmann, B., H. Schäfer, and R. Zagler, 1986, J. Less-Common Met. **118**, 43.

Englezos, P., 1993, Ind. Eng. Chem. Res. **32**, 1251.

English, N. J. and J. S. Tse, 2009, Phys. Rev. Lett. **103**, 015901.

English, N. J. and J. S. Tse, 2010, Energies **3**, 1934.

English, N. J. and J. S. Tse, 2011, Phys. Rev. B **83**, 184114.

English, N. J., P. D. Gorman, and J. M. D. MacElroy, 2012, J. Chem. Phys. **136**, 044501.

Ekimov, E. A., V. A. Sidorov, E. D. Bauer, N. N. Mel'nik, N. J. Curro, J. D. Thompson, and S. M. Stishov, 2004, Nature **428**, 542.

Ettingshausen, A. V. and W. Nernst, 1886, Ann. Phys. Chem. **265**, 343.

Euchner, H., S. Pailhés, L. T. K. Nguyen, W. Assmus, F. Ritter, A. Haghighirad, Y. Grin, S. Paschen, and M. de Boissieu, 2012, Phys. Rev. B **86**, 224303.

Falmbigl, M. and P. F. Rogl, 2012, in *Modules, Systems, and Applications in Thermoelectrics*, edited by D. M. Rowe (CRC Press, Taylor and Francis Group, Boca Raton, Florida), **9**, pp. 1-23.

Fano, U., 1960, Phys. Rev. **118**, 451.

Faraday, M., 1823, Quart. J. Sci. **15**, 71.

Freeman, J. J and A. C. Anderson, 1986, Phys. Rev. B **34**, 5684.

Fritzsche, H., 1971, Solid. St. Commun. **9**, 1813.

Flubacher, P., A. J. Leadbetter, J. A. Morrison, and B. P. Stoicheff, 1959, J. Phys. Chem. Solids **12**, 53.

Fujita, I., K. Kishimoto., M. Sato, H. Anno, and T. Koyanagi, 2006, J. Appl. Phys. **99**, 093707.

Fujiwara, A., K. Sugimoto, C. H. Shih, H. Tanaka, J. Tang, Y. Tanabe, J. Xu, S. Heguri, K. Tanigaki, and M. Takata, 2012, Phys. Rev. B **85**, 144305.

Fukuoka, H., K. Iwai, S. Yamanaka, H. Abe, K. Yoza, and L. Häming, 2000, J. Solid State Chem. **151**, 117.

Gallmeier, J., H. Schäfer, and A. Weiss, 1969, Z. Naturforsch. B **24**, 665.

Gatti, C., L. Bertini, N. P. Blake, and Bo. B. Iversen, 2003, Chem. Eur. J. **9**, 4556.

Goldsmid, H. J. and R. W. Douglas, 1954, British J. Appl. Phys. **5**, 386.

Goldsmid, H. J., 2010, in *Intorduction to Thermoelectricity*, (Springer-Verlag, Berlin).

Gonçalves, A. P. and C. Godart, 2013, in *New Materials for Thermoelectric Applications: Theory and Experiment*, edited by V. Zlatic and A. Hewson (Springer-Verlag, Dordrecht, 2013), pp. 1-24.

Graebner, J. E., B. Golding, and L. C. Allen, 1986, Phys. Rev. B **34**, 5696.

Grannan, E. R., M. Randeria, and J. P. Sethna, 1990, Phys. Rev. B **41**, 7784.

Grannan, E. R., M. Randeria, and J. P. Sethna, 1990, Phys. Rev. B **41**, 7799.

Gou, W., Y. Li, J. Chi, J. H. Ross, Jr, M. Beeckman, and G. S. Nolas, 2005, Phys. Rev. B **71**, 174307.

Gutt, C., J. Baumert, W. Press, J. S. Tse, and S. Janssen, 2002, J. Chem. Phys. **116**, 3795.

Hashimoto, D. and K. Shimizu, 2011, J. Opt. Soc. Am. **28**, 2227.

Hayashi, M., K. Kishimoto, K. Kishio, K. Akai, H. Asada, and T. Koyanagi, 2010, Dalton Trans. **39**, 1113.

He, H., A. Zevalkink, Z. M. Gibbs, G. J. Snyder, and S. Bobev, 2012, Chem. Mater. **24**, 3596.
Helen, B., E. Courtens, R. Vacher, A. Yamanaka, M. Kataoka, and K. Inoue, 2000, Phys. Rev. Lett. **84**, 5355.
Hermann, R. P., W. Schweika, O. Leupold, R. Rüffer, G. S. Nolas, F. Grandjean, and G. J. Long, 2005, Phys. Rev. B **72**, 174301.
Hermann, R. P., F. Grandjean, and G. J. Long, 2005, Am. J. Phys. **73**, 110.
Hermann, R. P., V. Keppens, P. Bonville, G. S. Nolas, F. Grandjean, G. J. Long, H. M. Christen, B. C. Chakoumakos, B. C. Sales, and D. Mandrus, 2006, Phys. Rev. Lett. **97**, 017401.
Hester, K. C. and P. G. Brewer, 2009, Annu. Rev. Marine. Sci. **1**, 303.
Hou, X., Y. Zhou, L. Wang, W. Zhang, W. Zhang, and L. Chen, 2009, J. Alloys Compd. **482**, 544.
Huo, D, T. Sakata, T. Sasakawa, M. A. Avila, M. Tsubota, F. Iga, H. Fukuoka, S. Yamanaka, S. Aoyagi, and T. Takabatake, 2005, Phys. Rev. B **71**, 075113.
Hunklinger, S. and A. K. Raychaudhuri, 1986, in *Progress in Low Temperature Physics*, **9**, pp.265-344.
Inamura, Y. , M. Arai, O. Yamamuro, A. Inabe, N. Kitamura, T. Otomo, T. Matsuo, S. M. Bennington, and A. C. Hannon, 1999, Physica B **263-264**, 299.
Inoue, R., H. Tanaka, and K. Nakanishi, 1996, J. Chem. Phys. **104**, 9569.
Ioffe, A. F., 1932, in *The socialist reconstruction and science*, No.1, p.23.
Ioffe, A. F. 1956, Izv. Akad. Nauk. SSSR, Ser. Fiz. **20**, 76.
Ioffe, A. F., 1958a, in *Semiconductor Thermoelements and Thermoelectric Cooling*, (Infosearch Ltd, London), pp.1-183.
Ioffe, A. F., 1958b, Scientific American **199**, 31.
Ioffe, A. V. and A. F. Ioffe, 1954, Dokl. Akad. Nauk. SSSR **98**, 757.
Ioffe, A. V. and A. F. Ioffe, 1956, Izv. Akad. Nauk. SSSR, Ser. Fiz. **20**, 65.
Ioffe, A. F. and A. R. Regel, 1960, Prog. Semicond. **4**, 237.
Ishii, I., H. Higaki, S. Morita, M. A. Avila, T. Sakata, T. Takabatake, and T. Suzuki, 2006, Physica B **383**, 130.
Ishii, I., Y. Suetomi, T. K. Fujita, K. Suekuni, T. Tanaka, T. Takabatake, T. Suzuki, and M. A. Avila, 2012, Phys. Rev. B **85**, 085101.
Iversen, B. B., A. E. C. Palmqvist, D. E. Cox, G. S. Nolas, G. D. Stucky, N. P. Blake, and H. Metiu, 2000, J. Solid State Chem. **149**, 455.
Jagannathan, A., R. Orbach, and O. Entin-Wohlman, 1989, Phys. Rev. B **39**, 13465.
Jeffrey, G. A., in *Inclusion Compounds*, edited by J. L. Atwood, J. E. D. Davies, and D. D. MacNicol (Academic Press, London, 1984) , pp. 135-190.
Jiang, Y., F. Bridges, M. A. Avila, T. Takabatake, J. Guzman, and G. Kurczveil, 2008, Phys. Rev. B **78**, 014111.
Johnsen, S., A. Bentien, G. K. H. Madsen, M. Nygren, and B. B. Iversen, 2007, Phys. Rev. B **76**, 245126.
Johnsen, S., M. Christensen, B. Thomsen, G. K. H. Madsen, and B. B. Iversen, 2010, Phys. Rev. B **82**, 184303.
Karttunen, A. J., T. F. Fässler, M. Linnolahti, and T. A. Pakkanen, 2011, Inorg. Chem. **50**, 1733.
Kanatzidis, M. G., 2010, Chem. Mater. **22**, 648.
Kaneshita, E. and T. Nakayama, 2009, Europhys. Lett. **86**, 56004.
Kasper, J. S., P. Hagenmuller, M. Pouchard, and C. Cros, 1965, Science **150**, 1713.
Kaye, G. W. C. and T H. Laby, 1966, in *Table of Physical and Chemical Constants*, (Longmans Green, London).
Keppens, V., B. C. Sales, D. Mandrus, B. C. Chakoumakos, and C. Laermans, 2000, Phil. Mag. Lett. **80**, 807.
Keppens, V., M. A. McGuire, A. Teklu, C. Laermans, B. C. Sales, D. Mandrus,and B. C. Chakoumakos, 2002, Physica B **316-317**, 95.
Kim, S. J., S. Hu, C. Uher, T. Hogan, B. Huang, J. D. Corbett, and M. G. Kanatzidis, 2000, J. Solid State Chem. **153**, 321.
Kim, J. H., N. L. Okamoto, K. Kishida, K. Tanaka, and H. Inui, 2007, J. Appl. Phys. **102**, 034510.
Kim, J. H., N. L. Okamoto, K. Kishida, K. Tanaka, and H. Inui, 2007, J. Appl. Phys. **102**, 094506.
Kirchner, S., F. Zamani and E. Muñoz, 2013, in *New Materials for Thermoelectric Applications: Theory and Experiment*, edited by V. Zlatic and A. Hewson (Springer-Verlag, Dordrecht, 2013), pp. 129-168.
Kishimoto, K., S. Arimura, and T. Koyanagi, 2006, Appl. Phys. Lett. **88**, 222115.
Kishimoto, K., T. Koyanagi, K. Akai, and M. Matsuura, 2007, Jpn. J. Appl. Phys. **46**, L746.
Kishimoto, K., N. Ikeda, K. Akai, and T. Koyanagi, 2008, Appl. Phys. Express **1**, 031201.
Kleinke, H. 2010, Chem. Mater. **22**, 604.
Klug, D. D., J. S. Tse, J. Y. Zhao, W. Sturhahn, E. E. Alp, and C. A. Tulk, 2011, Phys. Rev. B **83**, 184116.
Kono, Y., N. Ohya, T. Taguchi, K. Suekuni, T. Takabatake, S. Yamamoto, and K. Akai, 2010, J. Appl. Phys. **107**, 123720.
Koumoto, K., I. Terasaki, and R. Funahashi, 2006, Mater. Res. Soc. Bull. **31**, 206.
Kovnir, K. A. and A. V. Shevelkov, 2004, Russ. Chem. Rev. **73**, 923.
Koza, M. M., M. R. Johnson, H. Mutka, M. Rotter, N. Nasir, A. Grysiv, and P. Rogl, 2010, Phys. Rev. B **82**, 214301.
Kozina, M., F. Bridges, Y. Jiang, M. A. Avila, K. Suekuni, and T. Takabatake, 2009, Phys. Rev. B **80**, 212101.
Krivchikov, A. I., V. G. Manzhelii, O. A. Korolyuk, B. Ya. Gorodilov, and O. O. Romantsova, 2005, Phys. Chem. Chem. Phys. **7**, 728.
Krishnan, R. S., 1953, Proc. Indian Acad. Sci. A **37**, 377.
Kröner, R., R. Nesper, and H. G. von Schnering, 1988, Z. Kristallogr. - New Cryst. Struct. **182**, 164.
Kumar, G. S., G. Prasad, and R. O. Pohl, 1993, J. Materials Science **28**, 4261.
Kume, T., S. Ohno, S. Sasaki, H. Shimizu, Y. Ohishi, N. L. Okamoto, K. Kishida, K. Tanaka, and H. Inui, 2010, J. Appl. Phys. **107**, 013517.
Kuznetsov, V. L., L. A. Kuznetsova, A. E. Kaliazin, and D. M. Rowe, 2000, J. Appl. Phys. **87**, 7871.
LaLonde, A. D., Y. Pei, H. Wang, and G. J. Snyder, 2011, Mater. Today **14**, 526.
Lasjaunias, J. C., A. Ravex, M. Vandorpe, and S. Hunklinger, 1975, Solid State Commun. **17**, 1045.
Lee, C. H., I. Hase, H. Sugawara, H. Yoshizawa, and H. Sato, 2006, J. Phys. Soc. Jpn. **75**, 123602.
Lee, C. H. and H. Yoshizawa, M. A. Avila, I. Hase, K. Kikou, and T. Takabatake, 2007, J. Phys. Conf. Ser. **92**, 012169.
Lee, C. H., H. Yoshizawa, M. A. Avila, I. Hase, K. Kihou, and T. Takabatake, 2008, J. Phys. Soc. Jpn. **77**, Suppl. A 260.
Leoni, S., W. Carrillo-Cabrera, and Yu. Grin, 2003, J. Alloys.

Compd. **350**, 113.
Li, D. C., L. Fang, S. K. Deng, K. Y. Kang, L. X. Shen, W. H. Wei, and H. B. Ruan, 2012, Physica B **407**, 1238.
Li, Y. and J. H. Ross Jr., 2003, IEEE Trans. Appl. Supercond. **13**, 3047.
Li, Y., J. H. Ross Jr., J. A. Larrea, and E. Baggio-Saitovitch, 2004, Physica C **408-410**, 869.
Liu, Y., L. M. Wu, L. H. Li, S. W. Du, J. D. Corbett, and L. Chen, 2009, Angew. Chem. Int. Ed. **48**, 5305.
Loidl, A., K. Knorr, J. M. Rowe, and G. J. McIntyre, 1988, Phys.Rev. B **37**, 389.
Lorenz, L., 1872, Ann. Phys. **147**, 429.
Lorenz, L., 1881a, Ann. Phys. **13**, 422.
Lorenz, L., 1881b, Ann. Phys. **13**, 582.
Lovesey, S. W., 1984, in *Theory of Thermal Neutron Scattering from Condensed Matter*, (Clarendon Press, Oxford).
Madsen, G. K. H., K. Schwarz, P. Blaha, and D. J. Singh, 2003, Phys. Rev. B **68**, 125212.
Madsen, G. K. H. and G. Santi 2005, Phys. Rev. B **72**, 220301(R).
Mahan, G. D., B. Sales, and J. Sharp, 1997, Phys. Today **50**, 42.
Mahan, G. D., 1998, in *Solid State Physics*, edited by H. Ehrenreich and F. Spaepen (Elsevier), **51**, pp. 81-157.
Mansour, A. N., J. Martin, W. Wong-Ng, and G. S. Nolas, 2012, J. Phys. Cond. Matter **24**, 485503.
Martin, J., S. Erickson, G. S. Nolas, P. Alboni, T. M. Tritt, and J. Yang, 2006, J. Appl. Phys. **99**, 044903.
Martin, J., S. Erickson, G. S. Nolas, H. Wang, and J. Yang, 2007, J. Appl. Phys. **102**, 103719.
Martin, J., H. Wang, and G. S. Nolas, 2008, Appl. Phys. Lett. **92**, 222110.
Matsumoto, H., T. Mori, K. Iwamoto, S. Goshima, S. Kushibiki, and N. Toyota, 2009, Phys. Rev. B **79**, 214306.
Melnychenko-Koblyuk, N., A. Grytsiv, P. Rogl, H. Schmid, and G. Giester, 2009, J. Solid State Chem. **182**, 1754.
Menke, H. and H. G. von Schnering, 1973, Z. Anorg. Allg. Chem. **395**, 223.
Morelli, D. T., G. P. Meisner, B. Chen, S. Hu, and C. Uher, 1997, Phys. Rev. B **56**, 7376.
Mori, T., S. Goshima, K. Iwamoto, S. Kushibiki, H. Matsumoto, N. Toyota, K. Suekuni, M. A. Avila, T. Takabataake, T. Hasegawa, N. Ogita, and M. Udagawa, 2009, Phys. Rev. B **79**, 212301.
Mori, T., K. Iwamoto, S. Kushibiki, H. Honda, H. Matsumoto, N. Toyota, M. A. Avila, K. Suekuni, and T. Takabataake, 2011, Phys. Rev. Lett. **106**, 015501.
Mott, N. F. and H. Jones, 1936, in *The Theory of the Properties of Metals and Alloys*, (Clarendon Press, Oxford) Chap. 7, Sec. 15.
Mudryk, Y., P. Rogl, C. Paul, S. Berger, E. Bauer, G. Hilscher, C. Godart, and H. Noël, 2002, J. Phys.: Condens. Matter **14**, 7991.
Müller, H. R. and M. von Stackelberg, 1952, Naturwissenschaften **39**, 20.
Myles, C. W., J. Dong, and O. F. Sankey, 2001, Phys. Rev. B **64**, 165202.
Myles, C. W., K. Biswas, and E. Nenghabi, 2007, Physica B **401-402**, 695.
Nakamura, M. and M. Arai, 2010, unpublished work.
Nakayama, T., 1998, Phys. Rev. Lett. **80**, 1244.
Nakayama, T., 2002, Rep. Prog. Phys. **65**, 1195.
Nakayama, T., 2009, Nucl. Instr. Meth. Phys. Res. A **600**, 266.
Nakayama, T., K. Yakubo, and R. Orbach, 1994, Rev. Mod. Phys. **66**, 381.
Nakayama, T. and R. Orbach, 1999a, Physica B **47**, 468.
Nakayama, T. and R. Orbach, 1999b, Europhys. Lett. **47**, 468.
Nakayama, T. and E. Kaneshita, 2008, Europhys. Lett. **84**, 66001.
Nakayama, T. and E. Kaneshita, 2011, J. Phys. Soc. Jpn. **80**, 104604.
Narayanamurti, V. and R. O. Pohl, 1970, Rev. Mod. Phys **42**, 201.
Nasir, N., A. Grytsiv, N. Melnychenko-Koblyuk, P. Rogl, I. Bednar, and E. Bauer, 2010, J. Solid State Chem. **183**, 2329.
Nathan, B. D., L. F. Lou, and R. H. Tait, 1976, Solid State Commun. **19**, 615.
Nenghabi, E. N. and C. W. Myles, 2008, Phys. Rev. B **77**, 205203.
Nenghabi, E. N. and C. W. Myles, 2008, J. Phys.: Condens. Matter **20**, 415214.
Nguyen, L. T. K., U. Aydemir, M. Baitinger, E. Bauer, H. Borrmann, U. Burkhardt, J. Custers, A. Haghighirad, R. Höfler,, K. D. Luther, F. Ritter, W. Assmus, Yu. Grin, and S. Paschen, 2010, Dalton Trans. **39**, 1071.
Nolas, G. S., G. A. Slack, T. M. Tritt, and D. T. Morelli, 1995, in *Proceedings of the 14th International conference on Thermoelectrics*, edited by M. V. Vedernikov (A.F. loffe Physical-Technical Institute, St. Petersburg, Russia) 236.
Nolas, G. S., G. A. Slack, D. T. Morelli, T. M. Tritt, and A. C. Ehrlich, 1996, J. Appl. Phys. **79**, 4002.
Nolas, G. S., G. A. Slack, J. L. Cohn, and S. B. Schujman,1998, in *Proceedings of the 17th International conference on Thermoelectrics*, (IEEE, New York) p.294.
Nolas, G. S., J. L. Cohn, G. A. Slack, and S. B. Schujman 1998, Appl. Phys. Lett. **73**, 178.
Nolas, G. S., J. L. Cohn, and G. A. Slack, 1998, Phys. Rev. B **58**, 164.
Nolas, G. S., T. J. R. Weakley, J. L. Cohn, and R. Sharma, 2000, Phys. Rev. B **61**, 3845.
Nolas, G. S. and C. A. Kendziora, 2000, Phys. Rev. B **62**, 7157.
Nolas, G. S., B. C. Chakoumakos, B. Mahieu, G. J. Long, and T. J. R. Weakley, 2000, Chem. Mater. **12**, 1947.
Nolas, G. S., J. Sharp, and H. J. Goldsmid, 2001a, in *Thermoelectrics: Basic Principle and New Materials Developments*, (Springer, New York).
Nolas, G. S., G. A. Slack, and S. B. Schujman, 2001b, in *Recent Trends in Thermoelectric Materials Research I: Semiconductors and Semimetals*, **69**, edited by T.M. Tritt, (Academic Press, San Diego), pp.255-300.
Nolas, G. S., 2003, in *Chemistry, Physics, and Materials Science of Thermoelectric Materials: Beyond Bismuth Telluride*, edited by M. G. Kanatzidis, S. D. Mahanti, and T. P. Hogan, (Kluwer Academic / Plenum Publishers, New York), pp.107-120.
O'Brien, B. J. and C. S. Wallace, 1958, J. Appl. Phys. **29**, 1010.
Onsager, L., 1931, Phys. Rev. **37**, 405.
Pauling, L., 1948, in *The nature of the Chemical Bond*, (Cornell Univ. Press, Ithaca, NY).
Pauling, L. and R. E. Marsh, 1952, Proc. Natl Acad. Sci. U.S. **38**, 112.
Pacheco, V., A. Bentien, W. Carrillo-Cabrera, S. Paschen,

F. Steglich, and Yu. Grin, 2005, Phys. Rev. B **71**, 165205.
Paschen, S., W. W. Carrillo-Cabrera, A. Bentien, V. H. Tran, M. Baenitz, Y. Grin, and F. Steglich, 2001, Phys. Rev. B **64**, 214404.
Paschen, S., V. H. Tran, M. Baenitz, W. Carrillo-Cabrera, Yu. Grin, and F. Steglich, 2002, Phys. Rev. B **65**, 134435.
Paschen, S., V. Pacheco, A. Bentien, A. Sanchez, W. Carrillo-Cabrera, M. Baenitz, B.B. Iversen, Yu. Grin, and F. Steglich, 2003, Physica B **328**, 39.
Peierls, R., 1929, Ann. Phys. **3**, 1055.
Peltier, J. C., 1834, Ann Chim. Phys. **56**, 371.
Phillips, W. A., 1972, J. Low Temp. Phys. **7**, 351.
Phillips, W. A., 1987,@Rep. Prog. Phys. **50**, 1657.
Pohl, R. O., 1981, in *Amorphous Solids: Low Temperature Properties*, edited by W. A. Phillips (Springer, Berlin), p. 27.
Qiu, L., I. P. Swainson, G. S. Nolas, and M. A. White, 2004, Phys. Rev. B **70**, 035208.
Randeria, M. and J. P. Sethna, 1988, Phys. Rev. B **38**, 12607.
Rachi, T., H. Yoshino, R. Kumashiro, M. Kitajima, K. Kobayashi, K. Yokogawa, K. Murata, N. Kimura, H. Aoki, H. Fukuoka, S. Yamanaka, H. Shimotani, T. Takenobu, Y. Iwasa, T. Sasaki, N. Kobayashi, Y. Miyazaki, K. Saito, F. Z. Guo, K. Kobayashi, K. Osaka, K. Kato, M. Takata, and K. Tanigaki, 2005, Phys. Rev. B **72**, 144504.
Rodriguez, S. Y., L. Saribaev, and J. H. Ross, Jr., 2010, Phys. Rev. B **82**, 064111.
Rogl, P., 2006, in *Thermoelectrics Handbook: Macro to Nano*, edited by D. M. Rowe (CRC Press, Taylor and Francis Group, Boca Raton, Florida), **32**, pp. 1-24.
Rowe, D. M., 1995, in *CRC Handbook of Thermoelctrics*, edited by D. M. Rowe (CRC Press, Boca Raton, Florida).
Roudebush, J. H., N. Tsujii, A. Hurtando, H. Hope, Y. Grin, and S. M. Kauzlarich, 2012, Inorg. Chem. **51**, 4161.
Rowe, D. M., 2003, in *Proceedings of the 22nd International Conference on Thermoelectrics*, 1.
Safarik, D. J., A. Llobet, and J. C. Lashley, 2012, Phys. Rev. B **85**, 174105.
Sales, B. C., D. Mandrus, , and R. K. Williams, 1996, Science **272**, 1325.
Sales, B. C., D. Mandrus, B. C. Chakoumakos, V. Keppens, and J. R. Thompson, 1997, Phys. Rev. B **56**, 15081.
Sales, B. C., 1998, Mater. Res. Soc. Bull. **23**, 15.
Sales, B. C., B. C. Chakoumakos, D. Mandrus, and J. W. Sharp, 1999, J. Solid State Chem. **146**, 528.
Sales, B. C., B. C. Chakoumakos, R Jin, J. R. Thompson, and D. Mandrus, 2001, Phys. Rev. B. **63**, 245113.
Sales, B. C., 2002, Science **295**, 1248.
Saramat, A., G. Svensson, A. E. C. Palmqvist, C. Stiewe, E. Mueller, D. Platzek, S. G. K. Williams, D. M. Rowe, J. D. Bryan, and G. D. Stucky, 2006, J. Appl. Phys. **99**, 023708.
Sasaki, Y., K. Kishimoto, T. Koyanagi, H. Asada, and K. Akai, 2009, J. Appl. Phys. **105**, 073702.
Schujman, S. B., G. S. Nolas, R. A. Young, C. Lind, A. P. Wilkinson, G. A. Slack, R. Patschke, M. G. Kanatzidis, M. Ulutagay, and S.-J. Hwu, 2000, J. Appl. Phys. **87**, 1529.
Seebeck, T. J., 1822-1823, Abhandlungen der Deutscher Akademie der Wissenschaften zu Berlin, pp.265-373.
Seebeck, T. J., 1826, Ann. Phys. **82**, 253.
Shevelkov, A. V. and K. Kovnir, in *Zintl Phases - Principles and Recent Developments*, edited by T. F. Fässler (Springer, Berlin Heidelberg, 2011) , pp. 97-142.
Shimizu, H., R. Oe, S. Ohno, T. Kume, S. Sasaki, K. Kishimoto, T. Koyanagi, and Y. Ohishi, 2009, J. Appl. Phys. **105**, 043522.
Shimizu, H., Y. Takeuchi, T. Kume, S. Sasaki, K. Kishimoto, N. Ikeda, and T. Koyanagi, 2009, J. Alloys. Compd. **487**, 47.
Simons, S., 1964, Proc. Phys. Soc. London **83**, 749.
Slack, G. A., 1995, in *CRC Handbook of Thermoelectrics*, edited by D. M. Rowe, (CRC Press, Boca Raton, Florida), pp.407-440.
Snyder, G. J. and E. S. Toberer, 2008, Nat. Mater. **7**, 105.
Sommerfeld, A., 1927, Naturwissenschaften **15**, 825.
Sommerfeld, A., 1928, Naturwissenschaften **16**, 374.
Sootsman, J. R., D. Y. Chung, and M. G. Kanatzidis, 2009, Angew. Chem. Int Ed **48**, 8616.
Squires, G. L., 1978, in *Introduction to the Theory of Thermal Neutron Scattering*, (Cambridge University Press, London).
Stephens, R. B., 1973, Phys. Rev. B **8**, 2896.
Struzhkin, V. V., B. Militzer, W. L. Mao, H. K. Mao, and R. J. Hemley, 2007, Chem. Rev. **107**, 4133.
Suekuni, K., M. A. Avila, K. Umeo, and T. Takabatake, 2007, Phys. Rev. B **75**, 195210.
Suekuni, K., M. A. Avila, K. Umeo, H. Fukuoka, S. Yamanaka, T. Nakagawa, and T. Takabatake, 2008, Phys. Rev. B **77**, 235119.
Suekuni, K., S. Yamamoto, M. A. Avila, and T. Takabatake, 2008, J. Phys. Soc. Jpn. **77**, Suppl. A, 61.
Suekuni, K., Y. Takasu, T. Hasegawa, N. Ogita, M. Udagawa, M. A. Avila, and T. Takabatake, 2010, Phys. Rev. B **81**, 205207.
Takabatake, T., E. Matsuoka, S. Narazu, K. Hayashi, S. Morimoto, T. Sasakawa, K. Umeo, and M. Sera, 2006, Physica B **383**, 93.
Takasu, Y., T. Hasegawa, N. Ogita, M. Udagawa, M. A. Avila, K. Suekuni, I. Ishii, T. Suzuki, and T. Takabatake, 2006, Phys. Rev. B **74**, 174303.
Takasu, Y., T. Hasegawa, N. Ogita, M. Udagawa, K. Suekuni, M. A. Avila, and T. Takabatake, 2007, J. Phys. Conf. Ser. **92**, 012151.
Takasu, Y., T. Hasegawa, N. Ogita, M. Udagawa, M. A. Avila, K. Suekuni, and T. Takabatake, 2008, Phys. Rev. Lett. **100**, 165503.
Takasu, Y., T. Hasegawa, N. Ogita, M. Udagawa, M. A. Avila, K. Suekuni, and T. Takabatake, 2010, Phys. Rev. B **82**, 134302.
Tanaka, T., T. Onimaru, K. Suekuni, S. Mano, H. Fukuoka, S. Yamanaka, and T. Takabatake, 2010, Phys. Rev. B **81**, 165110.
Tang, X. F., L. M. Zhang, R. Z. Yuan, L. D. Chen, T. Goto, T. Hirai, J. S. Dyck, W. Chen, and C. Uher, 2001, J. Mater. Res. **16**, 3343.
Tang, J., R. Kumashiro, J. Ju, Z. Li, M. A. Avila, K. Suekuni, T. Takabatake, F. Guo, K. Kobayashi, and K. Tanigaki, 2009, Chem. Phys. Lett. **472**, 60.
Tang, J., Z. Li, T. Nishiro, K. Sato, and K. Tanigaki, 2010, J. Phys. Chem. Solids **71**, 480.
Tang, J., J. T. Xu, S. Hegri, K. Akai, and K. Tanigaki, 2011, J. Electronic Mater. **40**, 769.
Toberer, E. S., M. Christensen, B. B. Iversen, and G. J. Snyder, 2008, Phys. Rev. B **77**, 075203.
Toberer, E. S., A. F. May, and G. J. Snyder, 2010, Chem. Mater. **22**, 624.
Topp, K. A. and R. O. Pohl, 2002, Phys. Rev. B **66**, 064204.
Tritt, T. M., 2001, in *Recent Trends in Thermoelectric Ma-*

terials Research I, Semiconductors and Semimetals, edited by T. M. Tritt, (Academic Press, San Diego).
Tse, J. S., V. P. Shpakov, V. V. Murashov, and V. R. Belosludov, 1997, J. Chem. Phys. **107**, 9271.
Tse, J. S., V. P. Shpakov, V. R. Belosludov, F. Trouw, Y. P. Handa, and W. Press, 2001, Europhys. Lett. **54**, 354.
Uemura, T., K. Akai, K. Koga, T. Tanaka, H. Kurisu, S. Yamamoto, K. Kishimoto, T. Koyanagi, and M. Matsuura, 2008, J. Appl. Phys. **104**, 013702.
Uher, C., J. Yang, and S. Hu, 1999, Mater. Res. Soc. Symp. Proc. **545**, 247.
Uher, C., 2001, in *Recent Trends in Thermoelectric Materials Research I, Semiconductors and Semimetals*, edited by T. M. Tritt (Academic Press, San Diego), **69**, pp. 139-252.
Umeo, K., M. A. Avila, T. Sakata, K. Suekuni, and T. Takabatake, 2005, J. Phys. Soc. Jpn. **74**, 2145.
Vedernikov, M. V. and E. K., Iordanishvili, 1998, in Proceeding of the 17th International Conference on Thermoelectrics, 37.
von Schnering, H. G., W. Carrillo-Cabrera, R. Kröner, E.-M. Peters, K. Peters, and R. Nesper, 1998, Z. Kristallogr. - New Cryst. Struct. **213**, 679.
von Stackelberg, M. and H. R. Müller, 1951, J. Chem. Phys. **19**, 1319.
von Stackelberg, M. and H. R. Müller, 1951, Naturwissenschaften **38**, 456.
Walton, D., H. A. Mook, and R. M. Nicklow, 1974, Phys. Rev. Lett. **33**, 412.
Wang, L., L-D. Chen, X-H. Chen, and W-B. Zhang, 2009, J. Phys. D: Appl. Phys. **42**, 045113.
Wiedemann, G. and Franz, R. 1853, Ann. Phys. **89**, 497.
Winterlich, M., R. Böhmer, and A. Loidl, 1995, Phys. Rev. Lett. **75**, 1783.
Woods, G. T., J. Martin, M. Beekman, R. P. Hermann, F. Grandjean, V. Keppens, O. Leupold, G. J. Long, and G. S. Nolas, 2006, Phys. Rev. B **73**, 174403.
Xu, J., J. Tang, K. Sato, Y. Tanabe, H. Miyasaka, M. Yamashita, S. Heguri, and K. Tanigaki, 2010, Phys. Rev. B **82**, 085206.
Xu, J., J. Tang, K. Sato, Y. Tanabe, S. Heguri, H. Miyasaka, M. Yamashita, and K. Tanigaki, 2011, J. Electron. Mater. **40**, 879.
Xu, J., J. Wu, S. Heguri, G. Mu, Y. Tanabe, and K. Tanigaki, 2012, J. Electron. Mater. **41**, 1177.
Yamakage, A. and Y. Kuramoto, 2009, J. Phys. Soc. Jpn. **78**, 064602.
Yamanaka, S., H. Horie, H. Nakano, and M. Ishikawa, 1995, Fullerene Sci. Tec. **3**, 21.
Yamanaka, S., E. Enishi, H. Fukuoka, and M. Yasukawa, 2000, Inorg. Chem. **39**, 56.
Yang, J., 2004, in *Thermal Conductivity: Theory, Properties, and Applications*, edited by T. M. Tritt, (Kluwer Academic/Plenum Publisher, New york), 1-20.
Zaikina, J. V., K. A. Kovnir, F. Haarmann, W. Schnelle, U. Burkhardt, H. Borrmann, U. Schwarz, Yu. Grin, and A. V. Shevelkov, 2008, Chem. Eur. J. **14**, 5414.
Zaikina, J. V., T. Mori, K. Kovnir, D. Teschner, A. Senyshyn, U. Schwarz, Yu. Grin, and A. V. Shevelkov, 2010, Chem. Eur. J. **16**, 12582.
Zeller, R. C. and R. O. Pohl, 1971, Phys. Rev. B **4**, 2029.
Zerec, I., V. Keppens, M. A. McGuire, D. Mandrus, B. C. Sales, and P. Thalmeier, 2004, Phys. Rev. Lett. **92**, 185502.
Zhang, Y., P. L. Lee, G. S. Nolas, and A. P. Wilkinson, 2002, Appl. Phys. Lett. **80**, 2931.
Zhang, H., H. Borrmann, N. Oeschler, C. Candolfi, W. Schnelle, M. Schmidt, U. Burkhardt, M. Baitinger, J. T. Zhao, and Yu. Grin, 2011, Inorg. Chem. **50**, 1250.
Zheng, X., S. Y. Rodriguez, and J. H. Ross Jr., 2011, Phys. Rev. B **84**, 024303.
Zheng, X., S. Y. Rodriguez, L. Saribaev, and J. H. Ross Jr., 2012, Phys. Rev. B **85**, 214304.